

12  
B.S.

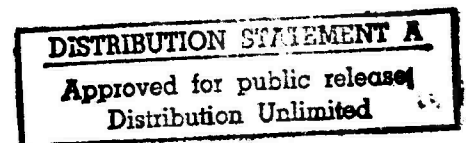
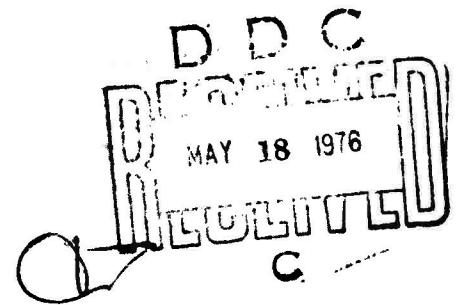
AD A 024463



AN EXPERIMENTAL AND ANALYTICAL INVESTIGATION OF A  
RADIAL FACE SEAL

TIMOTHY W. SWAFFORD

January 1976

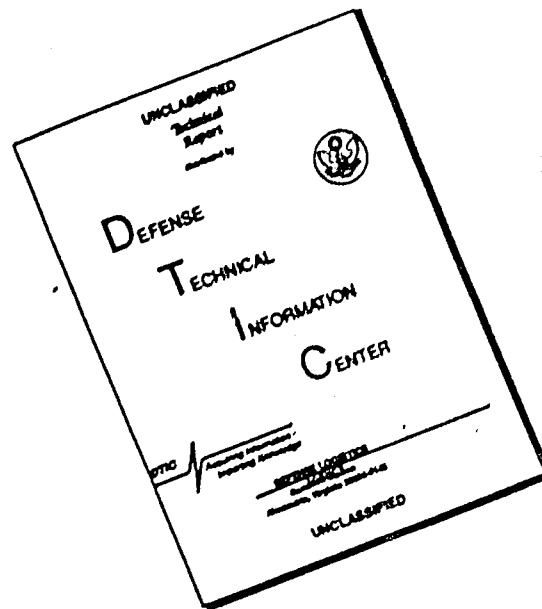


DEPARTMENT OF MECHANICAL AND AEROSPACE ENGINEERING

**The University of Tennessee**

Knoxville, Tennessee

# DISCLAIMER NOTICE



THIS DOCUMENT IS BEST QUALITY AVAILABLE. THE COPY FURNISHED TO DTIC CONTAINED A SIGNIFICANT NUMBER OF PAGES WHICH DO NOT REPRODUCE LEGIBLY.

ME-76-T57-22

January 1976

The University of Tennessee  
Department of Mechanical and Aerospace Engineering  
Knoxville, Tennessee 37916

An Experimental and Analytical Investigation of a Radial Face Seal

Timothy W. Swafford

Prepared under

Office of Naval Research Contract N00014-75-C-390

DISTRIBUTION STATEMENT A

Approved for public release;  
Distribution Unlimited

Reproduction in whole or in part is permitted for any purpose of  
the United States Government.

DDC  
RECEIVED  
MAY 18 1976  
C


404 721

## Foreword

This document is submitted as an interim report covering the second phase of an experimental investigation of a radial face seal. It contains a description of the experimental apparatus as well as a description of a theoretical analysis along with the results of both theory and experimentation. Support for this work was provided by Contract N00014-75-C-390 with the Office of Naval Research.

This report was submitted to the University of Tennessee by F. W. Swafford in partial fulfillment of the requirements for the Master of Science Degree; it is presented here with minor changes in format.

Approved: \_\_\_\_\_

  
H. J. Wilkerson  
Project Manager

## ABSTRACT

A complete description concerning the interface region of a parallel radial face seal has been conducted both experimentally and analytically. Analytical predictions stem from a FORTRAN IV computer program designed such that density and viscosity variation with temperature can be simulated. The equations of motion were solved on an incremental basis to yield a "closed form, finite difference" solution. For comparison purposes, predictions assuming non-temperature dependent fluid properties are also given.

Experimentally determined parameters include vertical load, torque, interface pressures, and temperatures, while interface clearance, supply pressure, and rotational speed were externally set parameters affecting seal performance. Unlike most other investigators, the test seal was rigidly mounted and both surfaces were constructed of stainless steel.

Numerically predicted temperature dependent and non-temperature dependent fluid property pressure profiles deviate substantially when fluid temperature rise becomes significant; thus decreasing the load carrying capacity of the seal. Predictions involving a temperature-dependent fluid indicate higher leakage rates and lower torque values when compared to predictions assuming a non-temperature dependent fluid.

Experimental testing was carried out under several sealing conditions. Supply pressures ranged from 17.1 to 87.5 psig ( $1.18 \times 10^5$  to  $6.03 \times 10^5$  N/m<sup>2</sup>) while average clearances and rotational

speeds ranged from 1995 to 3528 micro-inches (50.7 to 89.6 microns) and from 0 to 1520 rpm, respectively.

Vertical loads obtained experimentally were normally lower than those predicted although differences decreased at higher supply pressures. Experimentally determined torque agreed favorably with theoretical predictions while measured leakage rates were consistently lower than those predicted by theory.

In contrast to several past experimenters reporting doubly fluctuating components of clearance and pressure per shaft revolution, this investigation revealed but a single clearance and pressure oscillation per shaft revolution. Measured average pressure values agreed somewhat with predictions although significant differences were noticed at high speeds and low clearances.

# TABLE OF CONTENTS

CHAPTER	PAGE
I. INTRODUCTION . . . . .	1
Review of Literature . . . . .	3
Statement of the Problem . . . . .	11
II. THEORETICAL FACE SEAL ANALYSIS . . . . .	12
General. . . . .	12
Pertinent Assumptions . . . . .	12
Development of Analytical Model . . . . .	14
Calculation Technique . . . . .	18
Mathematical Modeling of Temperature Dependent	
Fluid Properties . . . . .	18
Detailed Discussion of Computer Program . . . . .	23
General. . . . .	23
Boundary conditions . . . . .	23
III. EXPERIMENTAL FACE SEAL TEST RIG AND INSTRUMENTATION.	27
General. . . . .	27
Test Apparatus . . . . .	27
Test (Stationary) Seal . . . . .	33
Rotating Seal . . . . .	36
Instrumentation . . . . .	36
External Transducers . . . . .	38
Interface and supply pressure . . . . .	38
Interface clearance . . . . .	42
Diaphragm temperature . . . . .	43

CHAPTER	PAGE
IV. INSTRUMENTATION CALIBRATION . . . . .	44
General . . . . .	44
Supply Pressure . . . . .	44
Interfacial Pressure . . . . .	45
Frictional Torque . . . . .	45
Vertical Load . . . . .	46
Clearance Probes . . . . .	46
Clearance Probe Pressure Compensation . . . . .	50
Flow Meter Calibration . . . . .	52
Thermocouple Calibration . . . . .	52
V. EXPERIMENTAL TESTS, DATA REDUCTION, AND RESULTS . . . . .	54
General . . . . .	54
Experimental Procedure . . . . .	54
Data Interpretation and Reduction . . . . .	55
Presentation of Data - Experimental and Analytical	
Results . . . . .	59
Analytical results . . . . .	59
Experimental results . . . . .	67
Comparisons of analytical and experimental	
findings . . . . .	76
VI. CONCLUSIONS AND RECOMMENDATIONS . . . . .	94
BIBLIOGRAPHY . . . . .	99
APPENDICES . . . . .	102
A. Computer Program . . . . .	103
B. Clearance Probe Installation Procedure . . . . .	125



CHAPTER	PAGE
C. Calibration Resistor ( $R_{Cal}$ ) Calculations . . . . .	127
D. Calibration Curves . . . . .	130
E. Clearance Probe Pressure Compensation-Determination of Actual Clearance Probe Movement . . . . .	144
VITA. . . . .	145

# LIST OF TABLES

TABLE	PAGE
I. Signal Conditioning Outline . . . . .	41
II. Theoretical Temperature-Dependent and Non-Temperature- Dependent Fluid Property Vertical Load Comparisons ( $P_o = 100$ psig, $h = 0.001$ inch) . . . .	64
III. Theoretical Temperature-Dependent and Non-Temperature- Dependent Fluid Property Vertical Load Comparisons ( $P_o = 100$ psig, $h = 0.003$ inch) . . . .	64
IV. Theoretical Temperature-Dependent and Non-Temperature- Dependent Fluid Property Leakage Rate Comparisons ( $P_o = 100$ psig, $h = 0.001$ inch) . . . .	65
V. Theoretical Temperature-Dependent and Non-Temperature- Dependent Fluid Property Leakage Rate Comparisons ( $P_o = 100$ psig, $h = 0.003$ inch) . . . .	65
VI. Experimental Data . . . . .	68
VII. Experimental Data . . . . .	69
VIII. Experimental, Temperature-Dependent, and Non- Temperature-Dependent Fluid Property Leakage Rate Comparisons (Runs 1 through 17) . . . . .	83
IX. Experimental, Temperature-Dependent, and Non- Temperature-Dependent Fluid Property Vertical Load Comparisons (Runs 1 through 17) . . . . .	89

## LIST OF FIGURES

FIGURE	PAGE
1. Typical Mechanical Face Seal . . . . .	2
2. Flow Geometry with Infinitesimal Fluid Element . . . . .	13
3. Tangential Direction Velocity Profile . . . . .	15
4. Computer Program Flow Chart . . . . .	19
5. Plot of Specific Gravity vs Temperature (Gulfspin 38 Oil) . . . . .	22
6. Pressure Acting on Upper Seal Face . . . . .	26
7. Test Apparatus . . . . .	28
8. Instrumented Section . . . . .	29
9. Strain Gage Placement on Instrumented Section . . . . .	31
10. Pressurization and Leakage Measurement System . . . . .	32
11. Test (Stationary) Seal . . . . .	34
12. Precision Measurement Company Model 150 Strain Gage Pressure Probe . . . . .	35
13. Rotating Seal . . . . .	37
14. Honeywell 24-Channel Oscillograph Recorder Console . . . . .	39
15. Typical Signal Path . . . . .	40
16. Vertical Load Influence on Torque . . . . .	47
17. Torque and Vertical Load Calibration Rig . . . . .	48
18. Clearance Probe Pressure Sensitivity . . . . .	51
19. Oscillograph Record (Run 12) . . . . .	56
20. Oscillograph Record (Run 13) . . . . .	57
21. Temperature Dependent and Non-Temperature Dependent Fluid Property Pressure Profiles . . . . .	60

FIGURE	PAGE
22. Seal Torque vs Clearance (Properties Temperature Dependent) . . . . .	61
23. Seal Torque vs Clearance (Properties Temperature Independent) . . . . .	62
24. Oil Outlet Temperature vs Clearance (Properties Dependent and Independent of Temperature) . . . . .	63
25. Clearance Probe Traces (Run 13) . . . . .	72
26. Pressure Probe Traces (Run 13) . . . . .	74
27. Seal Pressure vs Radius (Run 6) . . . . .	78
28. Seal Pressure vs Radius (Run 12) . . . . .	79
29. Seal Pressure vs Radius (Run 4) . . . . .	81
30. Seal Pressure vs Radius (Run 17) . . . . .	82
31. Seal Torque vs Clearance (Runs 2, 3, and 4) . . . . .	85
32. Seal Torque vs Clearance (Runs 6, 7, and 8) . . . . .	86
33. Seal Torque vs Clearance (Runs 15, 16, and 17) . . . . .	87
34. Temperature vs Radius (Run 13) . . . . .	90
35. Temperature vs Radius (Run 4) . . . . .	91
36. Temperature vs Radius . . . . .	93
37. Supply Pressure Calibration Curve . . . . .	131
38. Pressure Probe SP1 Calibration Curve . . . . .	132
39. Pressure Probe SP2 Calibration Curve . . . . .	133
40. Pressure Probe SP3 Calibration Curve . . . . .	134
41. Pressure Probe SP5 Calibration Curve . . . . .	135
42. Torque Calibration Curve . . . . .	136
43. Vertical Load Calibration Curve . . . . .	137

FIGURE	PAGE
44. Clearance Probe A1 Calibration Curve . . . . .	138
45. Clearance Probe B2 Calibration Curve . . . . .	139
46. Clearance Probe C3 Calibration Curve . . . . .	140
47. Clearance Probe F5 Calibration Curve . . . . .	141
48. Flow Meter Calibration Curve (Large Glass) . . . . .	142
49. Flow Meter Calibration Curve (Small Glass) . . . . .	143

# LIST OF SYMBOLS

$C_p$	Fluid specific heat
$E_f$	Friction energy
$E_p$	Flow work
$h$	Seal clearance
$M$	Seal moment
$\dot{m}$	Mass flow rate
$p$	Seal pressure at any radius
$Q$	Volumetric flow rate
$r$	Radial distance from seal centerline
$R_1$	Seal inside radius
$R_2$	Seal outside radius
$u_r$	Fluid radial velocity
$u_\theta$	Fluid tangential velocity
$y$	Normal distance from rotating seal face
$\rho$	Fluid density
$\mu$	Fluid absolute viscosity
$\nu$	Fluid kinematic viscosity
$\tau_r$	Radial direction fluid shear stress
$\Delta r$	Small radial increment
$\omega_f$	Fluid angular velocity
$\omega_s$	Seal angular velocity

## CHAPTER I

### INTRODUCTION

The parallel radial face seal, shown in Figure 1, has been the subject of numerous investigations in past years both from the standpoint of experimental and theoretical aspects. The process by which the seal actually operates remains basically somewhat of a mystery. Some of the early investigators were interested in merely establishing that a continuous fluid film actually exists between the two sealing surfaces. This hypothesis is generally accepted as valid although boundary lubrication may occur under certain conditions. Other experimenters were primarily interested in a more complete analysis of the interface conditions such as pressure and temperature profiles, frictional torque, wear, leakage rate, loading, and film thickness.

Some theoretical analyses have agreed favorably with experimental results with respect to leakage rate, frictional torque, and pressure profile. However, most of these tests were carried out under conditions where fluid temperature rise was insignificant. It is the overall purpose of this thesis to present and compare both theoretical and experimental data concerning the radial face seal. The theoretical data will take into account the possibility of temperature dependent fluid properties.

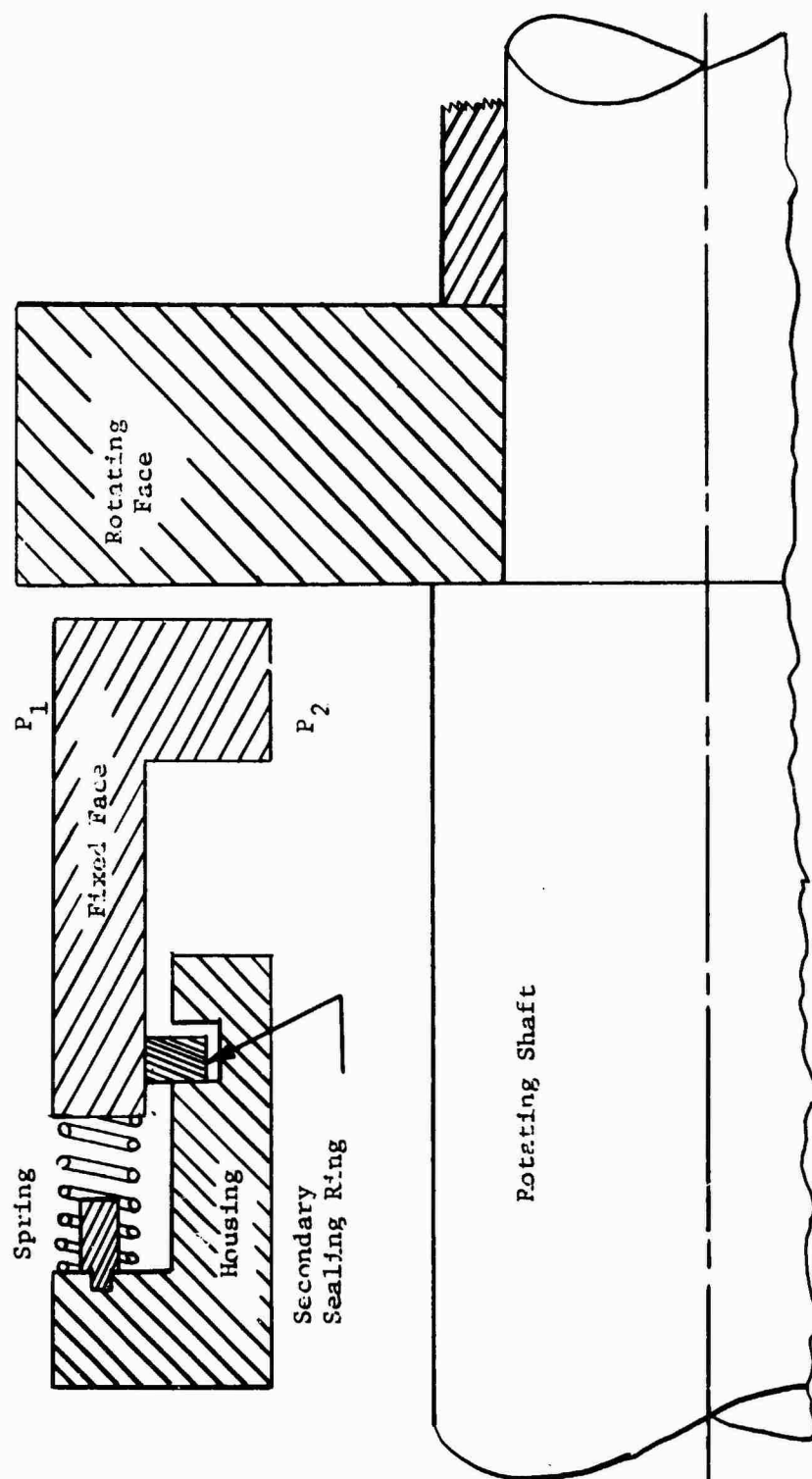


Figure 1. Typical Mechanical Face Seal.



### Review of Literature

Some of the earliest and most extensive research concerning radial face seals was carried out in 1960 by Denny (1), who was mainly concerned with studying the interface pressure profiles and clearances. Denny's experimental seal was artificially loaded by either a pneumatic piston or a lever-fulcrum system and clearance was determined by a capacitance method. Interface pressures were measured with pressure taps located radially around the seal. Also, to gain some idea of the interface temperature profile, thermocouples were also placed radially around the seal and lapped flush with the stationary carbon face. The leakage rate was determined by volumetric measurement over a period of time.

Denny's results indicated a number of interesting points, one of which was the ability of the rotating seal to withstand considerable loading with no pressure difference across the seal face (i.e., the seal was simply submerged in an oil bath and rotated). This was apparently due to a cyclic "generated pressure" at a frequency twice the rotating shaft speed. Also, the clearance appeared to fluctuate similarly to the pressure with peak clearance 180 degrees out of phase with the shaft rotation.

This generated pressure was deemed the cause of the seal to develop a radially inward pumping action. In some cases, this pumping action was sufficiently strong to induce a flow against a substantial pressure difference. In all tests conducted, the pressures measured were higher than predicted by theoretical analysis. However, frictional torque and leakage rate agreed somewhat with theory.

Denny's work confirmed the existence of a fluid film in a properly operating face seal but failed to define precisely what produces the actual sealing mechanism.

The following year, Ishiwata and Hirabayshi (2) suggested that an oil film would not occur naturally between two perfectly parallel surfaces but would appear, due to an oil wedge, if the two surfaces were actually wavy. Although no interface clearance measurements were attempted, a number of other parameters were recorded. Frictional torque was determined via a spring balance system. Surface (carbon) temperature was measured by embedding thermocouples in the stationary surface. The waviness and roughness of the sealing surfaces were determined by an interference-microscope and an optical flat employing sodium light. Seal performance was evaluated by examining the sealing surfaces by regular intervals. Seal leakage was measured rather uniquely by illuminating the contact part of the seal with ultraviolet light from a high-pressure mercury vapor lamp. When the oil emerged from the seal cavity, it fluoresced under the ultraviolet light, thus making it easily detectable.

Ishiwata's and Hirabayshi's coefficient of friction results were somewhat scattered in spite of the fact that some tests were carried out under identical conditions. They noticed that the friction coefficient decreased with increased loading employing motor oil but had a tendency to increase with load when spindle oil was used. They also noted that friction was lower when leakage occurred than when the seal was operating in a sealing mode.

Also in 1961, Summers-Smith (3) was conducting research with regard to the radial face seal. Like Ishiwata and Hirabayshi, Summers-Smith determined frictional torque employing a spring balance system. The sealing apparatus was loaded artificially with the aid of a system of pulleys and weights. Similarly to some other investigators, water was used as the fluid sealant. Although direct measurement of interface temperature was not attempted, it could be estimated from a series of thermocouples embedded at different depths normal to the sealing surface.

Friction and wear studies resulted in the conclusion that a fluid film of thickness of approximately 100 micro-inches was generated. Another result was that in a properly operating seal, leakage was extremely small and when volatile liquids were used as the sealant the leakage takes place by evaporation. Summers-Smith concluded his study by stating that the main limitation to the use of radial face seals at high pressures and rotational speeds is the temperature rise of the fluid film, i.e., when the fluids viscosity decreased resulting in a decrease in clearance, vaporization of the liquid may occur resulting in boundary lubrication.

Similar to Denny, Batch and Iny's (4) face seal investigations in 1964 revealed the twice shaft speed fluctuation of film thickness and pressure (pressure increased as film thickness decreased and vice-versa). Also like Denny, Batch and Iny used a carbon stationary face and determined clearance by a capacitance method. However, unlike Denny and other previous investigators, interface pressures were determined by piezo-electric pressure probes mounted behind a

thin diaphragm, thus leaving the fluid film undisturbed. Similarly to Summers-Smith, interface temperature was estimated from a bank of thermocouples normal to the sealing surface (temperature across the fluid film was assumed constant). The seal was loaded artificially by a pneumatic piston and leakage determined by a volumetric method. However, due to the experimental apparatus used, frictional torque measurements were not attempted.

The aforementioned film thickness fluctuation was found to be independent of supply pressure, speed, and temperature but was affected by seal loading. The fluctuations were concluded to have been induced by small vibrations of both faces.

Although Batch and Iny's work did not establish the sealing mechanism, the confirmation of pressure and clearance fluctuations was of valuable use to future investigators.

Also in 1964, Bremner (5) conducted a study of stationary face seals operating in the purely viscous flow regime. Employing a modified form of the Reynolds number ( $\rho u h^2 / \mu R_2$ ) as a flow criteria, he experimentally determined leakage rates, vertical loading, and pressure profiles. The majority of tests were carried out at an externally set clearance of 0.003 inch.

Again similarly to Denny, Bremner determined pressure profiles with radially spaced pressure taps. Although temperature profile measurements were not attempted, an average operating temperature could be estimated by the oil outlet temperature. Loading was determined by measuring the inlet and outlet pressures. .

Bremner's pressure profile and leakage rate results agreed somewhat with theory although viscosity change due to temperature rise

resulted in non-linear experimental relations influencing the leakage. Results also indicated that the modified Reynolds number was appropriate for at least an initial evaluation of the validity of the purely viscous flow relations.

In 1968, Pape (6) conducted research primarily aimed at studying the lubrication mechanism in face seals. His experimental apparatus consisted of a rotating and stationary piece similar to other experimenters. The seal was loaded artificially by a pneumatic piston. Torque was measured by a strain gage torque arm and clearance determined by a capacitance method. Unfortunately, due to the temperature sensitivity of the clearance measurement system, accurate film thickness values were unobtainable. Pape did not attempt to obtain local interface pressures but did determine film temperature by placing thermocouples 0.025 inch below the stationary face. Much attention was paid to obtaining local film temperatures by employing extremely small thermocouples and insulating the area immediately surrounding each thermocouple. The error in temperature readings was estimated at being no more than 1°C.

Similar to past investigators, Pape's results indicated a twice shaft speed fluctuation of gap size, apparently due to surface waviness. Since experiments yielded good reproducibility, he concluded that unreliable results obtained by other experimenters could possibly have been due to an ever-changing surface topography of the stationary carbon face.

Pape also conducted a theoretical analysis assuming that the sealing surface macroroughness accounted for the observed data and concluded that results indicate strong support that the concept of

considering the aforementioned sealing surface macroroughness is of major importance in the analysis of face seals.

Stanghan-Batch (7) performed experiments in 1970 primarily to attempt to account for the way in which a face seal develops a fluid film between the two sealing surfaces. His experimental seal closely resembled that of commercial face seals. Employing a stainless steel stationary disc, the seal was artificially loaded with the aid of a pneumatic piston. Thermocouples were embedded 0.25 mm from the sealing surface to give some indication of the interface fluid temperature. Film pressure was determined by piezo-electric pressure transducers mounted immediately behind a thin diaphragm. A capacitance method using a carbon rotating face determined the film thickness.

Stanghan-Batch's results indicated that the hydrodynamic process is induced by surface waviness of one or more of the seal faces. Again, the twice shaft speed fluctuation of clearance and pressure was noticed, apparently due to the wavy surfaces.

In 1971, from a purely theoretical standpoint, Wilhelm (8) used an order of magnitude analysis to derive equations of motion from the Navier-Stokes equations for both laminar and turbulent flow in a radial face seal. For reasons of simplicity, the possibility of variable fluid properties and surface waviness was not considered. Greater emphasis was put on the study of leakage rate than any other seal parameter.

Wilhelm concluded that for laminar flow, inclusion of the centrifugal inertia term only is adequate for most sealing conditions.

He also concluded that the inertia term tends to increase leakage if pressure flow is outward and decrease leakage when pressure flow is inward.

Before Wilhelm, in 1964, Snapp (9) did an analytical study of fluid films between sealing surfaces of mechanical face seals for six radial profiles: parallel, converging, diverging, and three types of parabolic profiles. His studies developed equations to evaluate the effect of seal contour on pressure profile, total seal vertical load, film thickness, and leakage rate. Assumptions used in the investigation were (1) laminar flow prevailed, (2) the fluid is Newtonian and incompressible, (3) the pressure is constant across the film thickness, (4) velocity varies in both the radial and tangential directions, (5) constant fluid properties, and (6) there is no circumferential variation of pressure.

Snapp's results indicated that a departure from parallelism within the seal cavity has a significant effect on face seal performance parameters, particularly on the face loading, primarily due to differences in pressure profiles.

Late in 1974, Kiber (10) performed an experimental investigation involving a radial face seal. This study was rather unique in that all data were collected without disturbing the fluid film. Clearance was determined by two inductance type probes mounted behind an epoxied-in-place diaphragm, outlined in detail by Duncan (11). Capacitance pressure probes mounted similarly to the clearance probes were employed to measure interface pressure. Torque and vertical load were determined by strain gages mounted in an instrumented piece to

which the stationary seal face was attached. Leakage measurements were not obtained.

Due to the physical condition of the stationary seal face, Kiber's tests were limited to relatively large clearances. This apparently was partly the reason for poor frictional torque data as compared to predicted results. (It should be noted that predicted results referred to here are from the computer program to be presented in Chapter II.) Also, the sensitivity of the torque strain gages was insufficient to sense small frictional changes from the null position.

Studies showed that the clearance probes employed by Kiber are pressure-sensitive as well as temperature-sensitive. Thus, clearance readings were observed before pressure was applied to the system. Also, as stated earlier, since the clearances at which tests were conducted were large, any temperature effects on clearance readings were neglected.

The measurement of local interface pressures by the capacitance method produced numerous uncertainties and problems in obtaining reliable pressure data. Due to these difficulties, only one interfacial pressure probe was operational. Pressure readings from this probe agreed somewhat poorly with predicted results. Also, vertical load measurements were consistently lower than those predicted.

Kiber concluded that inconsistencies in computed and measured data were due to the experimental calibration constants. That is, the sensitivities of certain probes (particularly that of frictional torque and vertical load) were too small to record minute changes



from the zero condition. In addition, extensive temperature profile presentation was omitted from Kiber's report because of the above inconsistencies.

#### Statement of the Problem

With some refinements, the experimental portion of this thesis is basically a continuation of Kiber's work. Commercially available strain gage pressure probes were used instead of the capacitance type probes employed by Kiber. A machined-in-place diaphragm was employed in place of Kiber's epoxied stainless steel diaphragm. Also, a new compound was employed in the installation of the clearance probes which is substantially harder than the epoxy previously used. Leakage was monitored by a volumetric type measurement system, by which longer run times were permitted. The torque strain gages were recalibrated such that smaller frictional effects could be monitored. The vertical load signal amplifier gain has been increased, increasing load measuring sensitivity.

As mentioned earlier, Kiber compared his results to a computer program developed by this author which permitted the possibility of temperature dependent fluid properties. This program will be examined in detail in Chapter II.

## CHAPTER II

### THEORETICAL FACE SEAL ANALYSIS

#### General

Development of the equations of motion and an accompanying numerical analysis concerning fluid flow within the sealing cavity of a radial face seal will be presented in this chapter. Since flow involving two relatively rotating surfaces is the subject of analysis, a cylindrical coordinate system is employed. The coordinate system and flow variables are given in Figure 2.

#### Pertinent Assumptions

Similar to those of Snapp (9), the assumptions important to the analysis are:

1. Laminar flow prevails.
2. The liquid is Newtonian and incompressible.
3. The pressure is constant across the film thickness.
4. The fluid velocity varies in both the radial and tangential directions.
5. The fluid properties, density and viscosity, are functions of fluid temperature.
6. There is no pressure variation in the tangential direction.
7. Steady state, steady flow conditions prevail.

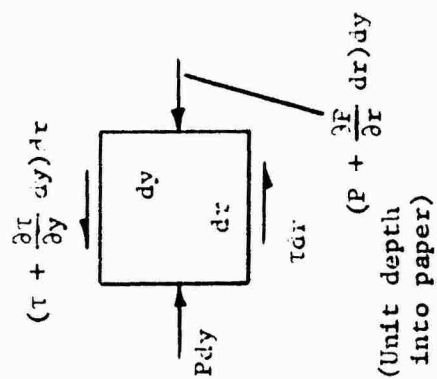
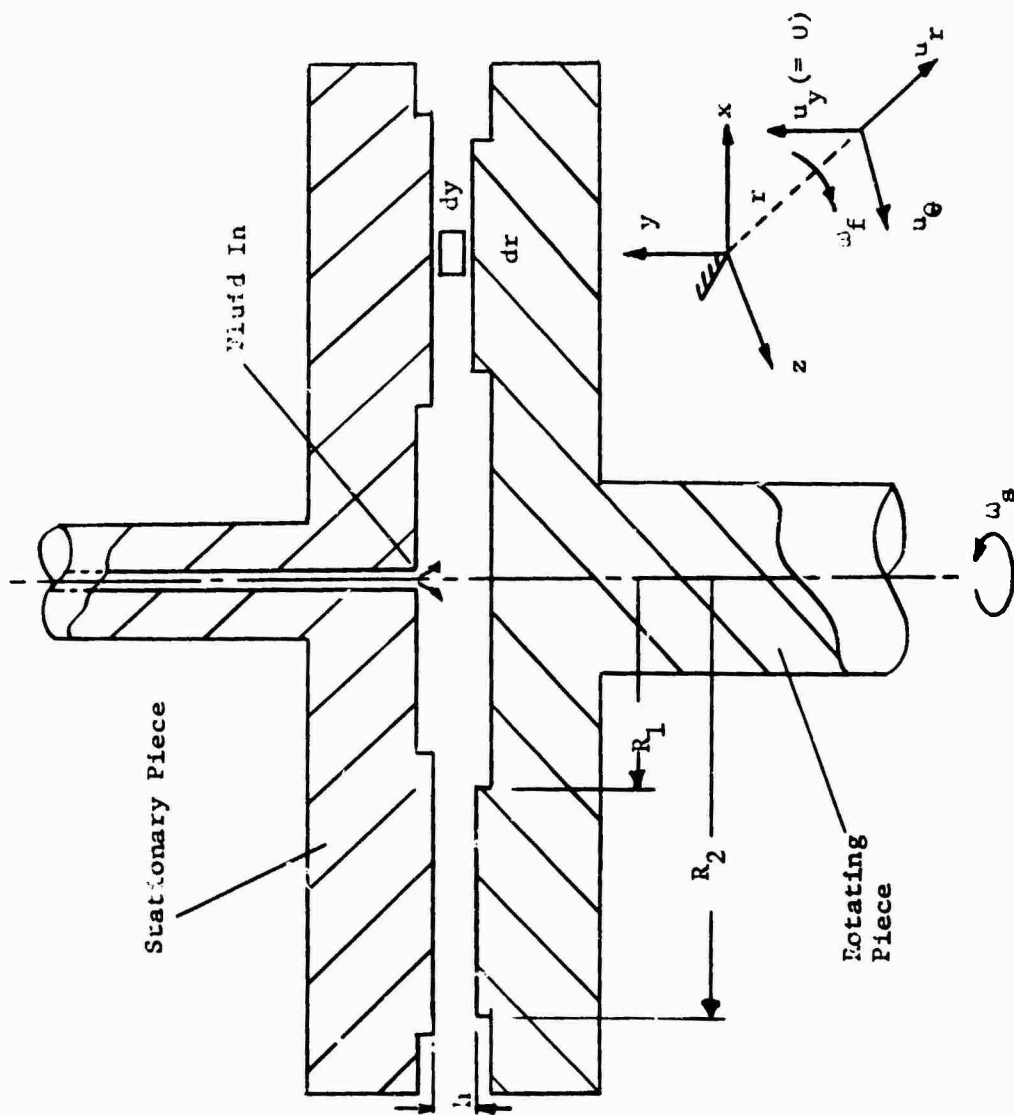


Figure 2. Flow Geometry with Infinitesimal Fluid Element.

8. Hydrodynamic entry length is assumed to be small in comparison with the total flow distance. This is a reasonable assumption for high Prandtl number fluids.

It should be noted that the possibilities of sealing surface waviness and surface roughness are not taken into account.

#### Development of Analytical Model

From the fluid element shown in Figure 2, by summing forces in the radial direction and considering parallel and smooth surfaces, the following relationship is obtained:

$$\frac{\partial P}{\partial r} - \frac{\partial \tau_r}{\partial y} - \rho r \omega_f^2 = 0. \quad (1)$$

Equation (1) was derived also by Sneek (20, 21) from an order of magnitude analysis. Further modification of Equation (1) is accomplished by fixing the radius  $r$  and working across the film thickness  $h$ . Substituting Newton's law of viscous fluids for laminar flow,

$$\tau_r = \mu \frac{\partial u_r}{\partial y},$$

Equation (1) now becomes

$$\frac{\partial P}{\partial r} - \mu \frac{\partial^2 u_r}{\partial y^2} - \rho r \omega_f^2 = 0. \quad (2)$$

Since the pressure is assumed to vary in the  $r$ -direction only, and for a given radius  $r$ ,  $u_r = u_r(y)$  only, Equation (2) becomes

$$\frac{\partial P}{\partial r} - \mu \frac{d^2 u_r}{dy^2} - \rho r \omega_f^2 = 0. \quad (3)$$

Consider now the assumed velocity profile in the tangential direction, shown in Figure 3.

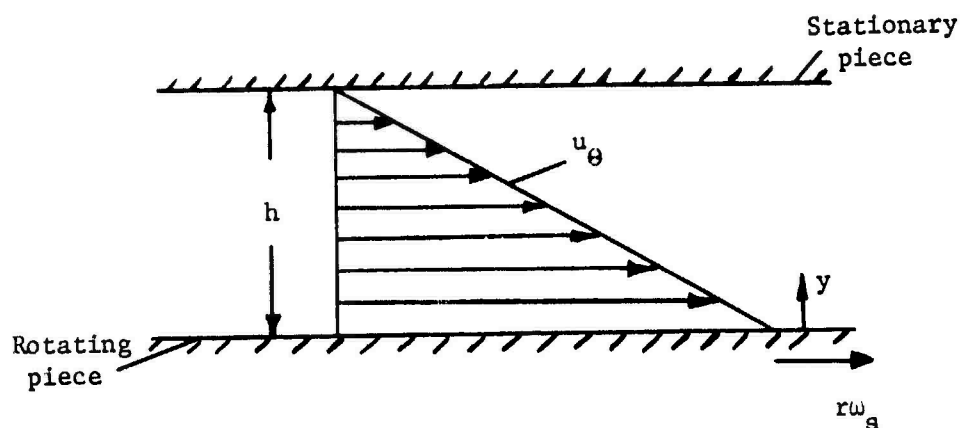


Figure 3. Tangential Direction Velocity Profile.

To satisfy the no-slip conditions at the upper and lower seal surfaces, it is seen that

$$\omega_f = \left(\frac{y}{h}\right)\omega_s. \quad (4)$$

Substituting the above into Equation (3) and integrating twice, it is seen that

$$u_r = \frac{1}{2\mu} \left[ \frac{dP}{dr} \right]_r y^2 - \frac{\rho r \omega_s^2}{12\mu h^2} y^4 + C_1 y + C_2. \quad (5)$$

Again from the no-slip condition at the upper and lower seal surfaces,  $C_1$  and  $C_2$  can easily be determined, yielding

$$u_r = \frac{1}{2\mu} \left[ \frac{dP}{dr} \right]_r (y^2 - hy) - \frac{\rho r \omega_s^2}{12\mu h^2} (y^4 - h^3 y). \quad (6)$$

The volumetric flow rate (at any radius  $r$ ) can now be determined from

$$Q = 2\pi r \int_0^h u_r dy. \quad (7)$$

Substituting and integrating,

$$Q = \frac{\pi r h^3}{6\mu} \left[ \frac{3\rho r \omega_s^2}{10} - \left( \frac{dP}{dr} \right)_r \right] \quad (8)$$

or

$$\left[ \frac{dP}{dr} \right]_r = \frac{3\rho r \omega_s^2}{10} - \frac{6\mu Q}{\pi r h^3} \quad (9)$$

By combining the mass conservation principle for steady flow and Equation (9), it is seen that

$$\int_{r=R_1}^{r=R_2} dp = \frac{3}{10} \omega_s^2 \int_{r=R_1}^{r=R_2} \rho r dr - \frac{6\mu}{\pi h^3} \int_{r=R_1}^{r=R_2} \frac{\mu}{\rho} \frac{dr}{r} \quad (10)$$

From the standpoint of variable properties, integration of Equation (10) would require that density and viscosity be known as a function of radius  $r$ . Most analytical solutions previously offered have made the assumption of constant properties and integrated across the total seal radius. For large clearances and supply pressures, the constant property assumption is normally adequate. However, at clearances which a face seal normally operates, the friction shear stress on the fluid is considerable and would impart a significant energy input to the fluid causing a notable temperature change.

Consider now integration of Equation (10). Over a very small increment of radius  $\Delta r$ , the fluid properties would remain essentially constant. Thus,

$$\int_{r=r}^{r=r+\Delta r} dp = \frac{3}{10} \omega_s^2 \rho \int_{r=r}^{r=r+\Delta r} r dr - \frac{6\mu}{\pi h^3} \int_{r=r}^{r=r+\Delta r} \frac{dr}{r}$$

or

$$P_{r+\Delta r} - P_r = \frac{3}{20} \omega_s^2 \rho (\Delta r^2 + 2r\Delta r) - \frac{6\mu}{\pi h^3} \ln \left( 1 + \frac{\Delta r}{r} \right) \quad (11)$$

Having determined  $dp/dr$  (evaluated at any radius  $r$ ), the volumetric flow rate can be found from Equation (8).

For the determination of seal moment and the accompanying temperature rise, Newton's fluid shear equation is again employed to yield

$$dM = \frac{2\pi\omega}{h} s \mu r^3 dr. \quad (12)$$

Integrating similarly to Equation (10) and multiplying by  $\omega_s$  gives the friction energy as

$$E_f = \frac{\pi\mu\omega^2}{2h} s [4r^3\Delta r + 6r^2\Delta r^2 + 4r\Delta r^3 + \Delta r^4]. \quad (13)$$

In addition, the change in flow energy (flow work) due to the change in pressure must be accounted for by

$$E_p = Q\Delta P \quad (14)$$

where  $\Delta P$  is given by Equation (11).

Assuming that all the input energy is absorbed by the fluid (i.e., no heat is convected to the seal), the temperature rise is predicted by the energy equation as

$$T_{r+\Delta r} - T_r = \frac{E_f + E_p}{mC_p}. \quad (15)$$

Having determined this temperature difference, the fluid properties at  $r = r + \Delta r$  can readily be evaluated, assuming that the "initial conditions" at  $r = r$  are known.

From the continuity equation

$$\dot{m} = \rho_r Q_r = \rho_{r+\Delta r} Q_{r+\Delta r} = \text{constant}, \quad (16)$$

it is noted that a change in fluid density would necessarily dictate that the volumetric flow rate also change to satisfy Equation (16).

Thus, with each evaluation of conditions at  $r = r + \Delta r$ , a new value of volumetric flow rate must be determined to compensate for the aforementioned density change and flow area change.

### Calculation Technique

A FORTRAN IV computer program has been developed to evaluate temperature, pressure, vertical load, and torque as a function of radial distance from the seal centerline. Initially, a mass flow rate is determined under the assumption of constant properties for a first approximation. Employing an assumed incremental value of  $\Delta r$ , pressure, volumetric flow rate, torque, temperature, density, viscosity, and mass flow rate are found at  $r_2 = r + \Delta r$ . If the mass flow has changed significantly, the process is repeated with a smaller  $\Delta r$  until less than one percent change is noticed.

When the outside seal radius is reached, the pressure is checked against the zero exit pressure criteria. If the pressure is significantly different from zero, a new trial mass flow rate is calculated in proportion to the error in the pressure difference. Employing this new mass flow rate, the entire process is repeated until the exit pressure is sufficiently close to zero (within plus or minus one percent). A flow chart describing the calculation technique is shown in Figure 4 (a more detailed discussion of the program is given later in this chapter).

### Mathematical Modeling of Temperature Dependent Fluid Properties

To apply the above model to a physical fluid, the fluid's properties needed to be determined as a function of temperature.



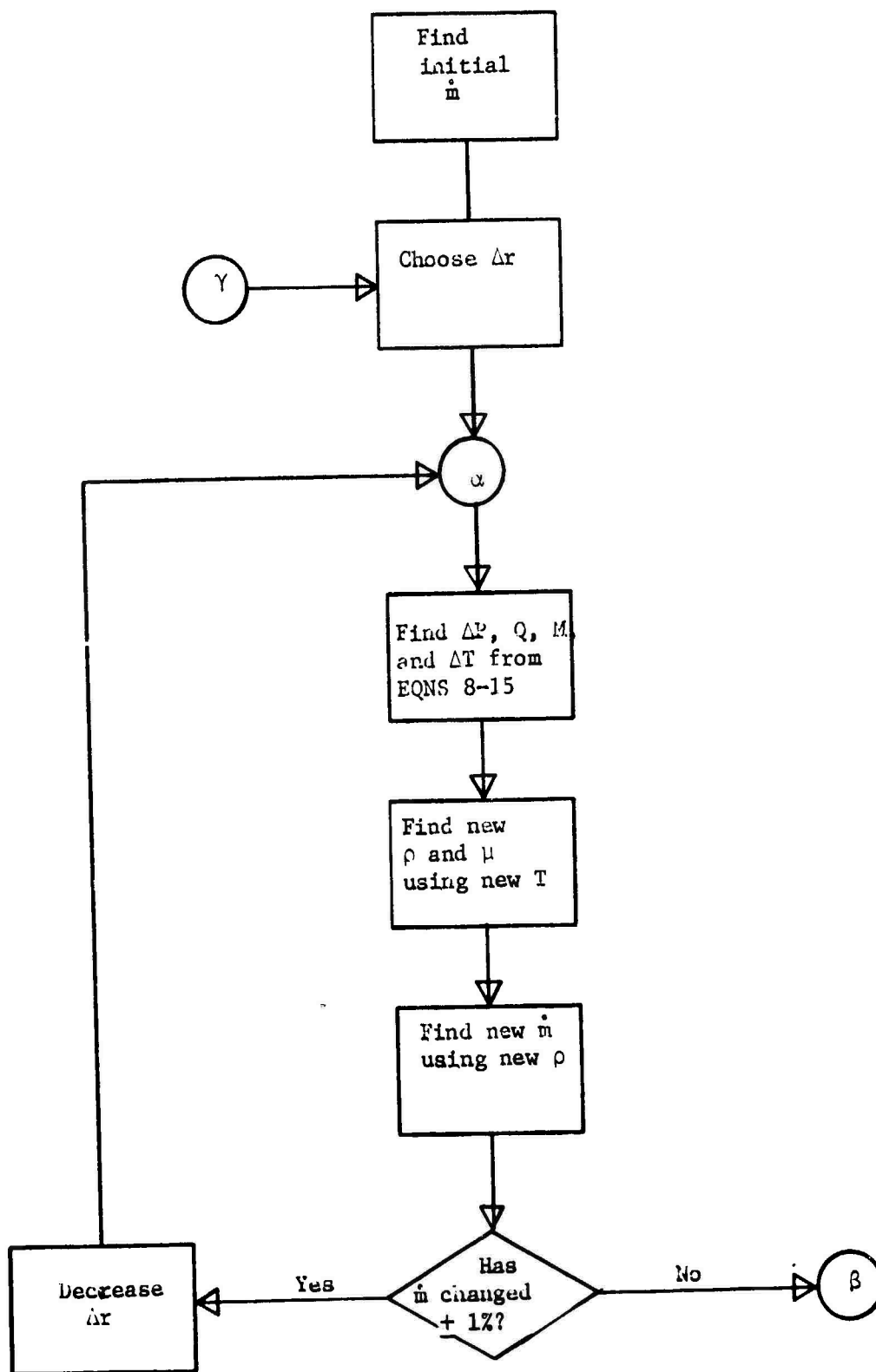


Figure 4. Computer Program Flow Chart.

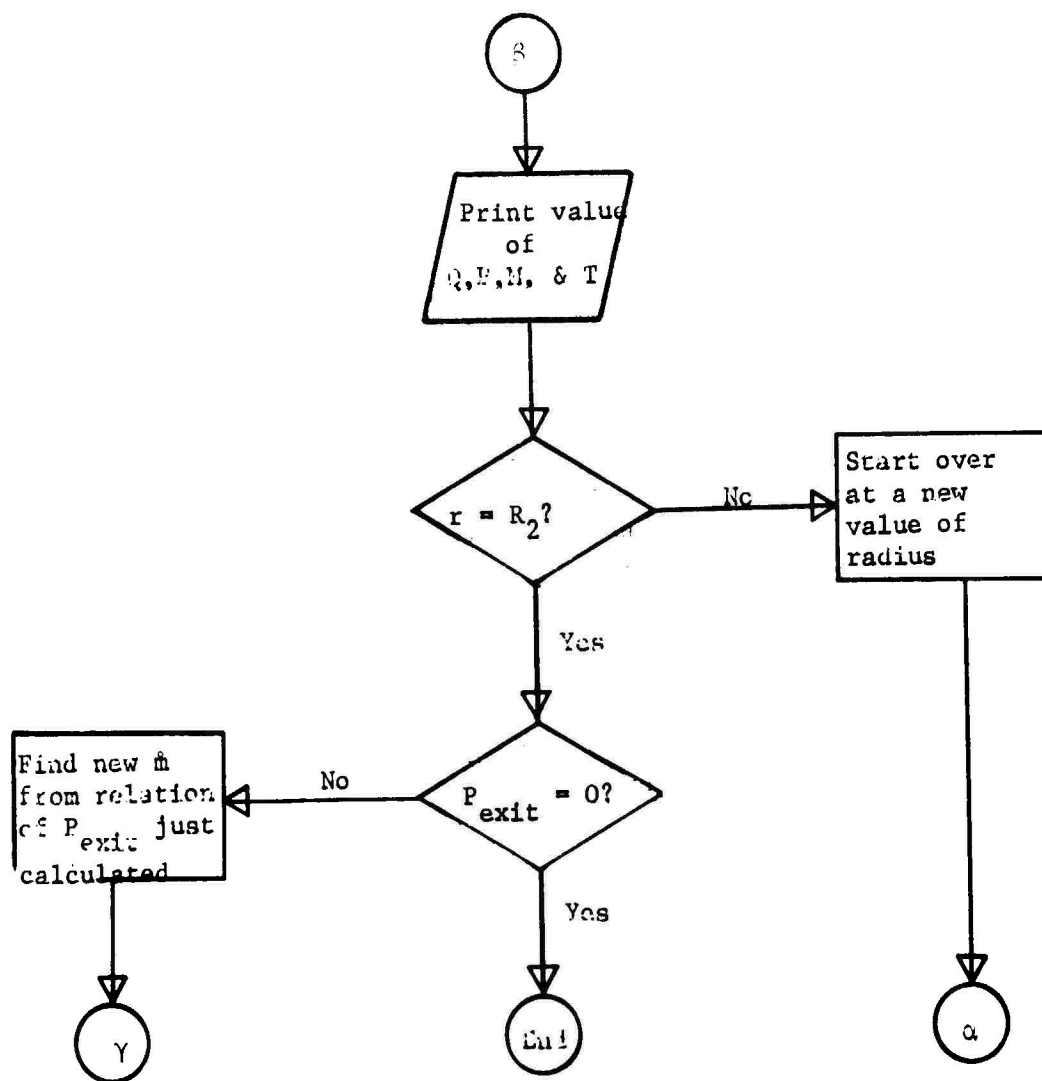


Figure 4 (Continued).

Gulfspin 38 oil was chosen as the working medium for the associated experimental investigation.

In determining oil density as a function of temperature, specific gravity was measured (using a Westphal Balance) at varying temperatures yielding a linear relationship, shown in Figure 5. For a mathematical relationship, a least squares polynomial curve fit gave the following:

$$\rho_{oil} = \rho_{H_2O} \underset{STP}{[SG]_{oil}} = \rho_{H_2O} \underset{STP}{[-(4.057 \times 10^{-4})(T) + 0.9031]} \quad (17)$$

where the oil temperature  $T$  is measured in degrees Rankine.

Viscosity on the other hand was determined as a function of temperature via a Saybolt Viscometer. From Fuller (12), the form of the equation of viscosity was suggested as:

$$\nu = \text{antilog}_{10} \text{ antilog}_{10}[n \log_{10}(T) + C] - 0.8 \quad (18)$$

where  $T$  is again measured in degrees Rankine. From plotting Saybolt Universal Seconds (SUS) versus oil temperature, the constants in Equation (18) were found to be

$$n = -3.80466$$

and

$$C = 10.53812.$$

Having determined Equations (17) and (18), computing numerical values of the oil properties at each incremental radius became a simple matter.

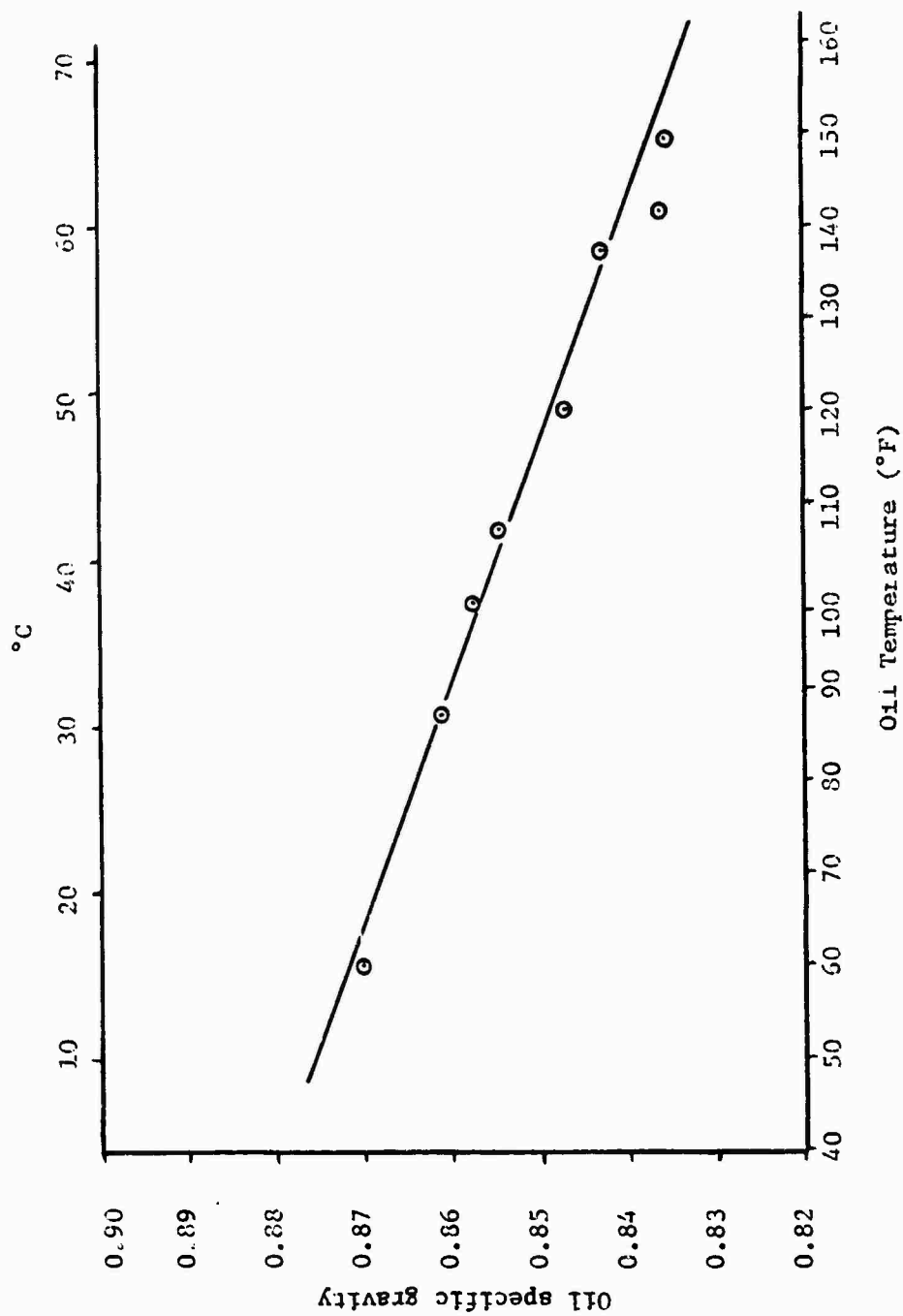


Figure 5. Plot of Specific Gravity vs Temperature (Gulfspine 38 Oil).

## Detailed Discussion of Computer Program

### General

The program used in this study is found in Appendix A. It was run on the IBM 360/65 digital computer at the University of Tennessee. In addition to the basic program, a CALCOMP plotting routine is also included. It was used by the author to gain knowledge of trends concerning the numerical results without actually examining the many numbers which were generated.

It was necessary to run the program in double precision to obtain the greatest possible accuracy in determining the mass flow rates and pressures which were the instrumental variables in making the program operational.

### Boundary Conditions

As mentioned earlier in this chapter, there were primarily two important boundary conditions to be met before any solution satisfied the physical flow criteria: (1) the pressure profile had to be such that the exit pressure corresponded to that physically present -- atmospheric in this case, and (2) the continuity relationship was satisfied throughout the total flow area of the seal.

This type of relationship necessitated that "one must know the solution before one can find the solution." That is, the correct mass flow rate had to be known at the beginning of the calculation process such that the zero exit pressure criteria was met. This was accomplished basically by a trial and error method to be discussed below.

After inputting sealing conditions for a particular run which are supply pressure ( $P_{\text{OLD}}$ ), film thickness ( $H$ ), seal rotational speed

(RPM), and inlet oil temperature (TFIRST), an initial mass flow rate assuming non-temperature-dependent fluid properties is calculated in SUBROUTINE MASS1 as a first approximation (the flow chart previously mentioned will be extremely helpful to the reader in following the program logic). After an initial  $\Delta r$  of 0.005 inch is assumed, density and viscosity ( $RH\phi$  and  $NU$ , respectively), pressure ( $PNEW$ ), volumetric flow rate ( $Q$ ), torque ( $M\phi$ MENT), friction energy plus flow work ( $EF$ ), and temperature rise ( $T$ ) is calculated employing Equations (11) through (16) at the new incremental radius. New oil properties, thus a new mass flow rate at this radius is calculated by SUBROUTINE CHECK1. The newly calculated mass flow rate is then checked against the old mass flow and if more than one percent change is noted, the process is repeated with a smaller value of  $\Delta r$  ( $DELTA R$ ) calculated in SUBROUTINE FIND. If less than one percent change is found, the calculated values of the above variables are printed by SUBROUTINE FOUND (the program is designed to print out data every 0.01 inch of radius), provided that the zero exit pressure stipulation is met. In other words, no calculated data are printed out until the correct mass flow rate has been determined.

The above process is repeated until the outside seal radius ( $R2$ ) is reached. The pressure at  $R2$  is checked to within plus or minus one percent of zero (atmospheric) pressure. If the exit pressure differs significantly from zero, a new trial value of mass flow rate is determined by SUBROUTINE MASS2 in proportion to the error in calculated exit pressure. This step was found to provide a radical improvement on convergence to the correct value of mass flow.

Finally, for comparison purposes, SUBROUTINE CONPRP calculates seal parameters assuming non-temperature-dependent fluid properties across the total seal flow area.

As a final note, it should be pointed out that the temperature-dependent fluid property portion of the program calculates vertical load in a different manner than the non-temperature-dependent fluid property subroutine. If non-temperature-dependent fluid properties are assumed, Equation (10) can readily be integrated to yield pressure as a function of radius  $r$ . Thus, total vertical load can be determined from the relationship

$$L = 2\pi \int_{r=R_1}^{r=R_2} rP(r)dr. \quad (19)$$

Figure 6 shows an exaggerated view of the upper (or lower) sealing surfaces. Having calculated the pressure at the outer incremental radius, the inner and outer pressures are averaged and multiplied by the incremental area, thus yielding an incremental value of vertical load. As the results will show, when temperature rise is insignificant, the two methods of vertical load calculation have excellent agreement.

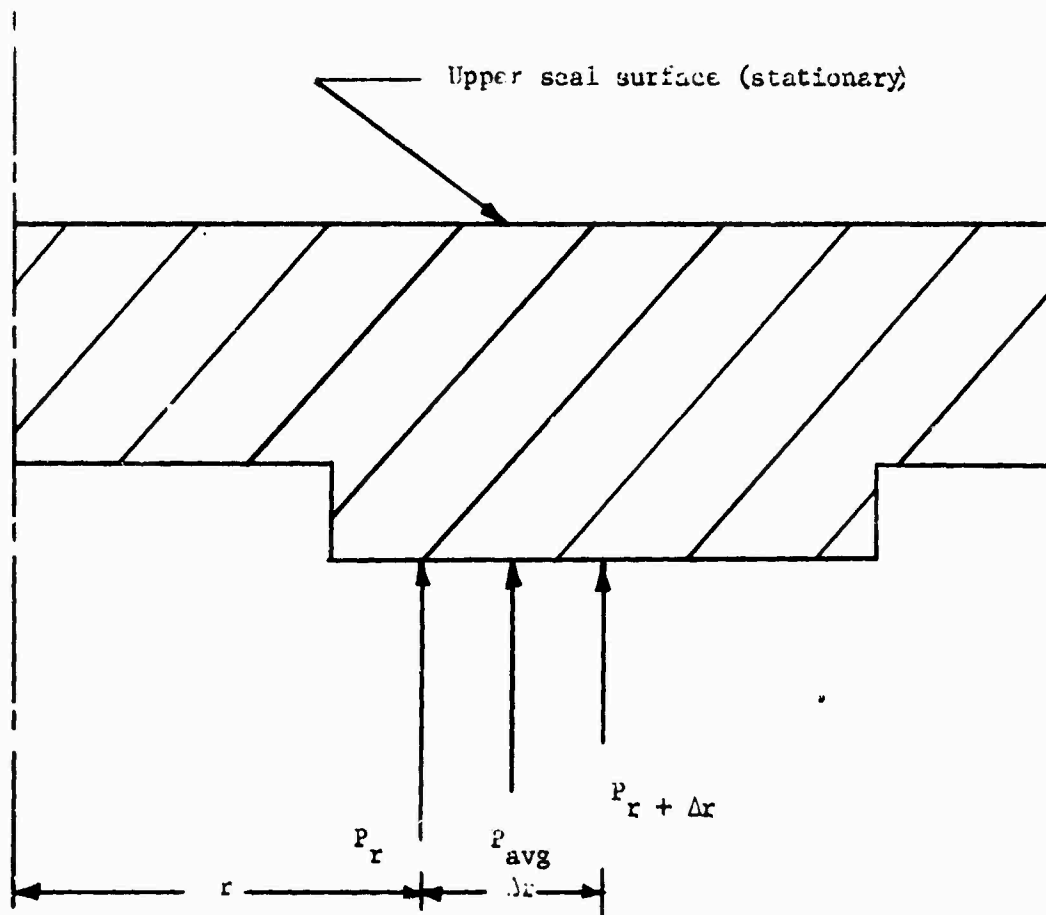


Figure 6. Pressure Acting on Upper Seal Face.



## CHAPTER III

### EXPERIMENTAL FACE SEAL TEST RIG AND INSTRUMENTATION

#### General

The experimental test rig along with all associated instrumentation is located in the dynamic sealing laboratory of the Mechanical and Aerospace Engineering Department of the University of Tennessee. The test rig and instrumentation will be described in this chapter with some detail; however, for a more detailed description of the associated experimental apparatus, particularly that concerning the instrumentation, the reader is referred to Kiber (10).

#### Test Apparatus

Figure 7 shows the basic experimental test rig. It has been designed such that a considerable wide range of sealing conditions can be simulated [see references (13) and (14) for the basic design].

The actual test seal, described in the next section, is mounted to an instrumented piece, Figure 3, which in turn is secured to a vertical support column. The support column is attached to a horizontal plate whose movement is controlled by three vertical adjustment columns. These three adjustment columns dictate the amount of tilt and clearance within the actual seal cavity. Between the vertical support column and horizontal plate is a set of adjustment screws by which the support column can be corrected for any

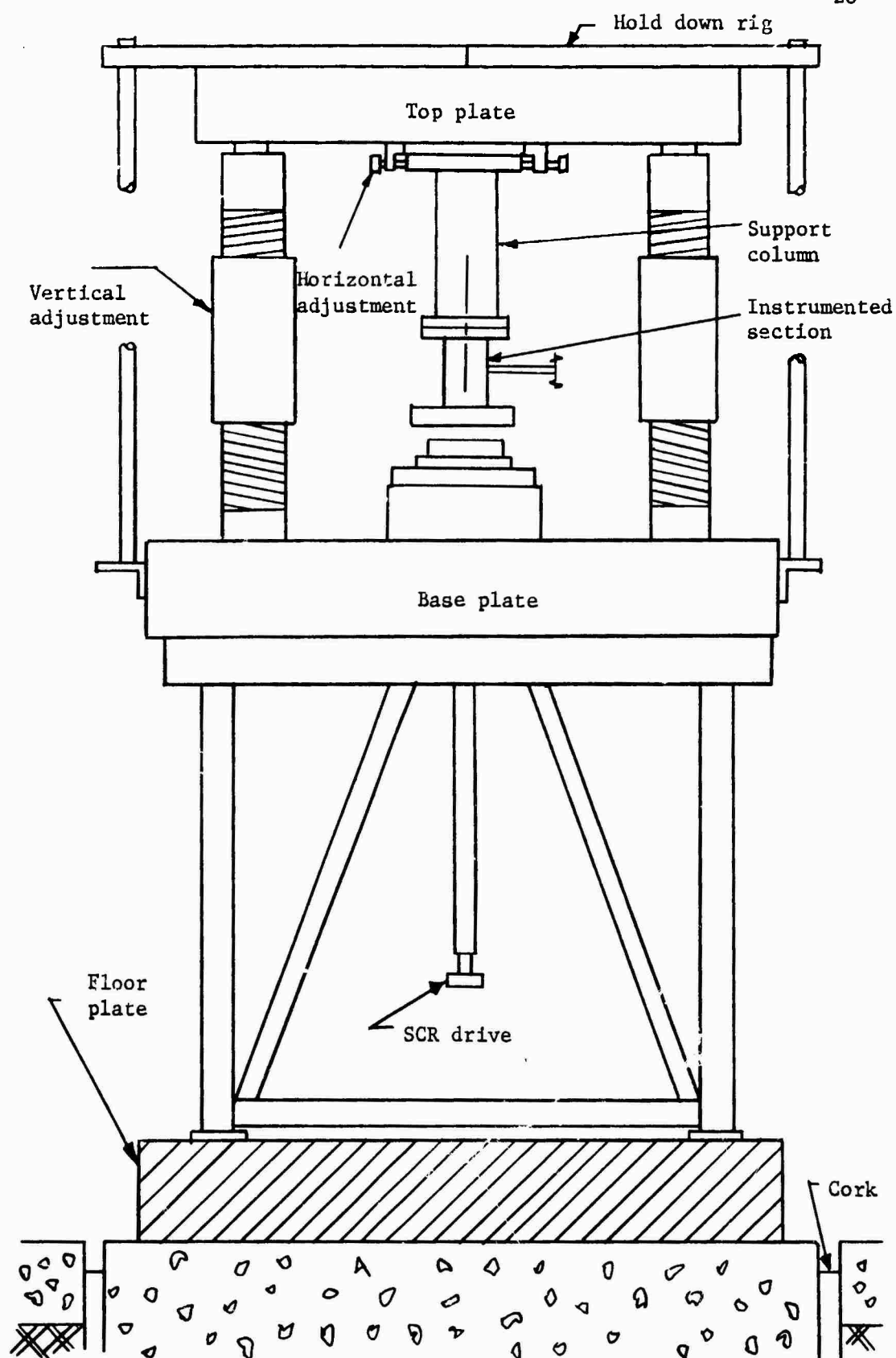


Figure 7. Test Apparatus.

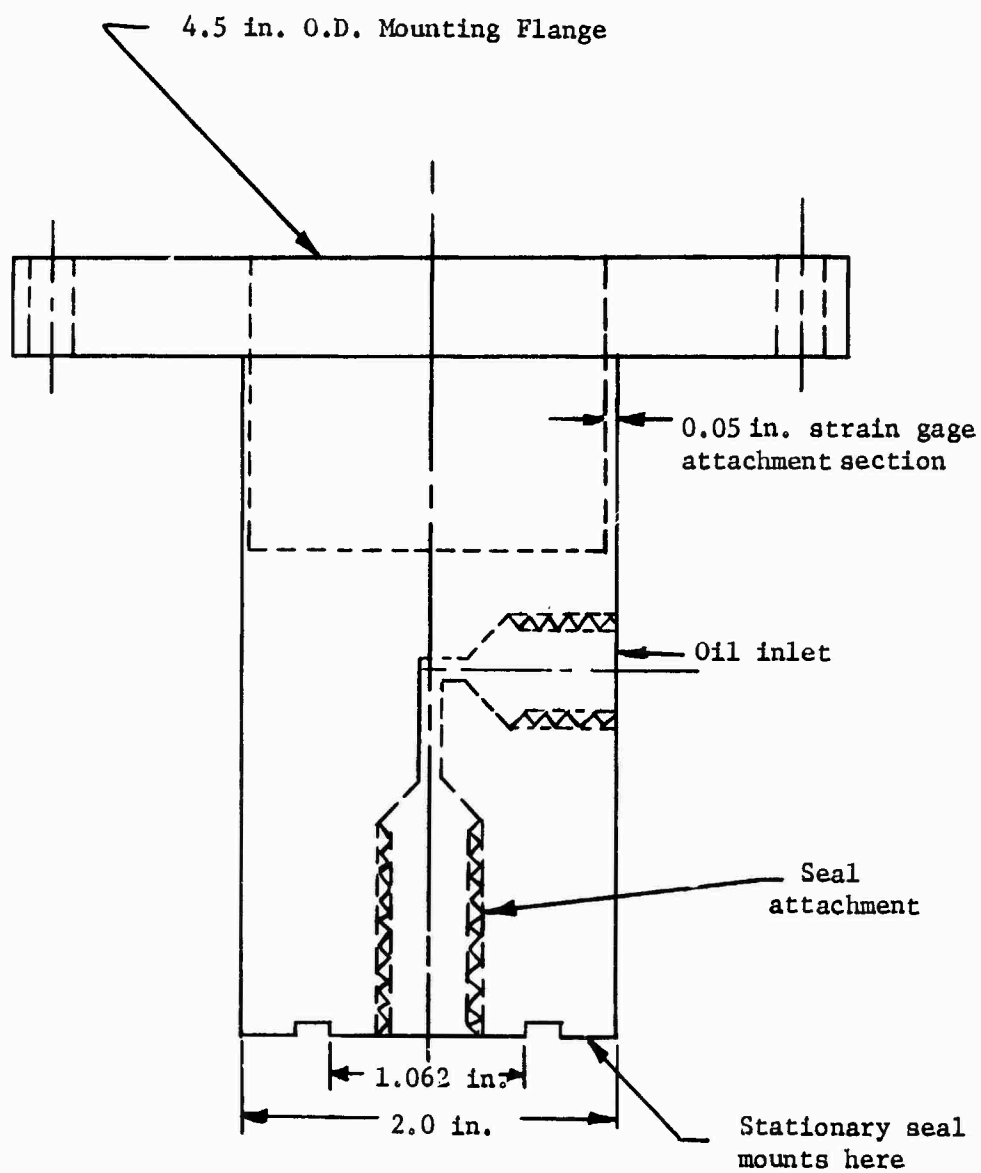


Figure 8. Instrumented Section.

misalignment between the stationary and rotating seal surfaces.

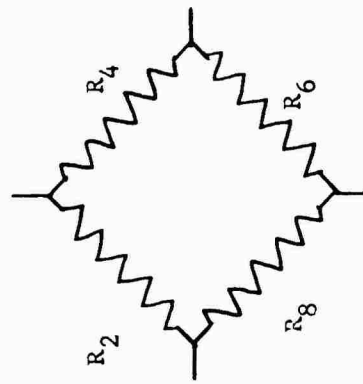
The instrumented section previously mentioned is fitted with two complete sets of strain gage bridge resistance circuits. One of these circuits, which consists of foil type gages, is for vertical load measurements while the other circuit, consisting of piezo-electric type gages, is for the determination of frictional torque. Figure 9 shows the manner by which these gages are physically located on the instrumented section.

An air spindle is the means by which the rotating seal surface remains in a flat horizontal plane. A variable speed SCR drive system provides the necessary range of rotational speeds needed for a complete simulation of face seal operation.

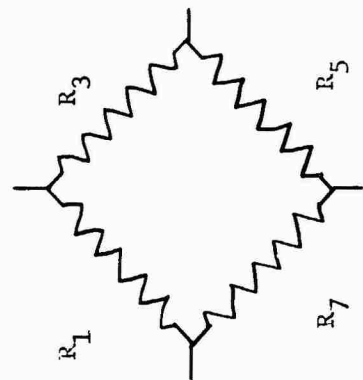
A newly installed pressurization and leakage rate measurement system, shown in Figure 10, is the means by which lubricant is supplied to the sealing apparatus. Two calibrated gage glasses are employed to determine leakage rates by volumetric analysis.

A Precision Measurement Company strain gage pressure transducer monitors the oil supply pressure prior to entering the instrumented section. Also, an oil filter located just upstream of the supply pressure transducer provides a means of final filtration before the oil actually flows through the seal.

To prevent any vertical movement of the horizontal plate, a hold-down rig was installed. This was necessary due to the "play" which was found to be in the joints of the vertical adjustment columns and the horizontal plate.



Vertical:  
 $R = 190\Omega$   
 $G.F. = 3.17$



Torque:  
 $R = 368.7\Omega$   
 $G.F. = 105.2$

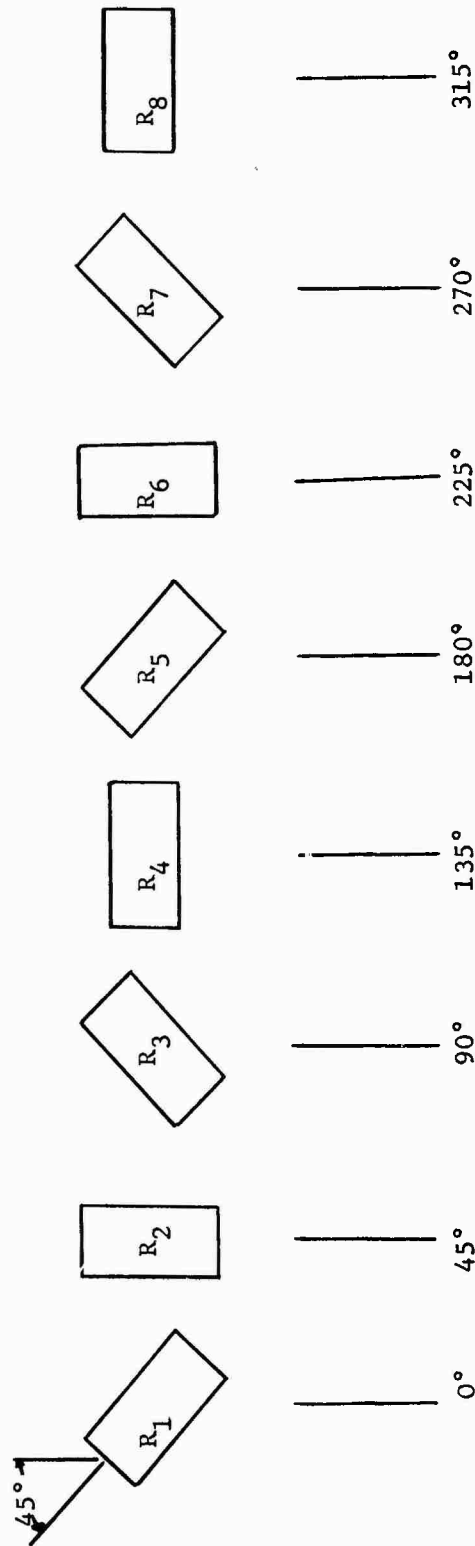


Figure 9. Strain Gage Placement on Instrumented Section.

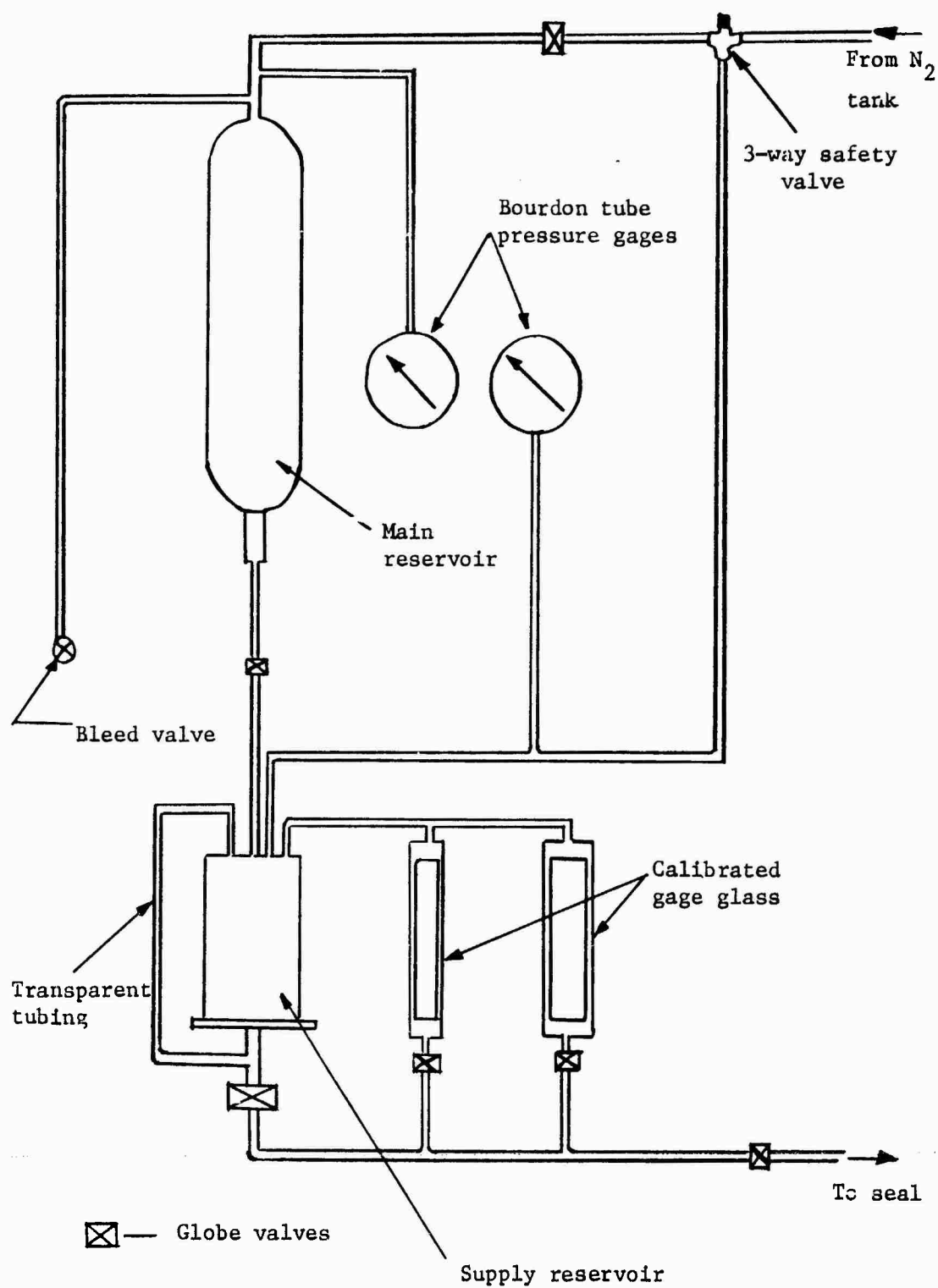


Figure 10. Pressurization and Leakage Measurement System.

As stated earlier, Gulfspin 38 oil was chosen as the working medium for the experimental investigation. Viscosity of this oil is approximately  $0.3294 \times 10^{-5}$  reyn at 25 degrees Celsius.

#### Test (Stationary) Seal

The stationary test seal used in this investigation is the end result of numerous seal fabrications. Shown in Figure 11, the test seal was machined from 316 stainless steel. With the seal in unfinished condition, the clearance probes were installed employing Devcon Aluminum Putty as the adhesive base. After clearance probe installation was accomplished, the sealing surface was slightly lapped. The step-by-step clearance probe installation procedure is given in Appendix B. A1, B2, C3, E4, and F5 refer to clearance probes in Figure 11. Clearance probe E4 was found to be inoperative after installation. This was probably due to the probe being shorted to the test seal itself.

After the initial lapping, five holes 0.150 inch in diameter were drilled from the sealing face side to accommodate installation of the pressure probes referred to by SP1, SP2, SP3, SP4, and SP5. The pressure probes, shown in Figure 12, were commercially available Precision Measurement Company Model 150 strain gage pressure transducers, consisting of a strain gage epoxied to a thin diaphragm. The pressure probes were installed such that approximately 0.002 inch protruded past the sealing surface. Again, Devcon Aluminum Putty was utilized as the adhesive base. After this assembly had thoroughly hardened, the sealing surface was lapped flat, thus removing the above protrusion. Unfortunately, one of the pressure probes (SP4) was

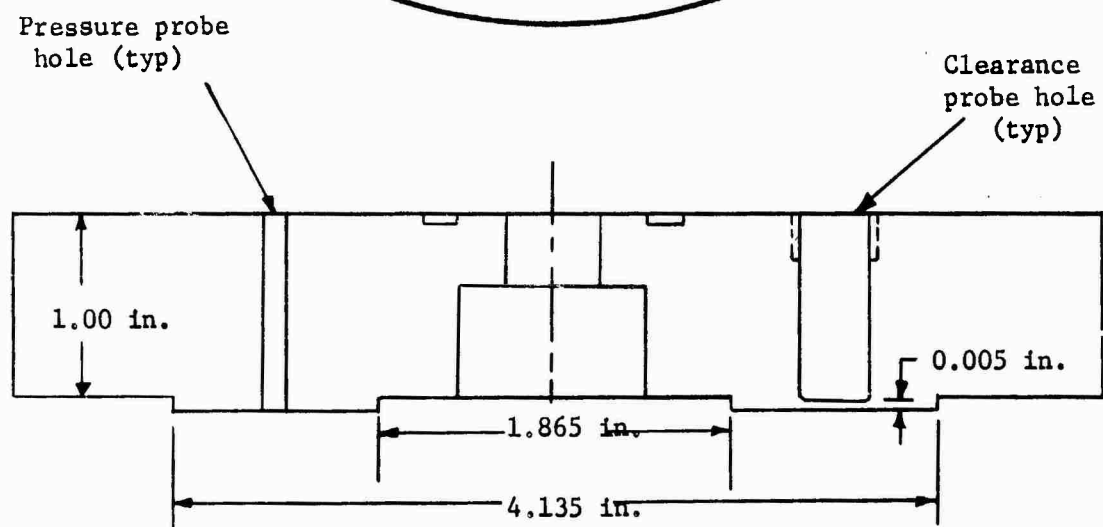
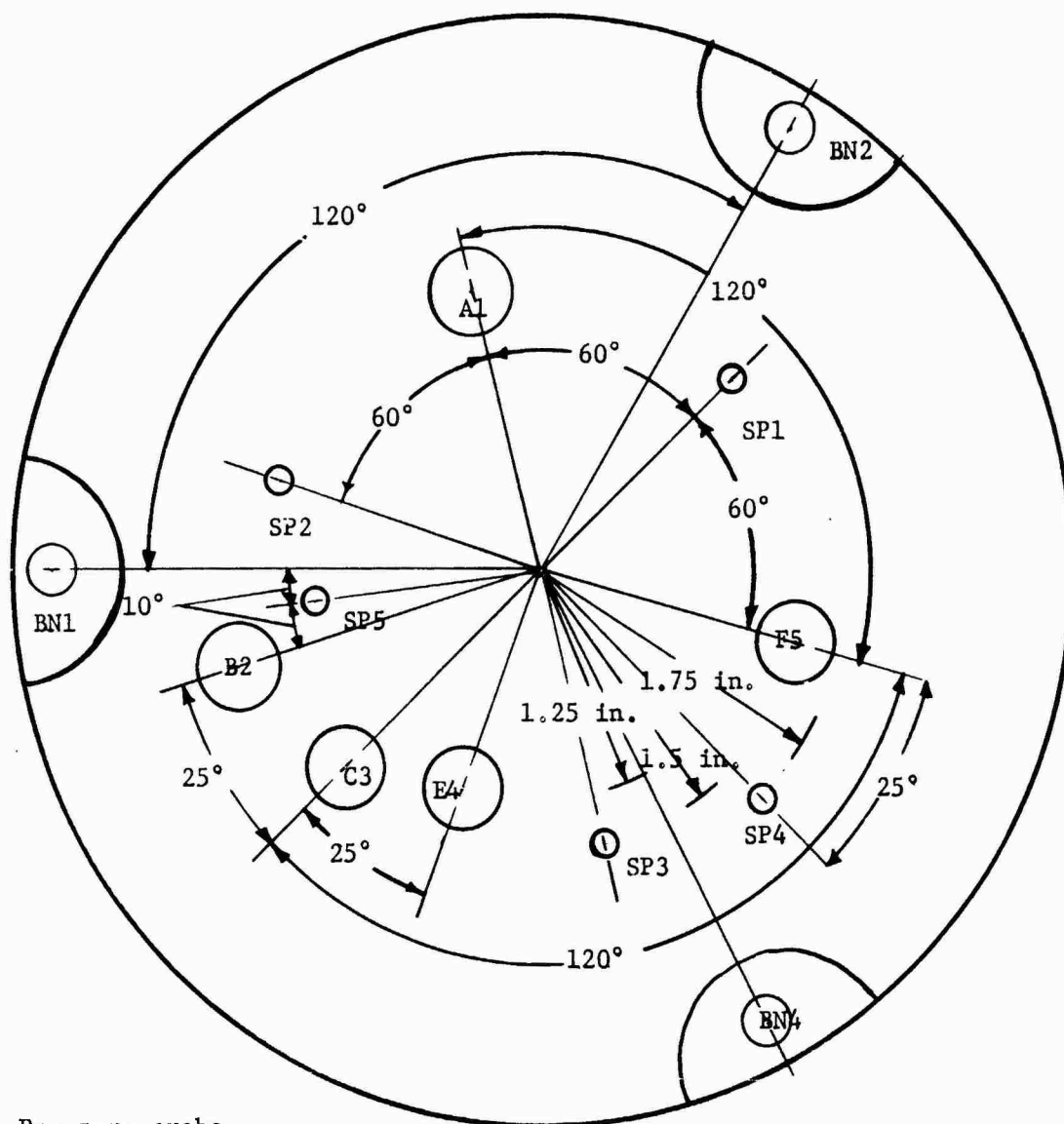


Figure 11. Test (Stationary) Seal.



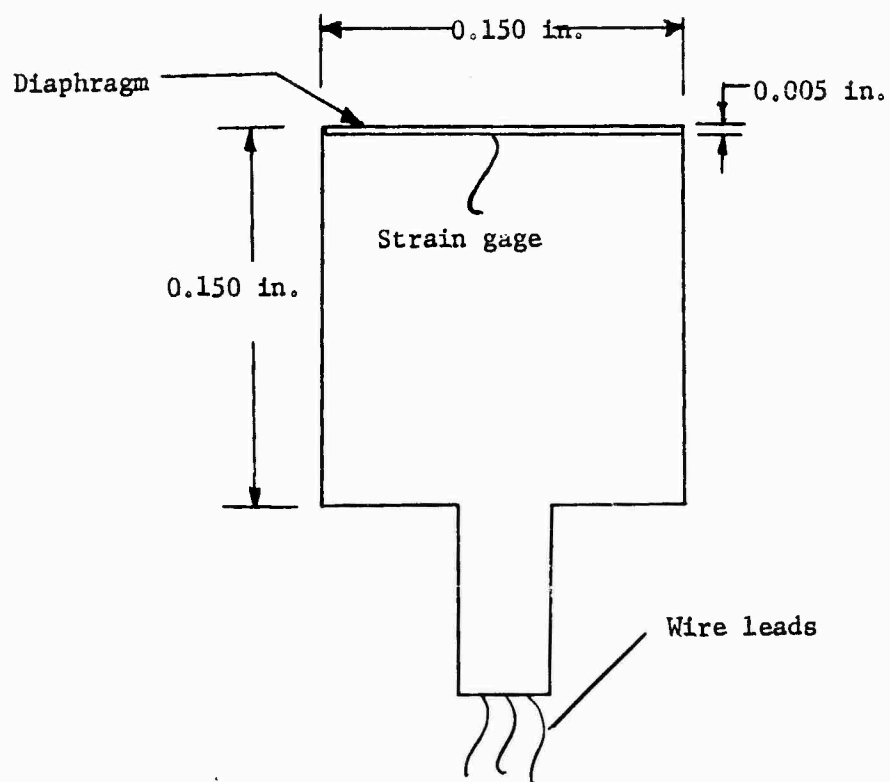


Figure 12. Precision Measurement Company Model 150 Strain Gage Pressure Probe.

destroyed during this process, and was probably caused by an excess amount of the probe protruding from the sealing surface. After this final lapping, the seal face was checked with an optical flat and was found to be approximately eight sodium lightbands (350 micro-inches) out-of-flat. The surface roughness was also checked and was found to have a CLA roughness of approximately 2.5 micro-inches.

#### Rotating Seal

Figure 13 shows the dimensions of the rotating piece used in this investigation which defines the sealing geometry. This piece was constructed similarly to the stationary piece in that it was machined from 316 stainless steel. After machining, the seal face was lapped and tested with an optical flat for degree of flatness. The optical flat revealed that this piece was approximately two sodium lightbands (90 micro-inches) out-of-flat. Similarly to the stationary seal, the CLA roughness was determined to be approximately 2.5 micro-inches.

#### Instrumentation

As described by Kiber (10), the instrumentation concerning this investigation consists of signal conditioning units, amplifiers, and recording devices. Since signals concerning the clearance probes were externally conditioned, no signal conditioning was required for measurement of film thickness. However, torque, vertical load, temperature, and pressure output was too small to be sensed directly; hence, signal conditioning had to be utilized in order to obtain a usable data acquisition system.

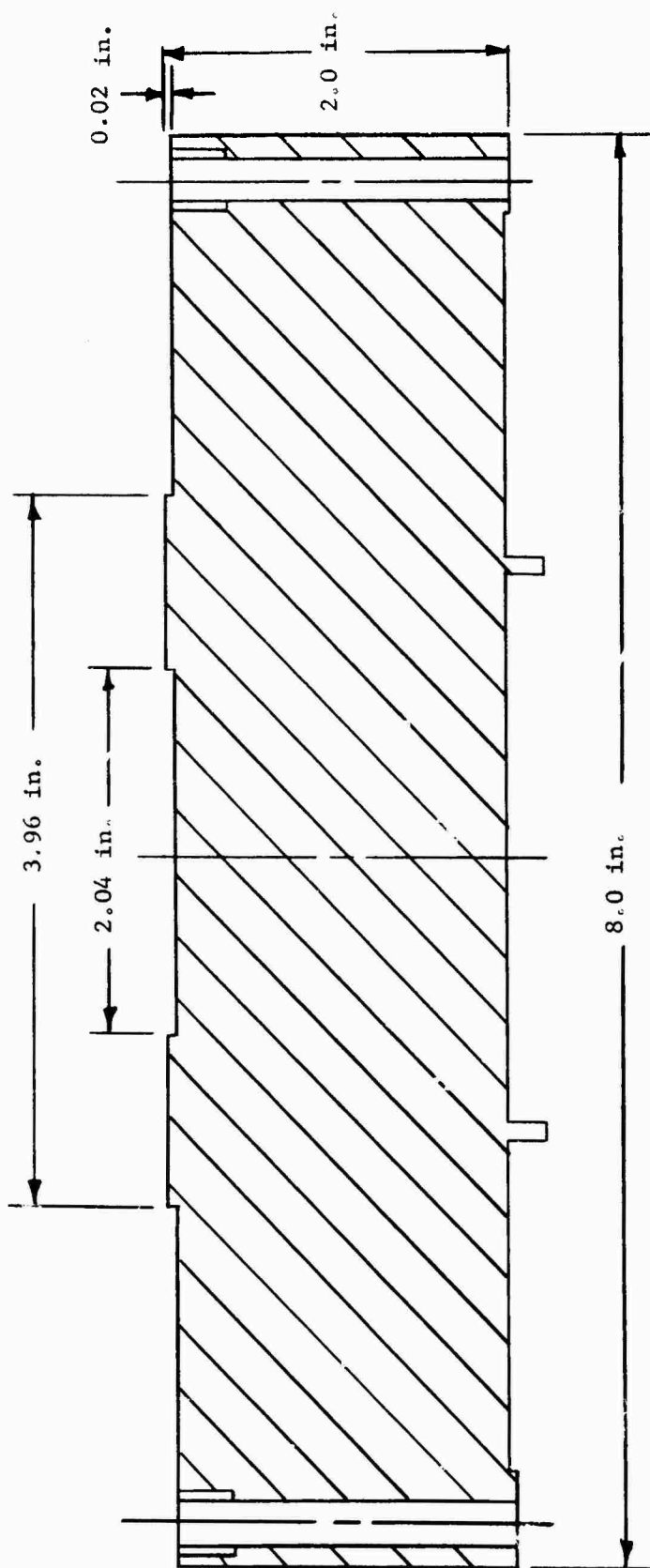


Figure 13. Rotating Seal.

The main instrumentation console, shown in Figure 14, is a Honeywell 24-channel oscillograph recorder. It contains strain gage signal conditioning units, low and high gain amplifiers, millivolt or thermocouple input signal conditioning units, and an oscillograph recorder. Also, due to an insufficient number of high gain amplifiers in the main console, two additional units containing thermocouple signal conditioning devices and high gain amplifiers were needed to complete the data acquisition system. These two additional units are not shown in Figure 14. An external signal can reach the galvanometer by one of two routes, both of which are shown in Figure 15 (only two signals were routed through the Reproduce BNC Jack in this investigation). Table I shows a summary of signal conditioning device name, abbreviation, and purpose.

#### External Transducers

##### Interface and Supply Pressure

As previously mentioned, the interface and supply pressure transducers consisted of Precision Measurement Company Model 150 strain gage pressure transducers with a 120 $\Omega$  strain gage epoxied to a 0.150-inch-diameter diaphragm. The transducer to monitor supply pressure was secured in a stainless steel pipe plug (again with Devcon Aluminum Putty) with approximately 0.002 inch of the transducer protruding from the plug. The transducer diaphragm was then lapped flush with the plug to provide a smooth, even surface.

Interface pressure was measured similarly to the supply pressure in that the transducers and the installation procedures were identical.

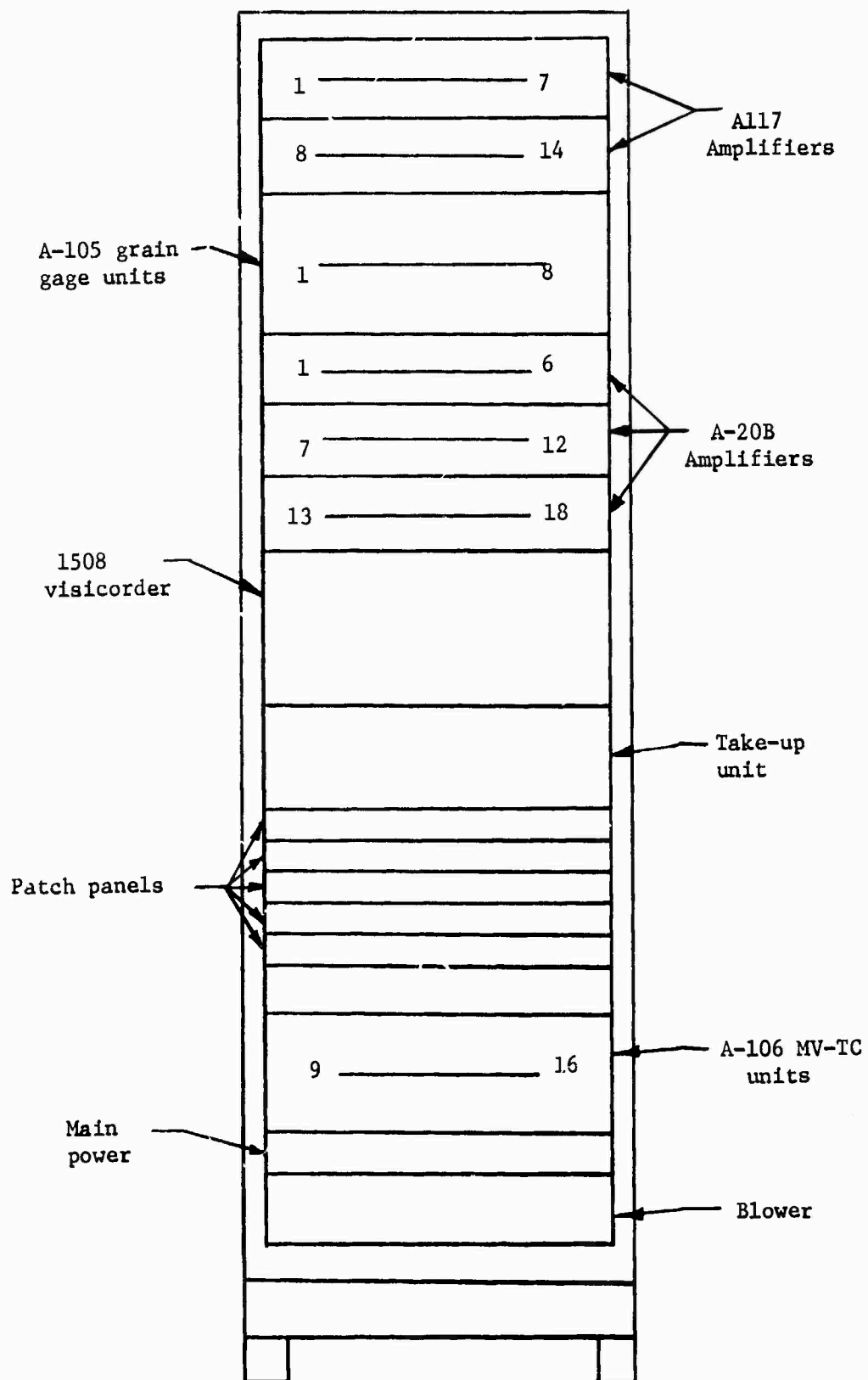


Figure 14. Honeywell 24-Channel Oscillograph Recorder Console.

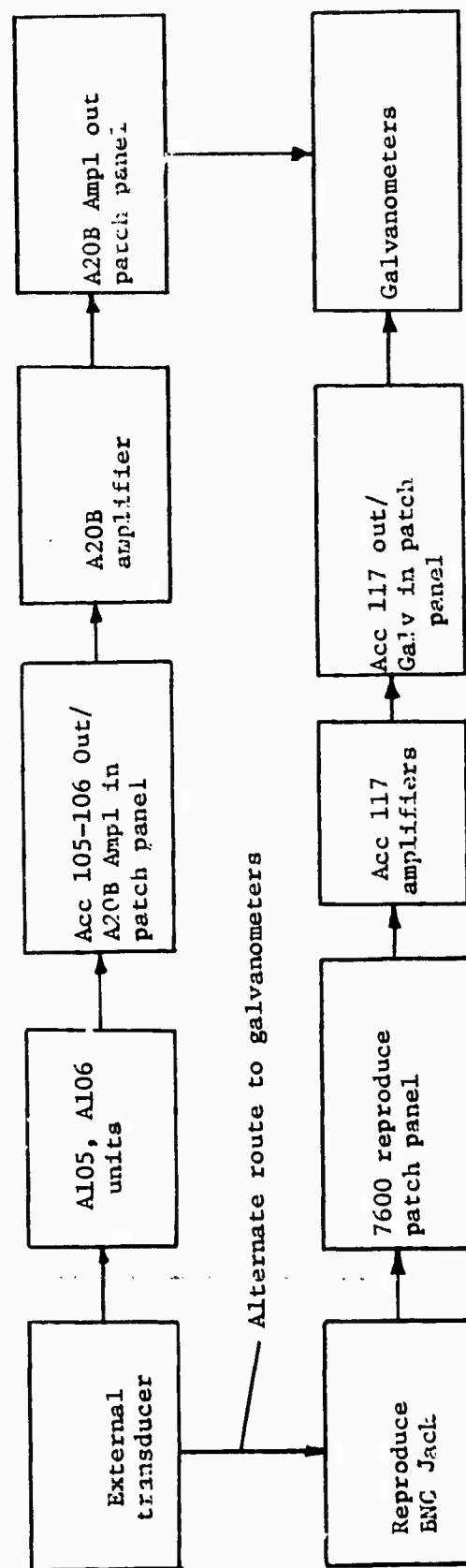


Figure 15. Typical Signal Path.

TABLE I  
SIGNAL CONDITIONING OUTLINE

Unit Name	Abbreviation	Purpose
Accudata 105	A-105	Strain gage signal conditioner
Accudata 106	A-106	Millivolt input or thermocouple input
Accudata 117	A-117	Low gain amplifiers
A20B	A-20B	High gain amplifiers

### Interface Clearance

Measurements of interface clearances in this investigation were made possible by the work of Duncan (11) with a non-penetrating inductance type clearance probe. Integrated with a substantial amount of electronic equipment, the probe provided a voltage output which was fed directly into the recording galvanometers.

Each clearance probe consisted of two pickup coils centered within two drive coils. Basically, a magnetic field is produced by the drive coils which induces eddy currents in the seal face which in turn induces a magnetic field in opposition to the drive coil magnetic field. The magnitude of this eddy current field is a function of the gap size between the two sealing surfaces. The two pickup coils, which are wound in opposite directions, are able to sense an induced voltage which is proportional to the total magnetic field of the drive coils plus that due to the induced eddy current. This total magnetic field is actually a vector difference between the drive coil field and the eddy current field. Since the pickup coils are wound in opposite directions, the voltage which appears at the probe output is actually the difference between that induced by each pickup coil thus producing a differential output signal from the probe. The associated electronic equipment then converts the amplitude modulated sine wave from the probe into a DC voltage which is a linear function of the clearance between the two sealing surfaces. Each probe has its own individual electronic null network which allows a zero voltage output at any clearance - in this case, zero clearance.



Diaphragm Temperature

With the aid of copper-constantan thermocouples, the actual interface fluid temperature could be estimated. One thermocouple was embedded inside each of the five clearance probes. Great care was taken so as to be sure that each thermocouple was as close to the bottom of the clearance probe as possible. This was to ensure that the thermocouple was in contact with the 0.005-inch diaphragm.

## CHAPTER IV

### INSTRUMENTATION CALIBRATION

#### General

Before any usable data concerning seal interface pressure, temperature, frictional torque, vertical load, film thickness, supply pressure, and leakage rate could be obtained, the various measuring devices had to be calibrated against known values of each respective variable. As with any experimental investigation, the data obtained are as valid only as each calibration represents.

#### Supply Pressure

The initial tests concerning the calibration of the supply pressure transducer were performed employing a Vishay Instruments Model P-350A strain indicator. Since the transducer was located upstream from the seal cavity, the oil outlet was simply plugged in order to obtain a static calibration system.

After an appropriate value of the internal calibration resistor (denoted by  $R_{cal}$ ) was determined, the supply pressure transducer was ready to calibrate in terms of galvanometer deflection. This was accomplished by employing a Bourdon tube pressure gage previously calibrated using a dead weight tester (for the  $R_{cal}$  calculation method and actual  $R_{cal}$  values, plus calibration curves concerning all instrumentation, the reader is referred to Appendices

C and D, respectively).

### Interfacial Pressure

Interface pressure probe calibration consisted mainly of devising a means by which the sealing cavity could be statically sealed. This was accomplished by fabricating an O-ring placed inside a confining plexiglass ring.

After  $R_{cal}$  values had been calculated for each interface pressure probe, calibration was carried out employing the previously calibrated supply pressure transducer. These calibration curves are given in Appendix D.

It should be pointed out that during the final lapping process, the degree of waviness of the sealing surface caused the diaphragms of three of the four pressure transducers (SP1, SP2, and SP5) to be lapped beyond the 0.002-inch tolerance. In addition to making the probes oversensitive, this apparently destroyed the linear output characteristics of these three probes.

### Frictional Torque

The friction torque strain gages had previously been calibrated by Kiber. His results, however, indicated that the highest torque encountered during a typical run was substantially below the lowest calibration point on the curve, also predicted by the computer program described in Chapter II. Hence, a new calibration curve needed to be determined.

From the computed torque results and from the vertical load effect on the torque strain gages (as shown in Figure 16) an appropriate  $R_{cal}$  value was determined. This being accomplished, torque as a function of oscillograph deflection was obtained employing the torque calibration rig given in Figure 17. The calibration curve obtained is given in Appendix D.

#### Vertical Load

The vertical load sensing strain gages were calibrated by Kiber employing a Baldwin SR-4 load cell connected to an Automation Industries strain indicator (the vertical load calibration rig is also given in Figure 17). The load was applied via a hydraulic jack. The load cell had a known output of 2 micro-inches per inch for every 1.0 lb<sub>f</sub> of vertical loading at the appropriate gage factor. The calibration procedure consisted of setting the load cell strain indicator to a known value of strain and applying load with the jack until the load cell strain indicator balanced. The strain readings from the vertical load strain gages were then recorded at that particular value of load. The calibration curve resulting from this procedure is also given in Appendix D.

It should be noted that an applied torque did not affect the output of the vertical load strain gages.

#### Clearance Probes

Before the clearance probes could be accurately calibrated, a means by which the actual clearance between the sealing (static)

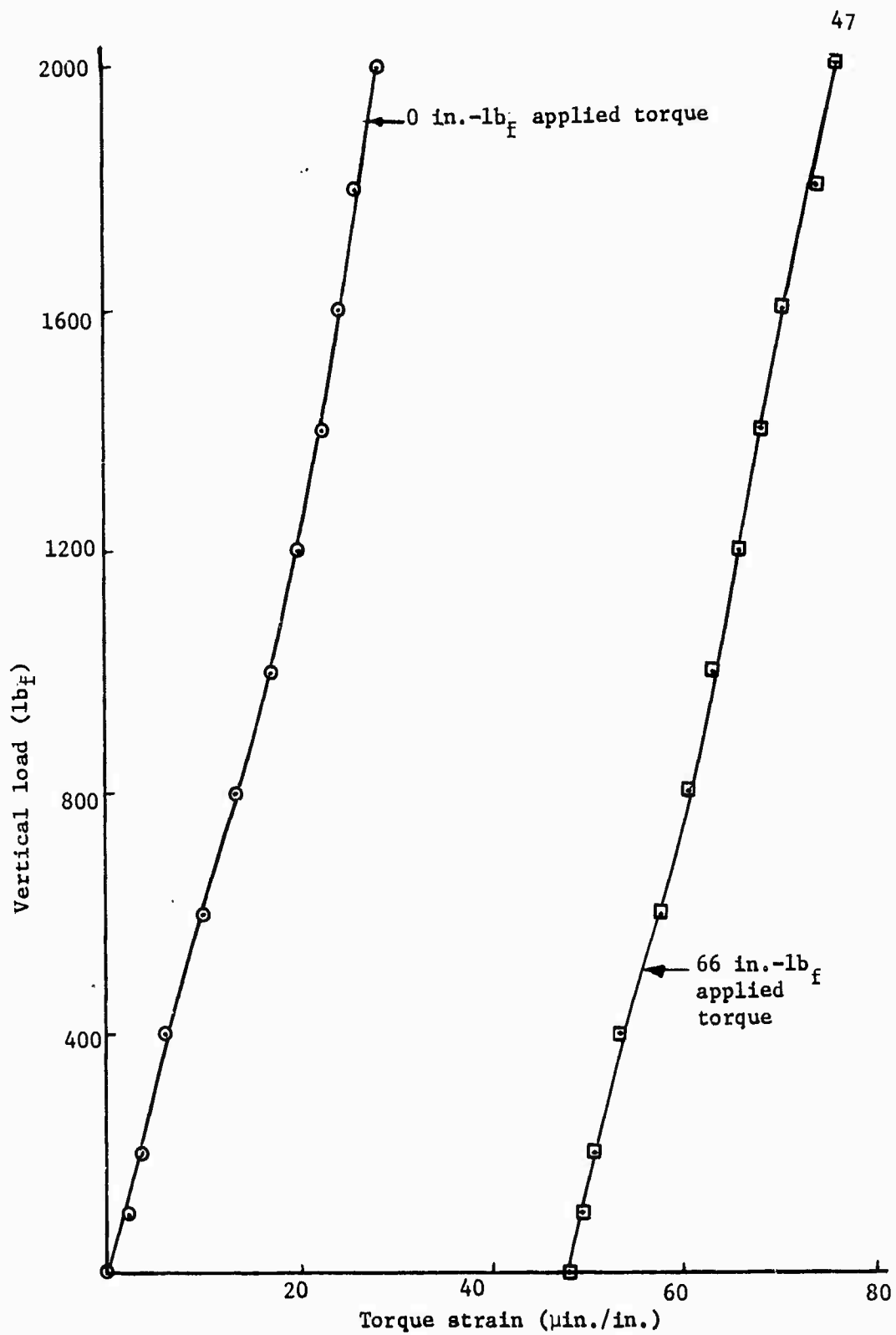


Figure 16. Vertical Load Influence on Torque.

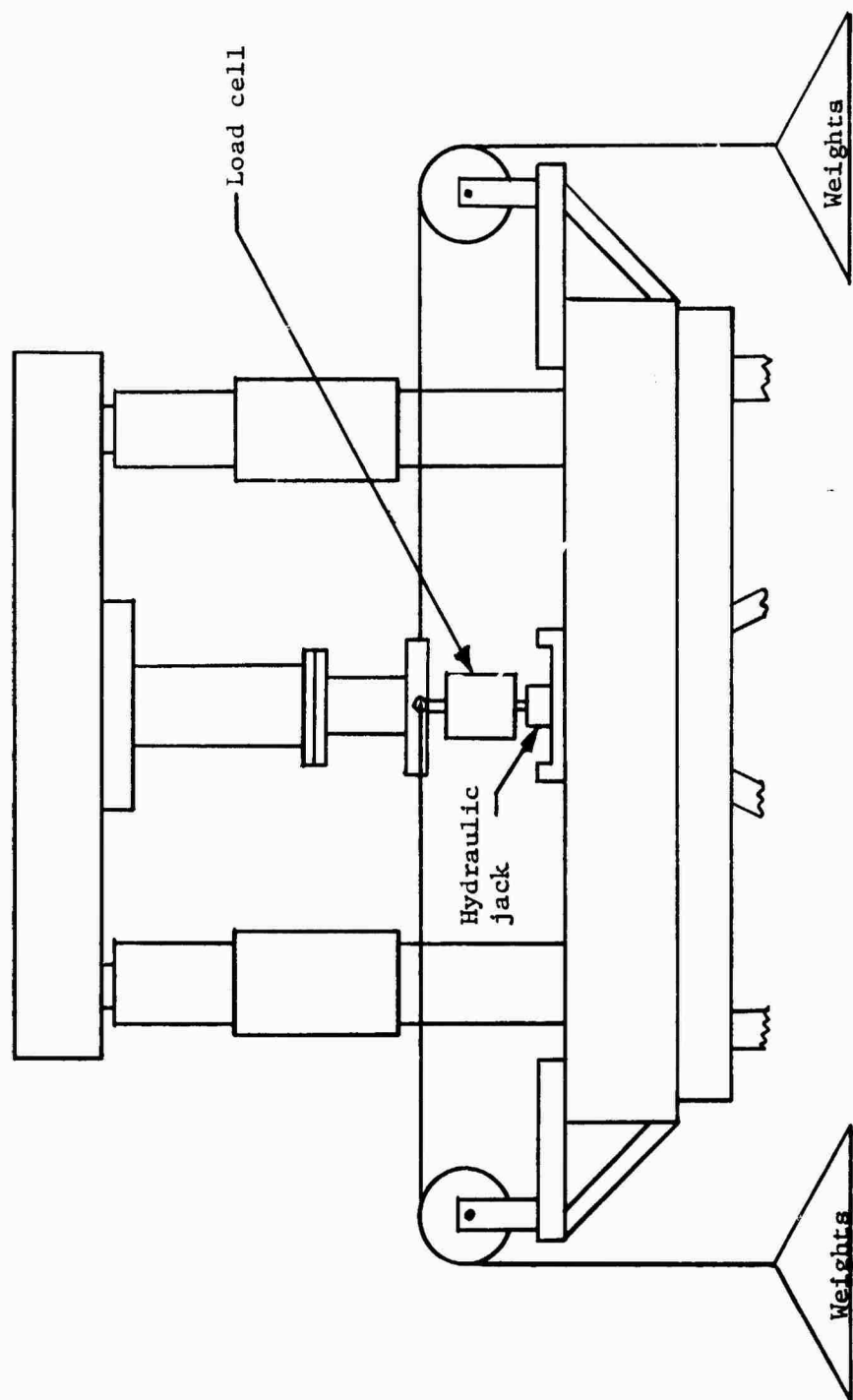


Figure 17. Torque and Vertical Load Calibration Rig.

surfaces had to be devised. This was accomplished by two methods: (1) by employing a Sheffield Proximity probe system and (2) from a Bentley-Nevada probe system. Basically, the Bentley-Nevada system was used primarily as a redundant clearance system and for checking the degree of seal tilt before each testing period.

Initially, the Bentley-Nevada system had to be calibrated such that for the range of clearances at which this investigation would take place, the output of the probes would be in their respective linear range. This was performed on a test assembly with the probe to be calibrated placed in a test seal which was dimensionally identical to that used in the actual tests.

From the results of the above tests, the output voltage of each probe's linear range was determined such that the highest possible clearance measuring sensitivity could be obtained over the expected clearance range.

With each external clearance system now statically calibrated, the clearance probes located within the sealing cavity were now ready to be calibrated. After the two sealing surfaces had been indexed, the upper instrumented seal was dropped down such that it was in physical contact with the lower sealing surface. This was defined as the zero clearance position. Each clearance indicating system, including that one being calibrated, was nulled for zero clearance (it should be noted that zero clearance for the Bentley-Nevada system was simply a "lower threshold" voltage which was at the low end of each probe's linear range). By carefully adjusting the vertical adjustment columns to an indicated clearance as

determined by the Sheffield system, an accurate calibration procedure had been established. Appendix D shows clearance probe calibration data. It should be noted that voltage as well as galvanometer deflection was plotted as a function of clearance. Probe output voltage as monitored on a digital voltmeter provided an accurate means to record individual probe sensitivities on a day-to-day basis to account for any small changes in system gain.

#### Clearance Probe Pressure Compensation

With the experimental test rig in the position for interfacial pressure probe calibration, the clearance probe output was monitored for various pressures. Since the actual "delta clearances" due to pressure were equal to the indicated delta clearance minus the actual movement of the upper sealing surface, this actual movement had to be determined. This was accomplished by observing the Bentley-Nevada output as well as the Sheffield system at the above varying pressures. However, since the Bentley-Nevada probes as well as the Sheffield probes were not in the same physical location as the clearance probes, a method was developed such that movement of each clearance probe could be determined from the change in clearance indicated by the Bentley-Nevada system as well as that of the Sheffield system. A brief description of this method is given in Appendix E.

From these tests, Figure 18 was produced. It should be noted that Kiber observed a linear pressure sensitivity curve. However, it seems that the compound employed to hold each probe in place concerning this investigation permitted much less deflection of the



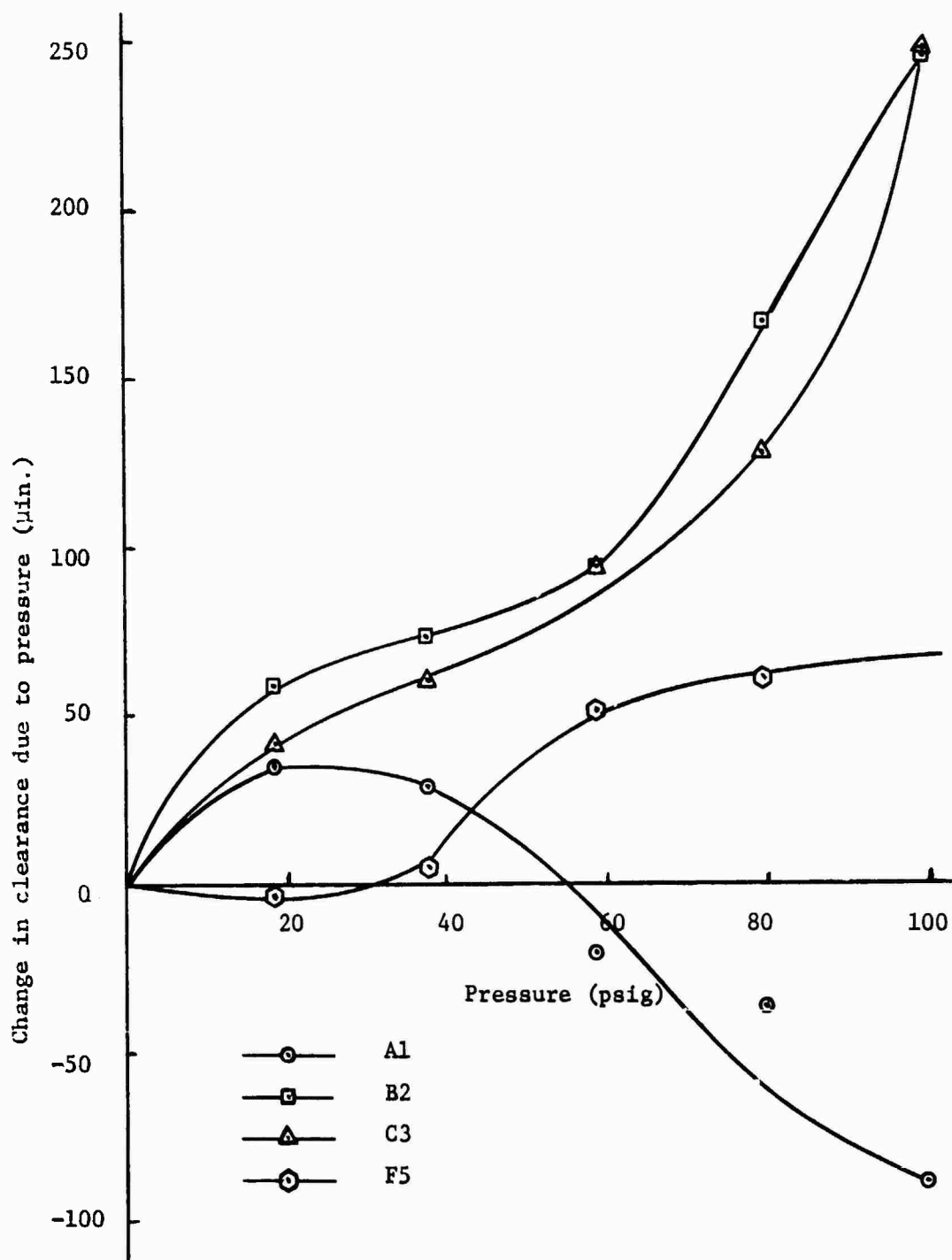


Figure 12. Clearance Probe Pressure Sensitivity.

0.005-inch diaphragm, thus causing the pressure sensitivity to decrease significantly.

#### Flow Meter Calibration

Calibration of the flow meters involved simply taking volume measurements with respect to the actual glass readings. For example, when the fluid meniscus was at the 100 mark on the glass, this volume of fluid was forced out and measured with a 100-ml graduated cylinder (zero volume was defined as the last reading on the glass). This procedure was repeated at each major division for each individual glass. Calibration curves for both glasses are also shown in Appendix D.

#### Thermocouple Calibration

The upper sealing surface diaphragm temperature was measured with copper-constantan thermocouples which had been epoxied inside and in the bottom of each clearance probe. The probes were then placed in physical contact with the 0.005-inch diaphragm.

The procedure for thermocouple calibration consisted of balancing the A20B high gain amplifiers such that a given millivolt input to the ACC106 unit would produce a favorable galvanometer deflection. For this investigation employing copper-constantan thermocouples, 4.00 mV represented approximately 200°F. Thus, the A20B amplifiers were balanced such that a 4.00-mV input produced a 3.0-inch galvanometer deflection. However, this was simply an approximation to yield the appropriate deflection. The actual thermocouple sensitivities were determined from the +1-mV calibrated

signal within the ACC106 unit. Before and after each experimental test, deflections produced from this +1-mV excitation were determined. This yielded the actual millivolt per inch deflection sensitivity with which each thermocouple responded for that particular day.

## CHAPTER V

### EXPERIMENTAL TESTS, DATA REDUCTION, AND RESULTS

#### General

The combination of each individual measuring device into one workable data acquisition system was extremely tedious and time consuming. The experimental procedure involved a substantial amount of system preparation and calibration. However, after each system had been nulled and set, data acquisition became a fairly simple matter.

#### Experimental Procedure

Before each test period, calibration and zero load deflections of each strain gage transducer ( $R_{cal}$  deflections) and also of each thermocouple ( $\pm 1$ -mV deflections) were obtained. This resulted in being able to compensate for any amplification gain changes due to changes in ambient conditions. Also before each test, the clearance probe system was nulled both of "infinity" and at zero clearance (the two sealing surfaces had been previously indexed in order to obtain a consistent reference point).

With the above accomplished, the test was ready to proceed. A test clearance was chosen and the stationary seal set at a value slightly higher than the chosen value to allow for the decrease in

clearance due to strapping the top support plate down. At this clearance (0 rpm), voltage readings and an oscillograph trace were taken. Dividing each clearance (indicated by voltage output) by its oscillograph deflection produced probe sensitivities in terms of galvanometer deflection for that particular test.

After strapdown, the rotating sealing surface was turned through 360 degrees and an oscillograph trace obtained. This trace revealed a sinusoidal output for each probe indicating the possibility that the rotating seal's spin axis was not normal to the rotating sealing surface.

Pressure was then applied to the system (at 0 rpm) and a trace was obtained. This configuration (which was a test condition itself) was the zero torque condition due to the vertical load effect on the torque strain gages. Flow measurements were obtained via the oil flow rate measuring system previously described.

The SCR drive was then turned on to the desired rotational speed and allowed to stabilize. While flow rate data were being taken, a burst of oscillograph data was obtained at a paper speed of 120 inches per second. Figures 19 and 20 show typical oscillograph traces obtained in this manner (for reasons of clarity, individual clearance and pressure oscillograph records will be presented later in this chapter).

#### Data Interpretation and Reduction

Reducing the data involved simply measuring the physical distance each individual trace deflected from its zero load

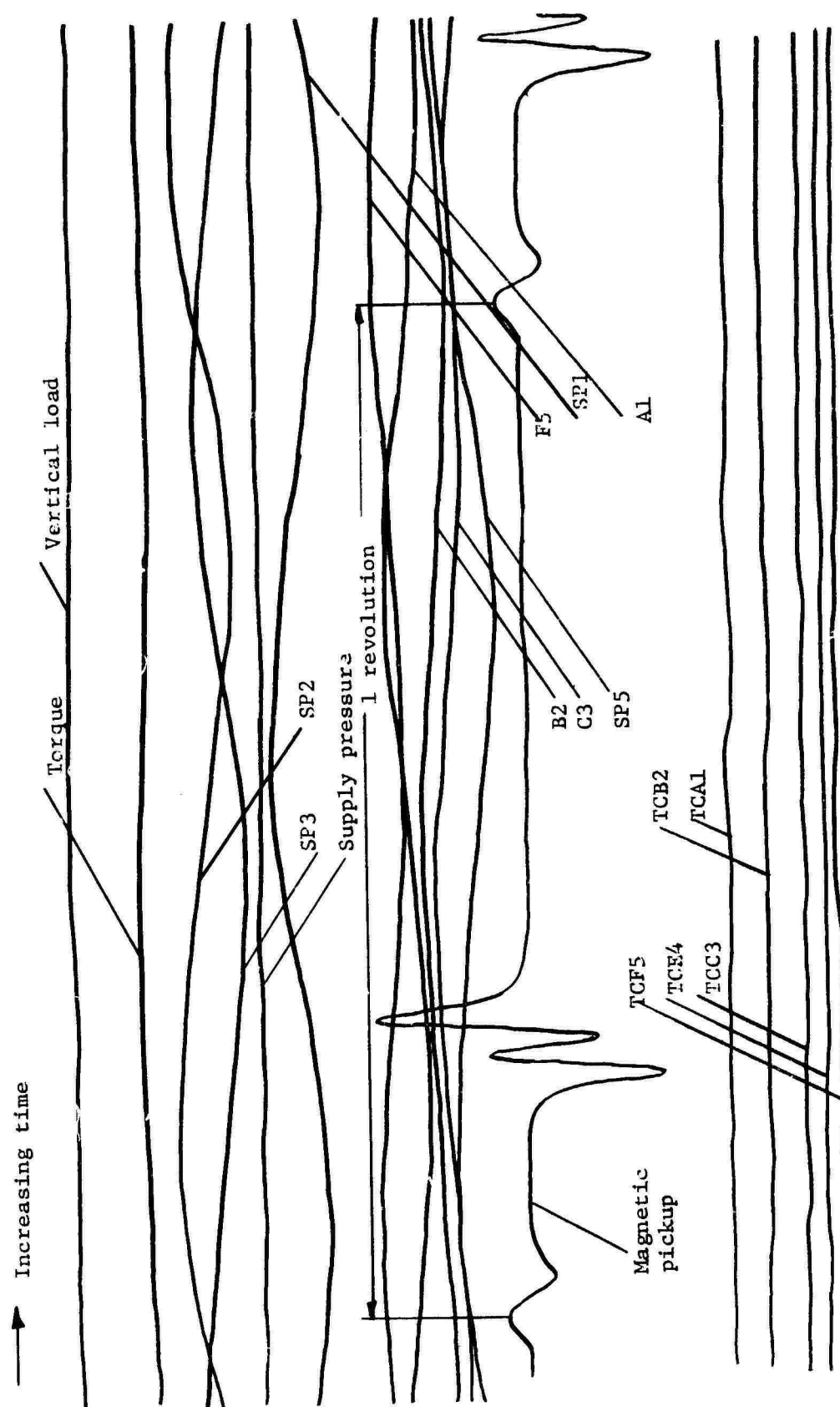


Figure 19. Oscilloscope Record (Run 12).

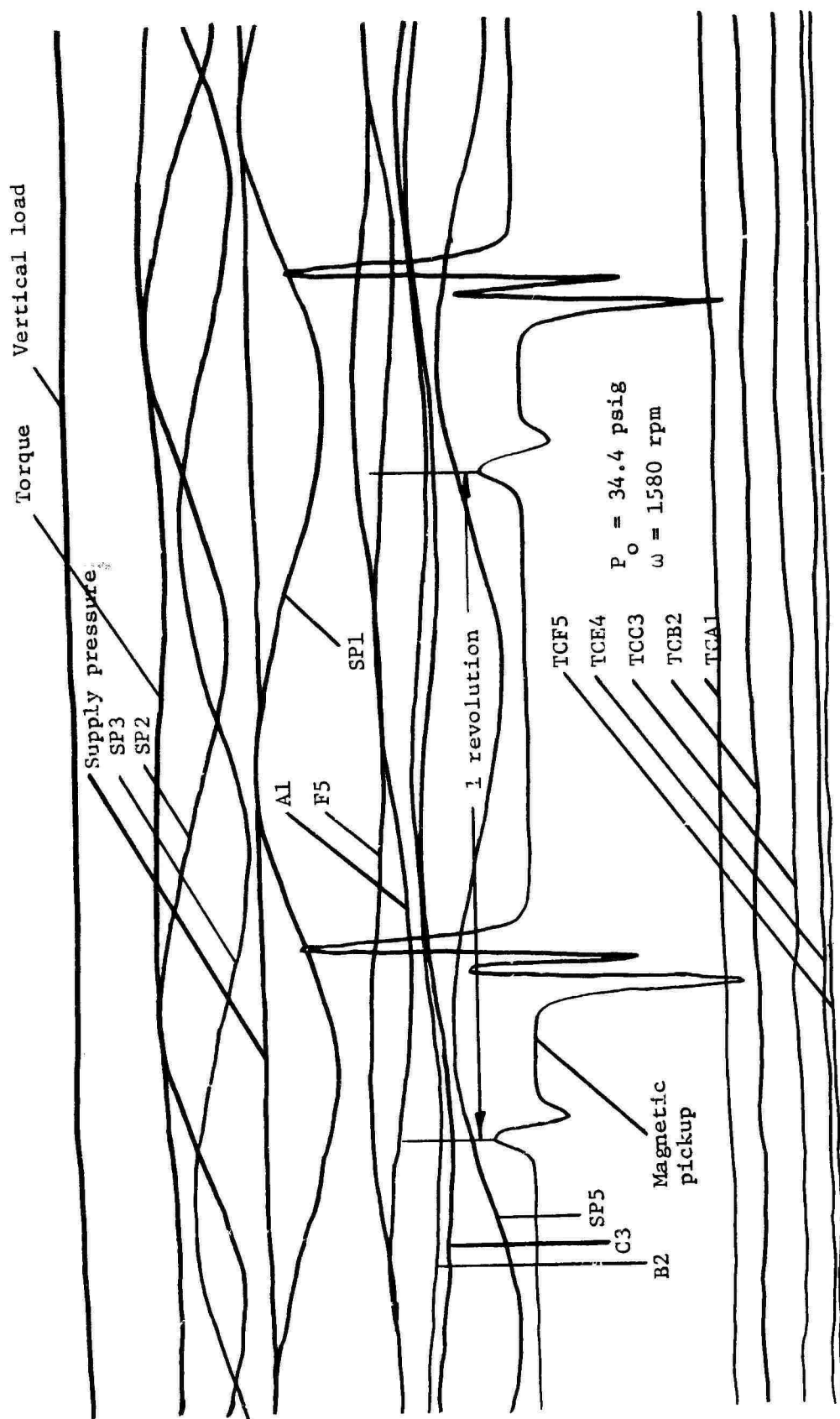


Figure 20. Oscilloscope Record (Run 13).

condition during any test. These deflections were then multiplied by an appropriate calibration constant to obtain physical parameters concerning each individual measuring device.

However, for data involving strain gages, any amplification gain changes had to be compensated for by utilizing each  $R_{cal}$  deflection during the test. This was accomplished from Equation (20):

$$\text{Physical load} = (\text{deflection})(\text{calibration constant}) \times \left( \frac{R_{cal} - cal}{R_{cal} - test} \right) \quad (20)$$

where

physical load = pressure, torque, or vertical load

deflection = trace deflection from zero position

calibration constant = slope of sensitivity curve

$R_{cal} - cal = R_{cal}$  deflection during calibration

$R_{cal} - test = R_{cal}$  deflection during test

However, since calibration curves of three pressure probes were non-linear, pressure readings had to be read directly from each calibration curve. Hence, Equation (20) was modified in this case to become

$$\text{Actual deflection} = (\text{Indicated deflection}) \left( \frac{R_{cal} - cal}{R_{cal} - test} \right) \quad (21)$$

where the above actual deflection was used to determine pressures from the calibration curves.

It should be noted that data involving a fluctuating parameter (such as clearance) were determined at the high and low points and then averaged to yield a constant component plus a fluctuating component.



Any clearance probe system gain changes from that during calibration was accounted for from the previously mentioned test procedure (the difference in sensitivities during calibration and testing were found to be very small).

Interpreting temperature data involved determining the deflection caused by a +1-mV input to the galvanometers to obtain each individual millivolt sensitivity for that particular test period. Thus, from the deflection determined during a test, a corresponding millivolt reading was calculated and the actual temperature read from copper-constantan thermocouple tables.

#### Presentation of Data — Experimental and Analytical Results

Due to the large amount of collected data, it is felt that the most efficient means of data presentation would be to examine and discuss three basic questions:

1. What did theory indicate of itself?
2. What did experiment indicate of itself?
3. How did theoretical and experimental results agree or differ?

To avoid repetition, some trends concerning both theoretical and experimental results will be pointed out in the discussion of how experiment and theory agreed or differed.

#### Analytical Results

The most significant results of the temperature-dependent fluid property face seal calculations are shown in Figures 21 through 24 and Tables II through V. For comparison purposes, face seal parameters

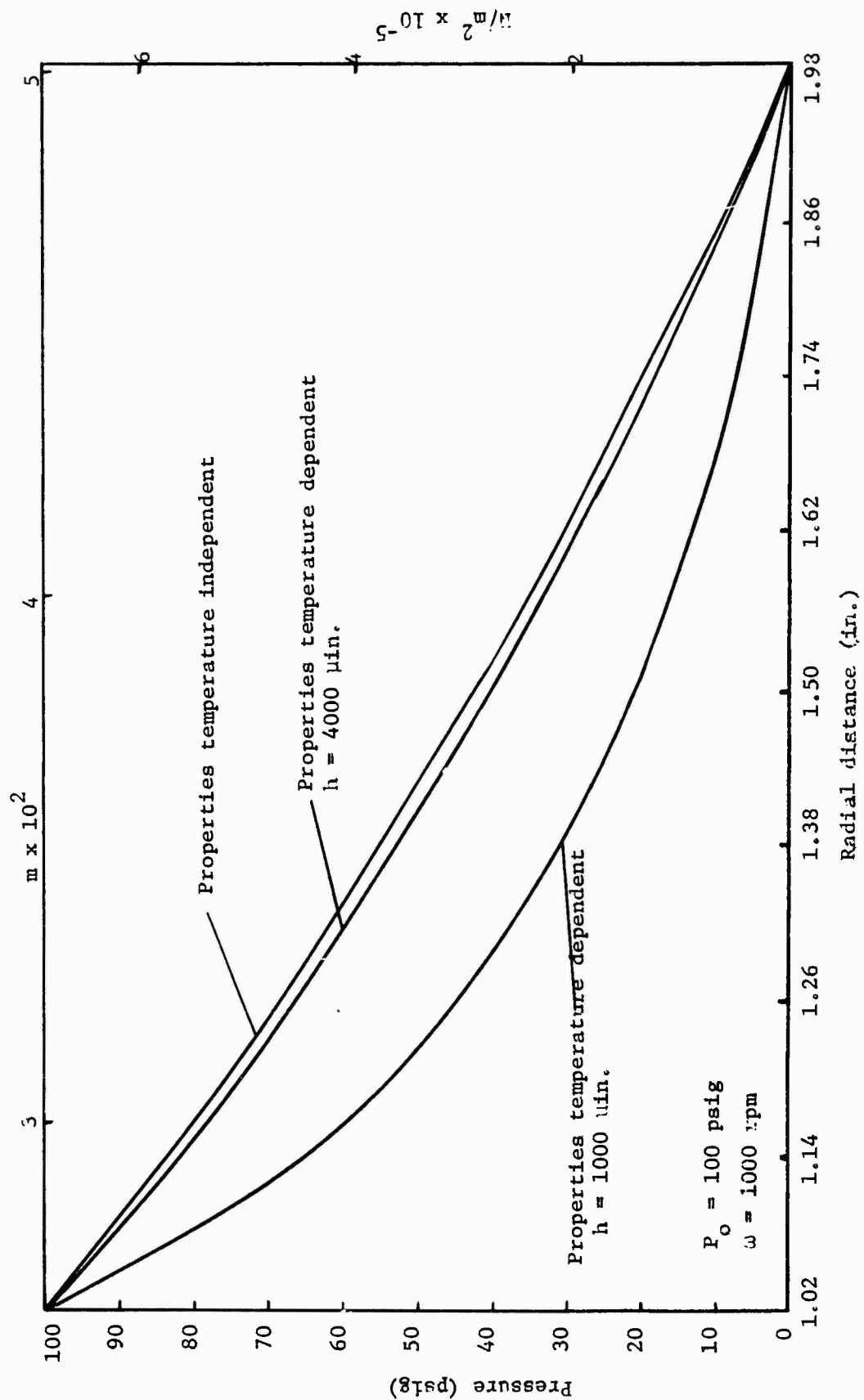


Figure 21. Temperature Dependent and Non-Temperature Dependent Fluid Property Pressure Profiles.

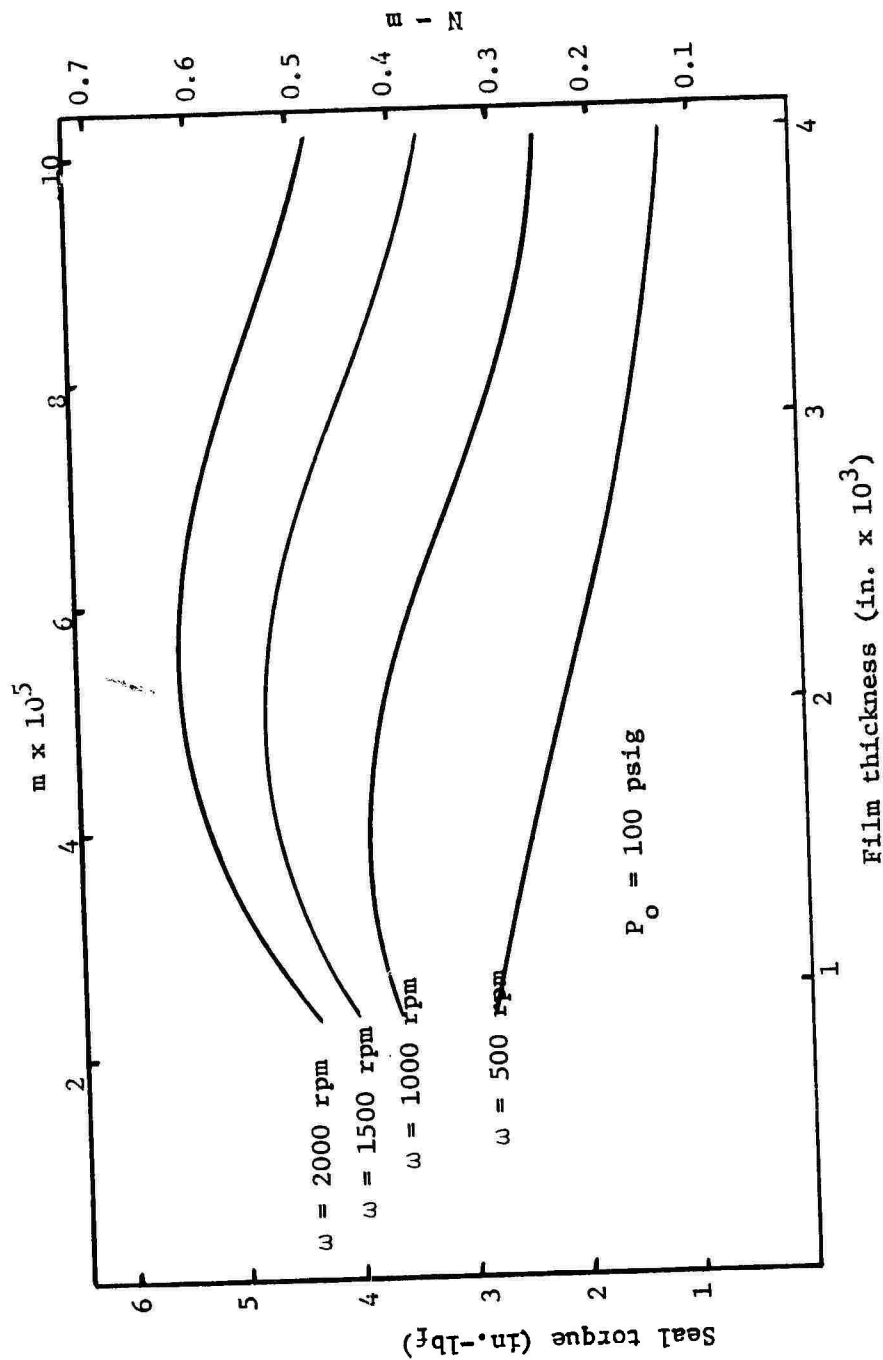


Figure 22. Seal Torque vs Clearance (Properties Temperature Dependent).

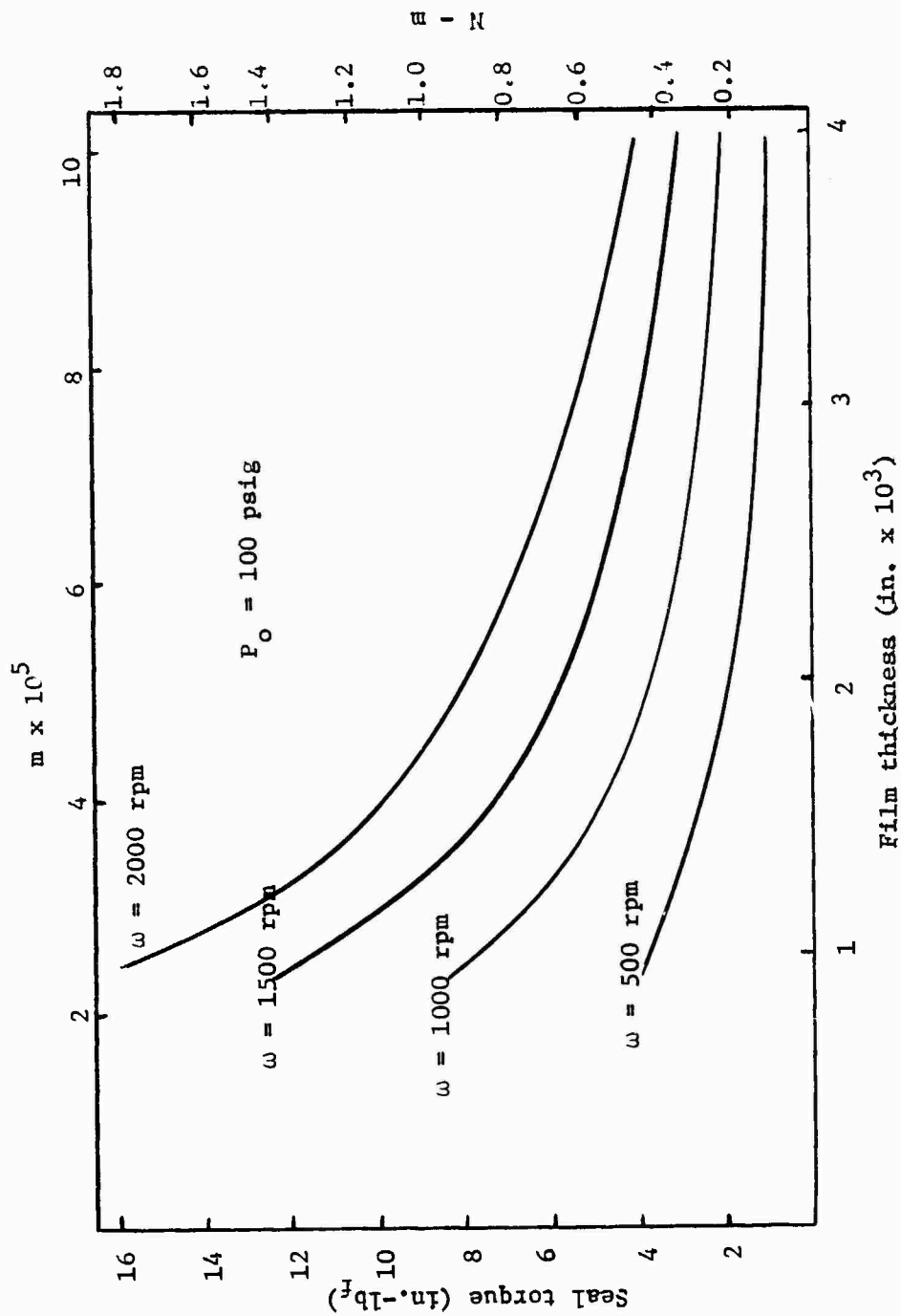


Figure 23. Seal Torque vs Clearance (Properties: Temperature Independent).

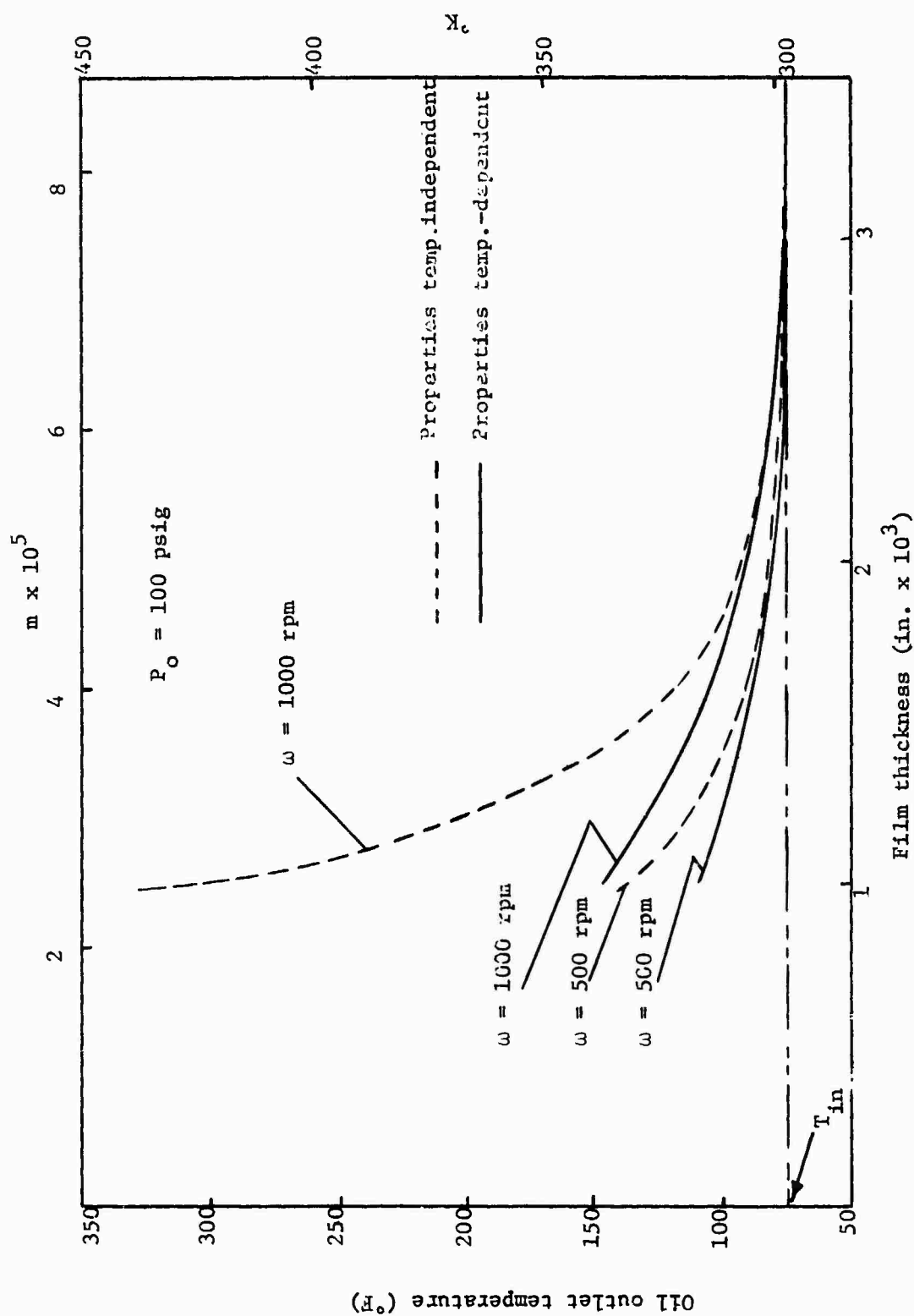


Figure 24. Oil Outlet Temperature vs Clearance (Properties Dependent and Independent of Temperature).

TABLE II

THEORETICAL TEMPERATURE DEPENDENT AND NON-TEMPERATURE DEPENDENT FLUID  
PROPERTY VERTICAL LOAD COMPARISONS ( $P_o = 100$  psig,  $h = 0.001$  inch)

RPM	Temperature Dependent Fluid Properties Load ( $lb_f$ )	Non-Temperature Dependent Fluid Properties Load ( $lb_f$ )
500	638.7	681.9
1000	595.0	681.6
1500	564.6	681.1
2000	553.3	680.5

TABLE III

THEORETICAL TEMPERATURE DEPENDENT AND NON-TEMPERATURE DEPENDENT FLUID  
PROPERTY VERTICAL LOAD COMPARISONS ( $P_o = 100$  psig,  $h = 0.003$  inch)

RPM	Temperature Dependent Fluid Properties Load ( $lb_f$ )	Non-Temperature Dependent Fluid Properties Load ( $lb_f$ )
500	686.6	681.9
1000	678.6	681.6
1500	671.7	681.1
2000	662.3	680.5

TABLE IV

THEORETICAL TEMPERATURE DEPENDENT AND NON-TEMPERATURE DEPENDENT FLUID  
PROPERTY LEAKAGE RATE COMPARISONS ( $P_o = 100$  psig,  $h = 0.001$  inch)

RPM	Temperature Dependent Fluid Properties $\dot{m}$ (lbm/min)	Non-Temperature Dependent Fluid Properties $\dot{m}$ (lbm/min)
500	0.057	0.045
1000	0.074	0.045
1500	0.091	0.045
2000	0.106	0.045

TABLE V

THEORETICAL TEMPERATURE DEPENDENT AND NON-TEMPERATURE DEPENDENT FLUID  
PROPERTY LEAKAGE RATE COMPARISONS ( $P_o = 100$  psig,  $h = 0.003$  inch)

RPM	Temperature Dependent Fluid Properties $\dot{m}$ (lbm/min)	Non-Temperature Dependent Fluid Properties $\dot{m}$ (lbm/min)
500	1.224	1.224
1000	1.256	1.227
1500	1.294	1.233
2000	1.346	1.241

assuming temperature independent fluid properties are also shown. It should be noted again that the results presented stem from the assumption of smooth, parallel, and aligned sealing surfaces.

Figure 21 (page 60) shows the effect of the temperature-dependent fluid property assumption on the interface region pressure profile. At low supply pressures and small clearances, the temperature rise is significant indicating a breakdown of the fluid property temperature independence assumption. Figure 21 illustrates also that at higher clearances, the temperature rise is almost negligible, causing the small differences in temperature-dependent and temperature-independent fluid property pressure profiles.

As expected, a deviation in pressure profiles indicates a difference in the load carrying capacity of the seal. Tables II and III (page 64) compare vertical load for temperature-dependent fluids and also for temperature-independent fluids.

To further illustrate the effect of varying viscosity and density on seal performance, Figures 22 and 23 (pages 62 and 63) show total seal torque plotted as a function of clearance at various seal speeds for temperature-dependent and temperature-independent fluids, respectively. Figure 22 illustrates that as the fluid temperature rise becomes large, its viscosity decreases thus causing a drop in seal torque at small clearances. However, as shown in Figure 23 (page 62), calculations involving a non-temperature-dependent property fluid cannot sense a viscosity change and thus predict a higher torque at low clearances.



Another interesting difference of the temperature-dependent fluid property assumption versus the temperature-independent fluid property assumption is the temperature of the fluid as it emerges from the seal. Figure 24 (page 63) shows fluid outlet temperature as a function of clearance at various rpms for fluid properties dependent and independent of temperature. Note that at large clearances and low seal speeds, solutions based on temperature-dependent and temperature-independent fluids yield essentially the same result.

Since the major role of a face seal is to prevent fluid leakage, a comparison of leakage rates for temperature-dependent and non-temperature-dependent fluid properties is in order. Tables IV and V (page 65) compare leakage rate for various sealing conditions. At conditions resulting in a low temperature rise, the two solutions are essentially identical. However, when the temperature rise becomes significant, there are important differences in the leakage rates.

### Experimental Results

All experimental data obtained during the course of this investigation are presented first in tabular form in Table VI. Particular experimental parameters will be compared to numerical results in the next section.

Trends regarding each individual measuring device will be discussed separately for clarity.

TABLE VI  
EXPERIMENTAL DATA

Run No.	Supply Pressure (psig)	RPM	Clearance Probe Output (min.)					Average*
			A1	B2	C3	F5		
1	17.4	0	2949	2896	2903	2686	2858	
2	17.4	490	3081 + 176	2724 + 209	2745 + 177	2809 + 176	2840	
3	17.1	980	3176 + 147	2835 + 176	2874 + 149	2928 + 144	2953	
4	17.1	1515	3294 + 118	2977 + 132	3079 + 112	3072 + 112	3106	
5	41.0	0	3169	3091	3134	2827	3055	
6	41.0	505	3360 + 170	2938 + 220	2968 + 186	2907 + 176	3043	
7	41.0	1000	3426 + 147	3015 + 165	3052 + 159	2979 + 152	3118	
8	41.2	1510	3499 + 118	3070 + 154	3211 + 130	2919 + 120	3175	
9	87.5	0	3762	3578	3636	3136	3528	
10	41.5	0	2308	2275	2390	2155	2282	
11	36.1	505	2436 + 184	2093 + 209	2216 + 177	2206 + 176	2238	
12	33.8	1020	2532 + 147	2225 + 187	2402 + 159	2354 + 144	2378	
13	34.4	1520	2671 + 110	2402 + 143	2635 + 112	2546 + 111	2564	
14	20.8	0	1875	1911	2174	2018	1995	
15	20.0	515	2120 + 169	1790 + 231	2076 + 196	2105 + 184	2022	
16	19.5	1015	2262 + 147	2009 + 176	2312 + 149	-	2194	
17	19.2	1520	2422 + 110	2174 + 121	2606 + 103	-	2401	

\*Clearance value used in computer run.

TABLE VII  
EXPERIMENTAL DATA

Run No.	Torque (in.-lb <sub>f</sub> )	Vertical Load (lb <sub>f</sub> )	Flow Rate (lbm/min)	Supply Pressure (psig)	Pressure Probe Output (psig)			
					SP1	SP2	SP3	SP5
1	0	96.2	0.168	17.4	6.0	6.5	6.7	10.0
2	1.25	87.5	0.174	17.4	6.5 + 1.0	5.0 + 1.0	7.2 + 1.5	11.0 + 2.0
3	2.37	96.2	0.178	17.1	6.0 + 2.5	3.5 + 2.5	7.1 + 2.2	10.0 + 3.0
4	3.13	91.8	0.183	17.1	7.0 + 3.5	2.0 + 2.0	7.6 + 3.0	8.5 + 4.3
5	0	296.9	0.486	41.0	15.5	15.6	16.2	31.2
6	1.25	303.4	0.499	41.0	15.8 + 0.5	14.3 + 0.5	16.6 + 1.3	30.4 + 0.6
7	2.23	275.1	0.499	41.0	16.8 + 1.4	12.8 + 1.3	15.8 + 2.3	29.4 + 1.1
8	2.99	270.7	0.519	41.2	17.3 + 1.9	11.6 + 1.4	16.4 + 2.9	27.7 + 1.7
9	0	523.9	-	87.3	34.6	32.2	33.9	65.6
10	0	279.1	0.207	41.5	17.5	16.5	15.2	30.0
11	-	210.4	0.180	36.1	15.5 + 2.5	14.0 + 1.5	13.5 + 1.9	27.0 + 1.0
12	-	171.8	0.175	33.8	14.5 + 2.5	12.3 + 3.3	12.3 + 3.5	25.0 + 2.0
13	-	171.8	0.171	34.4	14.0 + 4.0	11.0 + 5.5	12.2 + 4.3	25.5 + 3.5
14	0	-	0.058	20.8	10.0	8.5	9.8	16.0
15	1.26	-	0.058	20.0	8.5 + 2.5	6.5 + 3.0	10.0 + 3.1	14.0 + 3.5
16	2.78	-	0.056	19.5	7.5 + 5.5	5.0 + 5.0	9.0 + 5.7	15.0 + 4.0
17	3.59	-	0.053	19.2	5.5 + 8.5	3.5 + 6.5	9.2 + 6.1	15.0 + 6.5

Clearance probes. In examining Table VI (page 68), perhaps the most distinguishable observation is noting that the clearance probes indicate fluctuating clearances, the magnitude of which decreases with increasing speed. However, the oscillatory magnitudes remain essentially constant with regard to varying supply pressures. These fluctuations were also found by Denny (1), Batch and Iny (4), Pape (6), Stanghan-Batch (7), and also by Kiber (10). Batch and Iny's results were contrary to findings concerning this investigation in that they noticed the magnitude of clearance oscillation to be independent of supply pressure, rotational speed, and temperature but was affected by vertical loading. This study indicates however clearance fluctuation to be highly dependent of rotational speed. Also contrary to other findings, this study revealed a single clearance oscillation per shaft revolution (pressure oscillations were also noticed which will be discussed later in this chapter).

Table VI also illustrates the trend of increasing average clearances with increasing seal rotational speed. Average clearance also increases with increasing supply pressures.

Examining degree of clearance probe fluctuation once again reveals that the magnitude of oscillation of clearance probe B2 (which is located on the outermost radius) is always greater than the fluctuation magnitudes of the other three clearance probes. This observation leads to considering the possibility that the plane of the rotating piece sealing surface was not normal to the spin axis of the rotating piece. This would account for the observed oscillatory output from all the clearance probes, and also for the generally equal magnitude of fluctuation of clearance probes A1, C3,

and F5. It should be pointed out also that magnitudes of oscillatory clearances generally decreased with decreasing average clearance.

Figure 25 shows individual clearance probe traces taken from Figure 20 (page 57). This is a representative trace of all clearance data experimentally obtained. Examination of Figure 25 reveals that clearance probes A1, F5, and C3 (which are on the same radius) are 120 degrees out of phase in the order given with clockwise rotation of the rotating seal. With the same rotational direction clearance probe B2 lags clearance probe C3 by 25 degrees. The above phase relationships support the "wobble" theory regarding the rotating seal since clearance probes A1, C3, and F5 are physically located 120 degrees apart while clearance probe B2 is located 25 degrees from clearance probe C3.

Pressure probes. Similar to the clearance probes, Table VII (page 70) indicates oscillating interface pressures. Oscillatory magnitudes increased with increasing rotational speed and also increased with decreasing clearance. Magnitude of fluctuation regarding pressure probes SP1, SP2, and SP3 (located on the same radius) remain about constant with respect to a certain seal rotational speed.

Table VI also illustrates the trend that average interface pressures generally (although not always) decrease with increasing rotational speed. Pressure probe SP2 exhibited this behavior throughout each testing period. Average pressures measured by pressure probe SP5 (located on the innermost radius) were always greater than pressures measured by the other three probes.

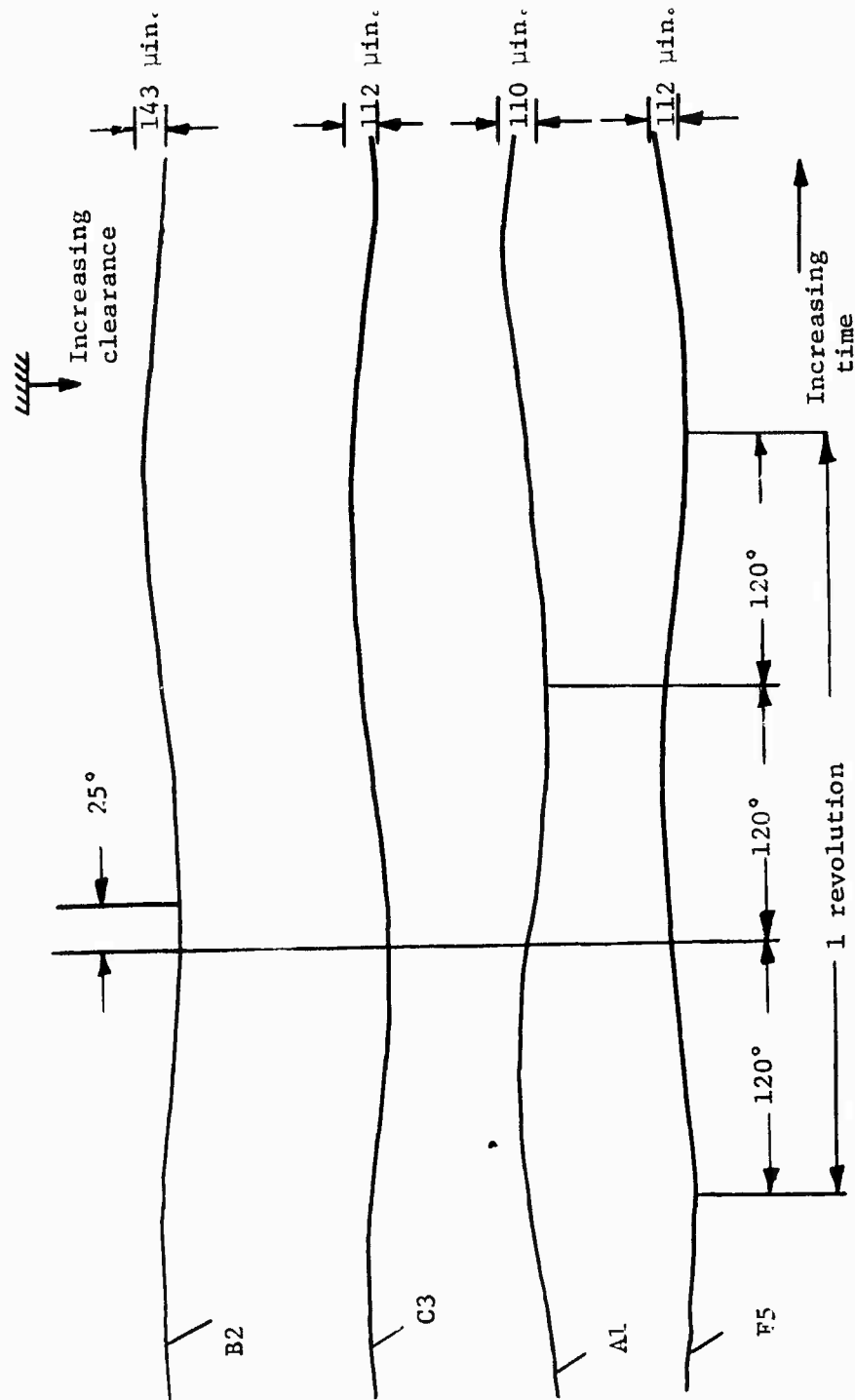


Figure 25. Clearance Probe Traces (Run 13).

Perhaps the most interesting observation regarding pressure fluctuation occurred during two high speed, low clearance runs, 16 and 17. Referring to Table VII (page 69), the reader will notice that the fluctuating components of pressure as measured by SP1 and SP2 were equal to or went below atmospheric pressure. Also, pressure probe SP5 noticed pressures higher than the inlet supply pressure during run 17. These occurrences were also noted by Denny (1); however, referring back to Figures 19 and 20 (pages 58 and 59) reveals a single pressure oscillation with respect to shaft rotation. Other investigators noticed a twice fluctuation of pressure per shaft revolution. This discrepancy could have been caused by the experimental seal's rigid mounting whereas other investigators have employed spring loaded test apparatus.

Figure 26 shows individual pressure probe traces taken again from Figure 20. Similar to the clearance probes, Figure 26 illustrates the 120-degree phase lag of pressure probes SP1, SP2, and SP3 for clockwise rotation; i.e., SP2 leads SP1 120 degrees, SP3 leads SP2 120 degrees, and SP1 leads SP3 120 degrees. Again similar to the clearance probes, the above phase relationships correspond exactly to the physical location which each pressure probe was installed. It should be noted also that pressure probe SP5 (located on the innermost radius) follows the above trend in that phase angle and physical location correspond (SP3 lags SP5 by 95 degrees).

Leakage rates. Referring again to Table VII, it is seen that leakage rates increased with increasing supply pressures but decreased with decreasing average clearance. Examining leakage data regarding

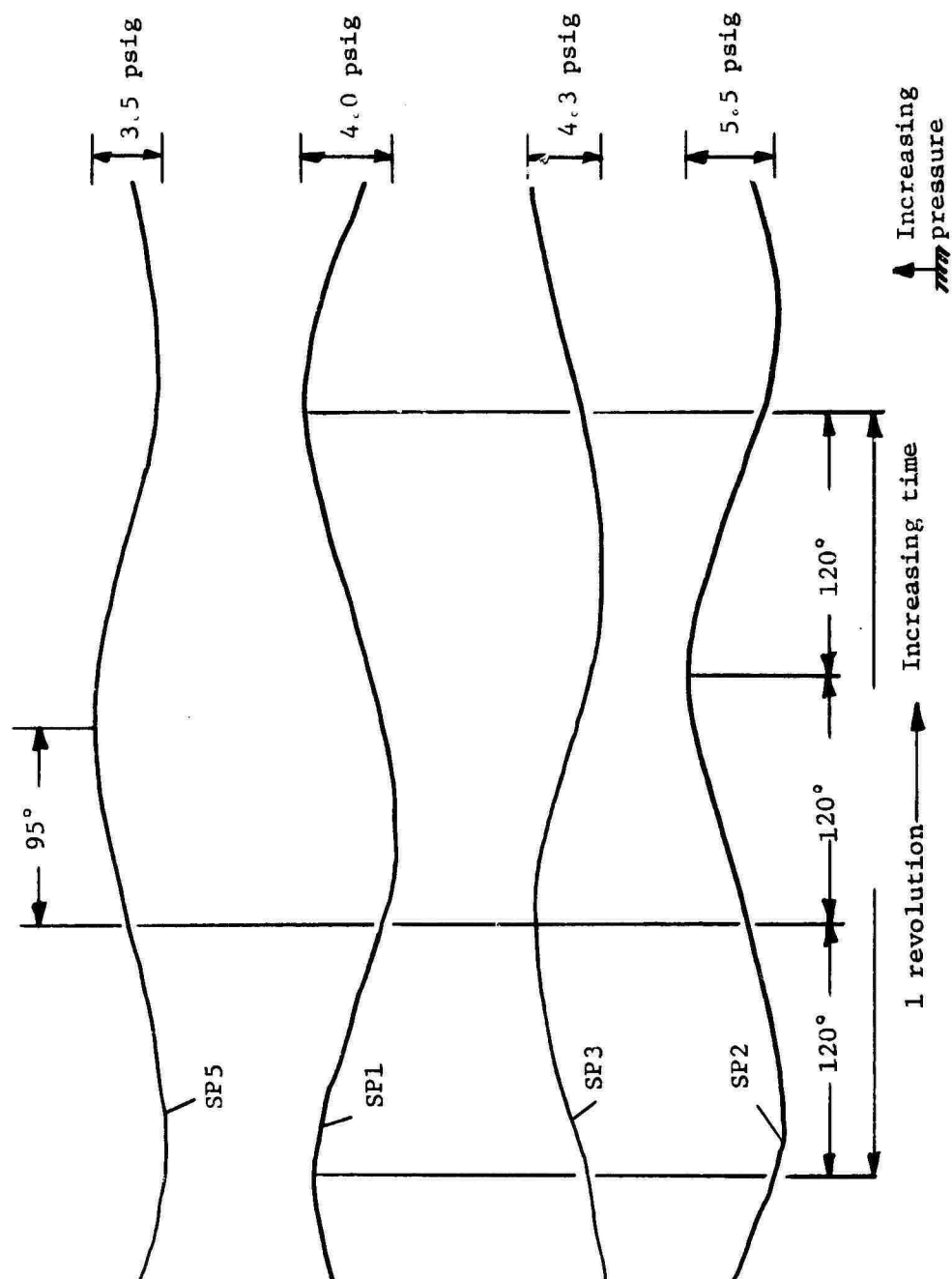


Figure 26. Pressure Probe Traces (Run 13).



Runs 1 through 8 (high clearance) indicates that as the seal rotational speed increased, mass flow rate increased likewise. However, a look at Runs 10 through 17 (low clearance) of Table VII reveals the opposite trend of decreasing leakage rates with increasing rotational speed. With regard to the latter observation, it seems possible that the test seal was approaching a sealing mode during these low clearance, high speed runs.

Torque. As would be expected, experimentally determined torque values consistently increased with increasing rotational speeds. Also, with exception to Runs 11 through 13, torque values tended to increase with decreasing average clearance. It is believed that the low torque values concerning Runs 11 through 13 were caused by vertical loading effects which will be discussed with some detail in the section concerning data comparison.

There is some evidence from Table VII that torque had a tendency to decrease with increasing supply pressures. Also, small torque fluctuations at a "once per revolution" frequency were noted at high speeds and low clearances. Again, it is believed that vertical load effects caused this notable observation.

Vertical load. Considering experimentally obtained vertical load values (again shown in Table VII), it is noted that loads are most strongly influenced by supply pressure values. It seems that load values were not affected strongly by speed or clearance. In general, vertical load decreased with increasing rotational speed although not always and not drastically.

Similar to torque data, small vertical load oscillations (again at a "once per revolution" frequency) were observed at high speed, low clearance experimental tests.

Temperature. More detailed temperature data will be given later in this chapter. However, certain trends are discussed below which will be supported by later presentations.

As previously mentioned, experimental testing began with the seal and oil in thermal equilibrium with ambient conditions. Experimental temperature data obtained towards the first of a test period revealed that diaphragm temperatures tended to increase with radius. However, as each test progressed, the test seal itself was heating up, causing diaphragm temperatures towards the seal center to become greater than those towards the outer seal radius (this observation was not always true). This indicates that heat conduction was taking place within the test seal itself.

Further observations lead to the conclusion that the test seal has a large thermal inertia; i.e., a substantial amount of time was required for the seal to relinquish the heat generated by the sealing process.

#### Comparisons of Analytical and Experimental Findings

It is felt that the most efficient means of comparing theory to actual experimental phenomena is by examining results concerning each individual seal parameter separately and then attempt to draw conclusions from these comparisons.

Interface clearance. The theoretical sealing parameters presented earlier resulted from the assumption that both sealing surfaces were smooth and mutually parallel. Experimental results indicate however the possibility of the rotating seal's spin axis being at an angle other than the normal with the rotating sealing surface. Also, predicted results are based upon the assumption that both sealing surfaces are perfectly flat where in actuality sealing surface out-of-flatness was of significant magnitude, particularly with that concerning the surface of the stationary instrumented seal.

Since the mathematical model presented has no provisions which consider deviations from sealing surface parallelism and smooth flat surfaces, differences concerning clearance measurement in theory and experiment should be expected.

Interface pressure. As illustrated in Figure 27, theoretical (both temperature-dependent and temperature-independent fluid property solutions) interface pressure data indicate a smooth parabolic shaped pressure profile with no fluctuating components while experimental results give evidence of oscillating interface pressures (average pressures and their respective degree of oscillation are shown in figures dealing with interface pressure). Figure 27 also shows that at relatively large clearances and low speeds, average pressures agree favorably with predicted results, both from the standpoint of temperature-dependent as well as temperature-independent fluid properties.

Figure 28 shows the predicted pressure profile at a higher speed and lower clearance. It is noticed that the theoretical

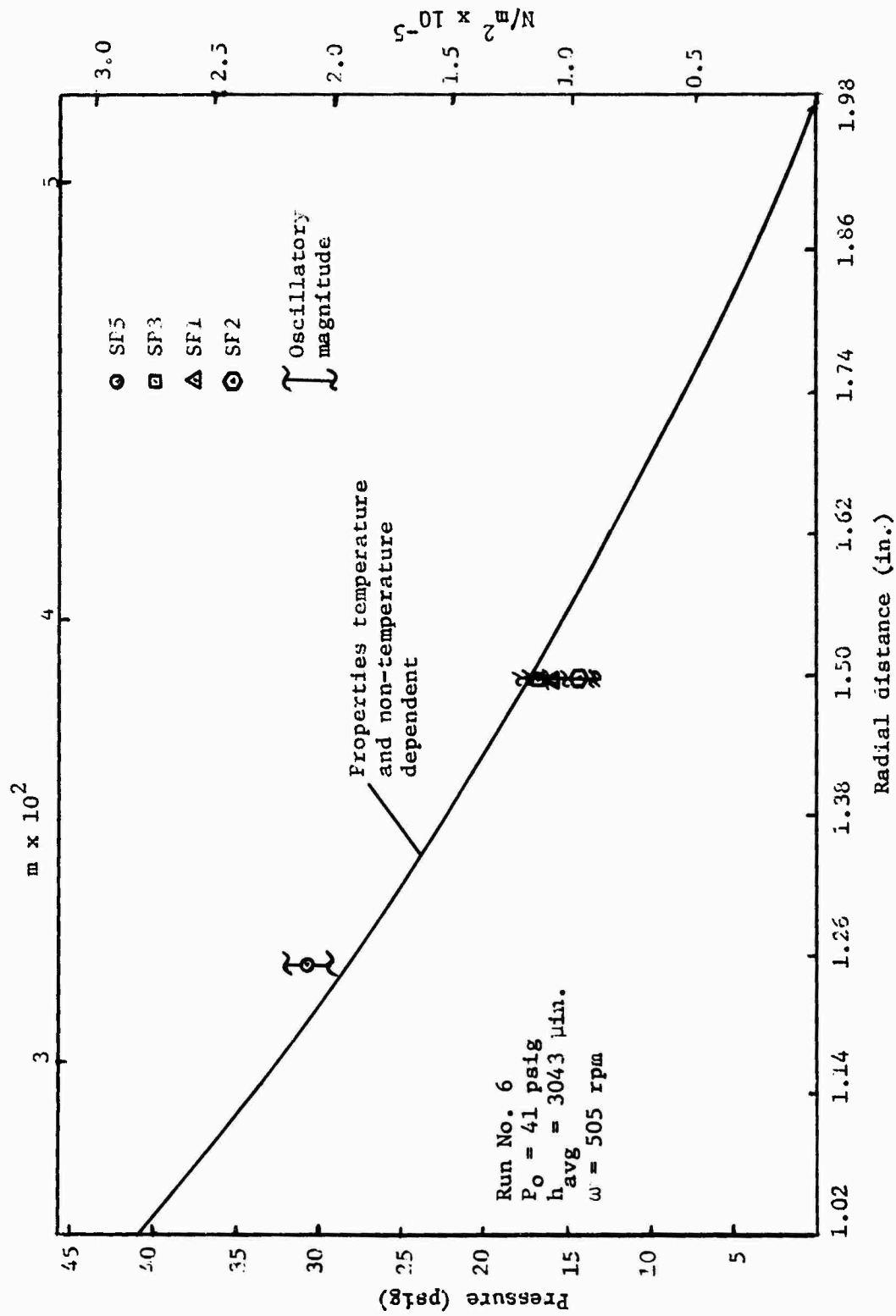


Figure 27. Seal Pressure vs Radius (Run 6).

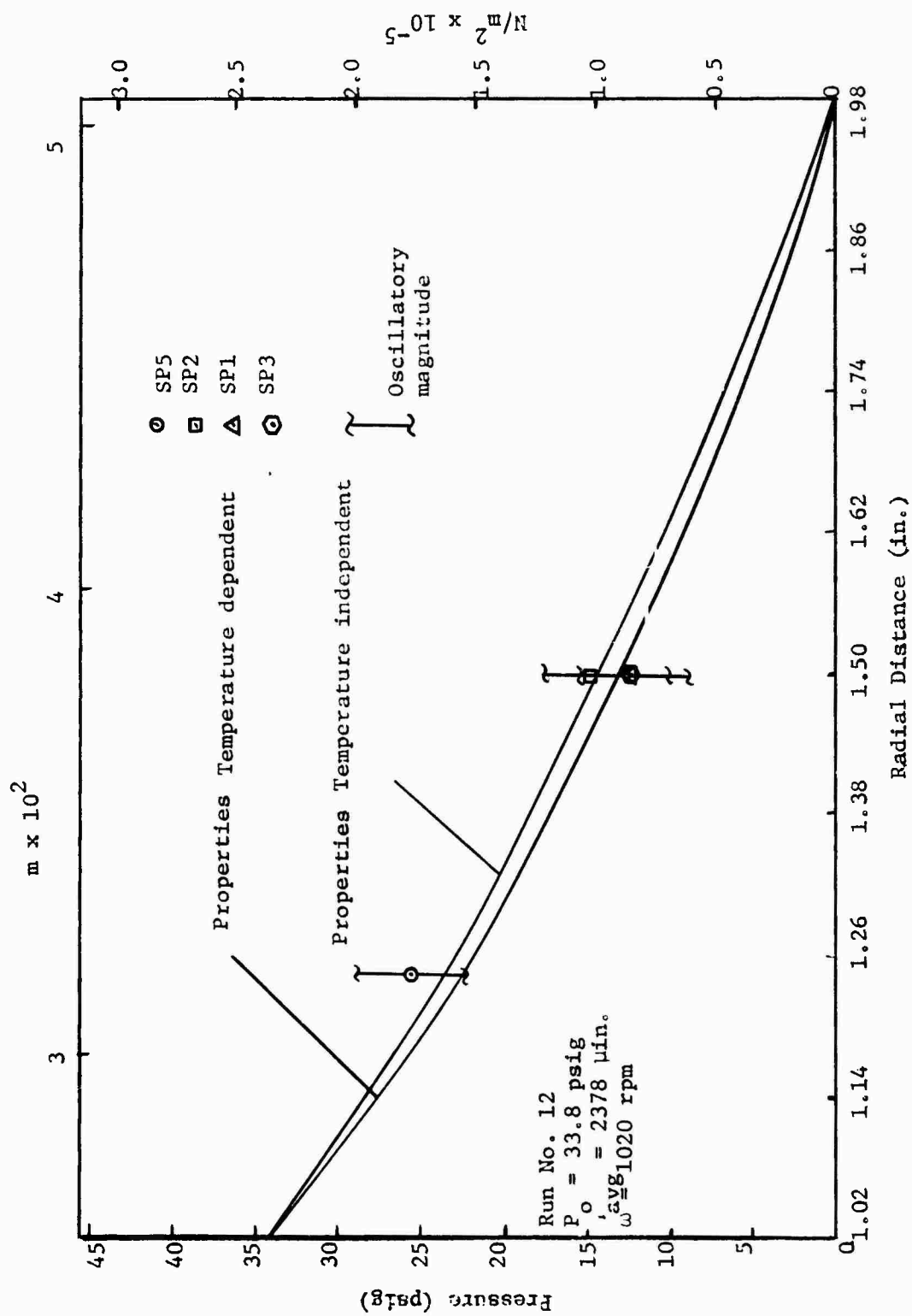


Figure 28. Seal Pressure vs Radius (Run 12).

solutions based on temperature-dependent and temperature-independent fluid properties have significant differences when rotational speed is high and clearance is low. Experimentally obtained interface pressure at the innermost radius is consistently higher than both theoretical methods indicate. At a radius of 1.5 inches, pressure probes SP1 and SP3 seem to agree very well with the temperature-dependent fluid property pressure profile. However, as Figure 29 shows, at a higher speed and lower supply pressure (which effects temperature rise similar to low clearances), pressure probe SP5 yielded an average pressure considerably lower than predicted values, while probes SP3 and SP1 agreed with the non-temperature-dependent fluid property value. Similar to probe SP5, probe SP2 output fell significantly lower than predicted. Note also that probe SP2 indicated a zero gage pressure at the lower end of its oscillation. As previously mentioned, this occurred during Run 17 as illustrated in Figure 30. Probe SP2 as well as probe SP1 indicated below atmospheric pressures. Also shown in Figure 30 is the "generated pressure" as indicated by probe SP5, which is above that of the supply pressure.

Leakage rates. Table VIII gives theoretical temperature-dependent and temperature-independent fluid property leakage rates as well as experimentally determined leakage rates. As Table VIII shows, experimental mass flow rates are consistently lower than those predicted by theory. One interesting trend is that theory predicts increasing leakage with increasing rotational speed which agrees with experimental tests at high clearances (Runs 1 through 8).

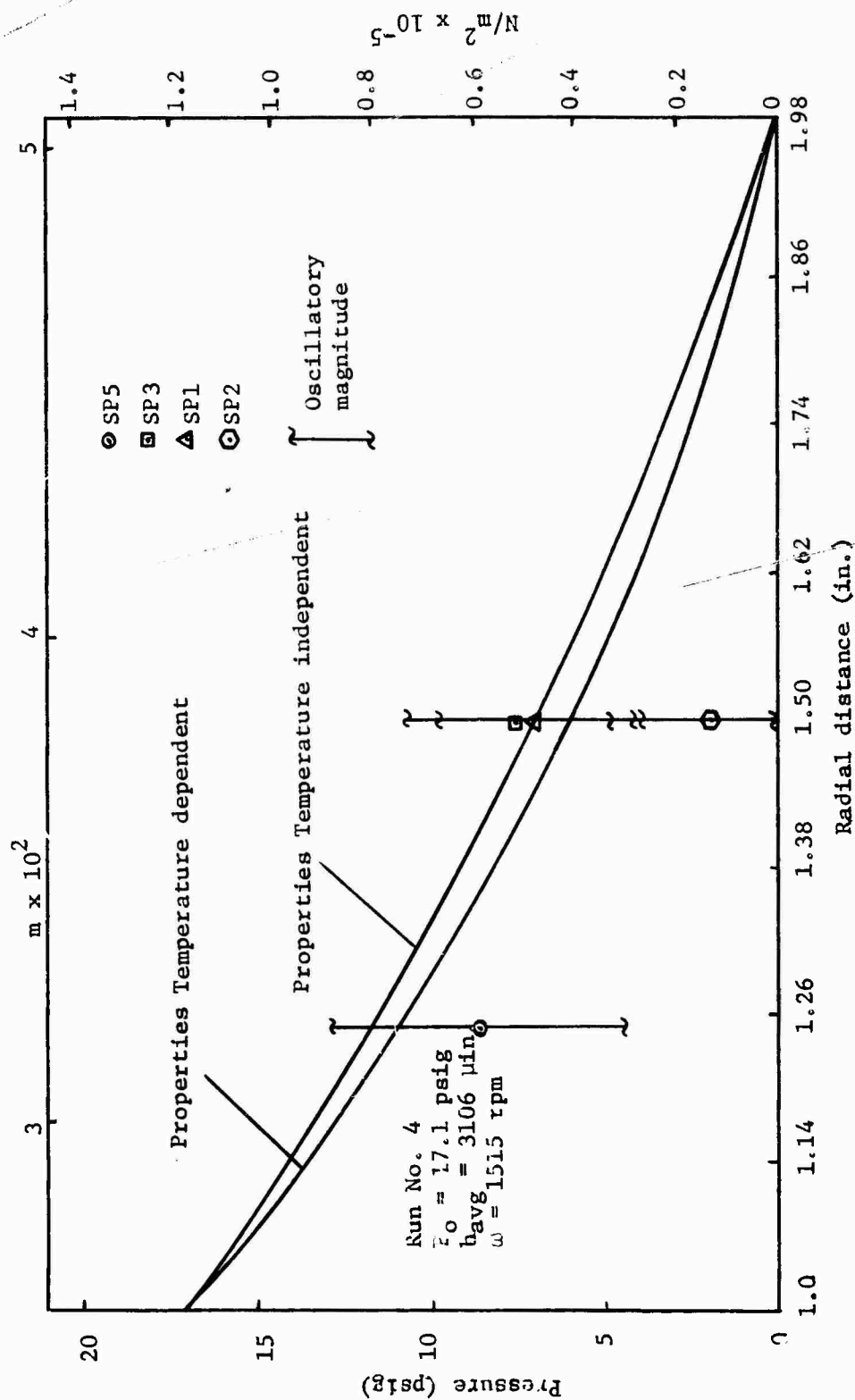


Figure 29. Seal Pressure vs Radius (Run 4).

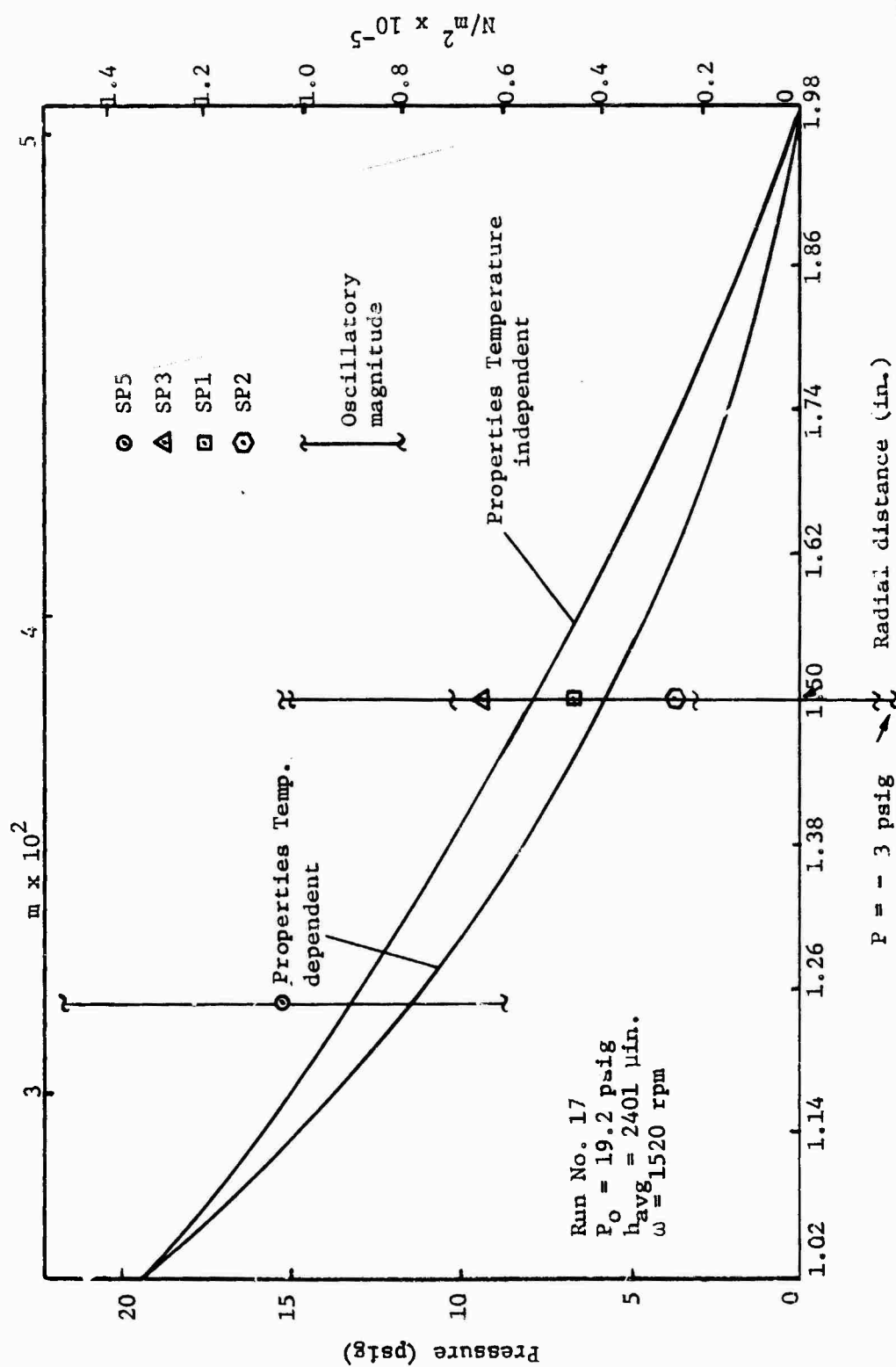


Figure 30. Seal Pressure vs Radius (Run 17).



TABLE VIII

EXPERIMENTAL, TEMPERATURE-DEPENDENT, AND NON-TEMPERATURE-DEPENDENT FLUID  
PROPERTY LEAKAGE RATE COMPARISONS (RUNS 1 THROUGH 17)

Run No.	Supply Pressure (psig)	Average Clearance ( $\mu$ in.)	RPM	Leakage Rate (lbm/min)		
				Exp.	T0	TI
1	17.4	2858	0	0.168	0.194	0.194
2	17.4	2840	490	0.174	0.196	0.190
3	17.1	2953	980	0.178	0.233	0.214
4	17.1	3106	1515	0.183	0.295	0.256
5	41.0	3055	0	0.486	0.555	0.555
6	41.0	3043	505	0.499	0.550	0.550
7	41.0	3118	1000	0.499	0.618	0.596
8	41.2	3175	1510	0.519	0.690	0.640
9	87.5	3528	0	-	1.825	1.825
10	41.5	2282	0	0.207	0.234	0.234
11	36.1	2238	505	0.180	0.200	0.193
12	33.8	2378	1020	0.175	0.244	0.218
13	34.4	2564	1520	0.171	0.330	0.283
14	20.8	1995	0	0.058	0.078	0.078
15	20.0	2022	515	0.058	0.088	0.079
16	19.5	2194	1015	0.056	0.122	0.099
17	19.2	2401	1520	0.053	0.174	0.132

Exp = experimental; T0 = properties temperature-dependent;  
TI = properties temperature-independent.

However, at low clearances (Runs 10 through 17), it seems that leakage decreases with increasing seal rotational speed which, in turn, causes substantial differences when comparing experimental and theoretical values.

However, as shown in Table VIII (page 83) theory and experiment do agree with respect to increasing leakage as supply pressures increase and also in that leakages decrease as clearances decrease. Table VIII also shows that differences between theoretical and experimental leakage rates increased with increasing supply pressure.

Torque. As previously mentioned, theory predicts no torque fluctuation while experiments give evidence that small torque oscillations did occur. However, it is felt that the observed torque oscillations occurred due to vertical load effects on the torque strain gages. Since pressure fluctuations did take place which in turn caused vertical load oscillations, it is entirely possible that these load oscillations would have an effect on torque output.

Figures 31, 32, and 33 show theoretically determined torque as a function of clearance at different seal speeds and supply pressures. Superimposed on these plots are experimentally determined torque values (torque values found during Runs 11 through 13 have been omitted due to obviously erroneous results caused again by vertical load effects). It is seen that results between experiment and temperature-dependent fluid property values agree quite favorably, especially at low seal speeds. However, as seal speeds increase, so do the differences between theory and experiment. These

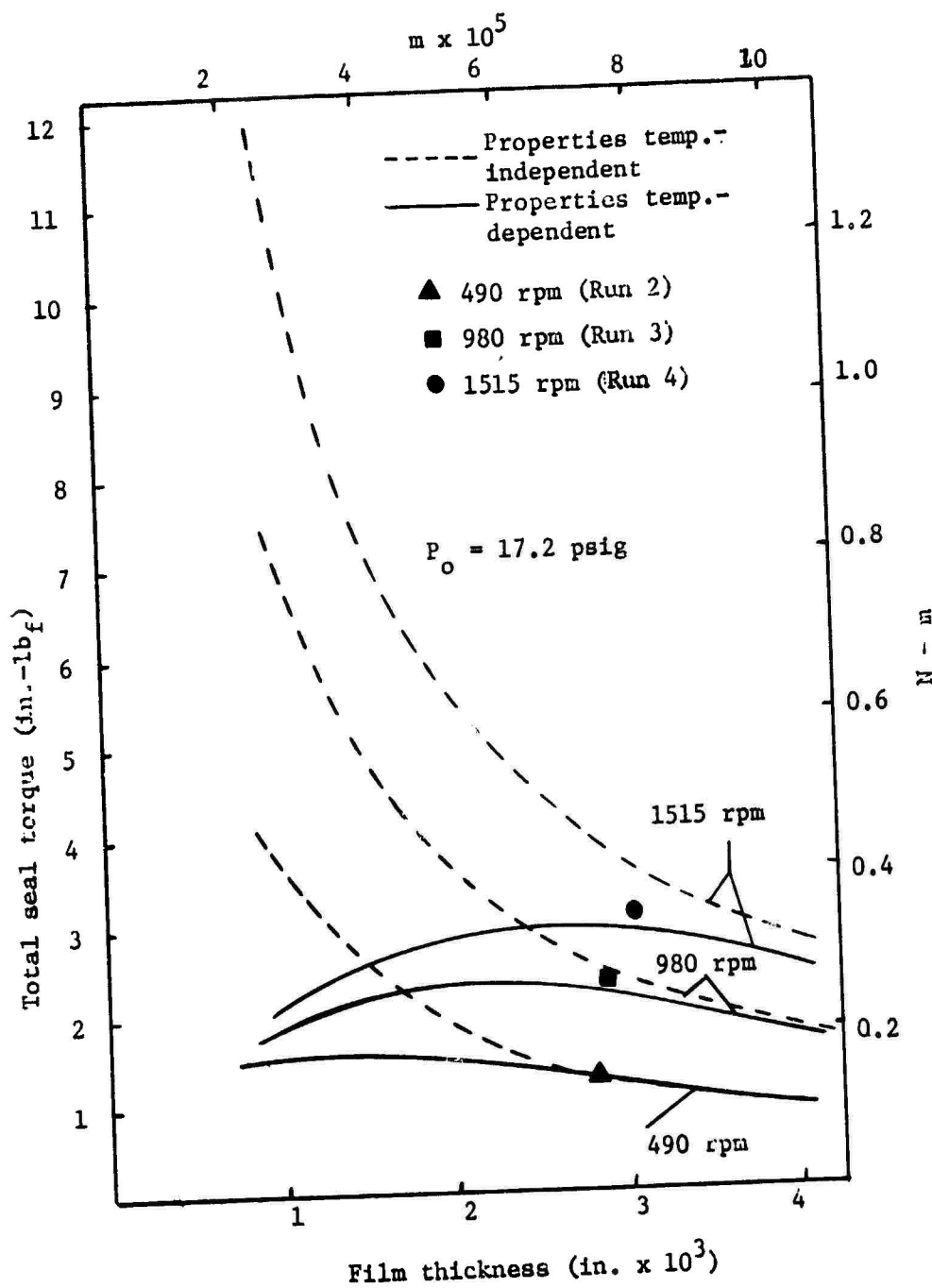


Figure 31. Seal Torque vs Clearance (Runs 2, 3, and 4).

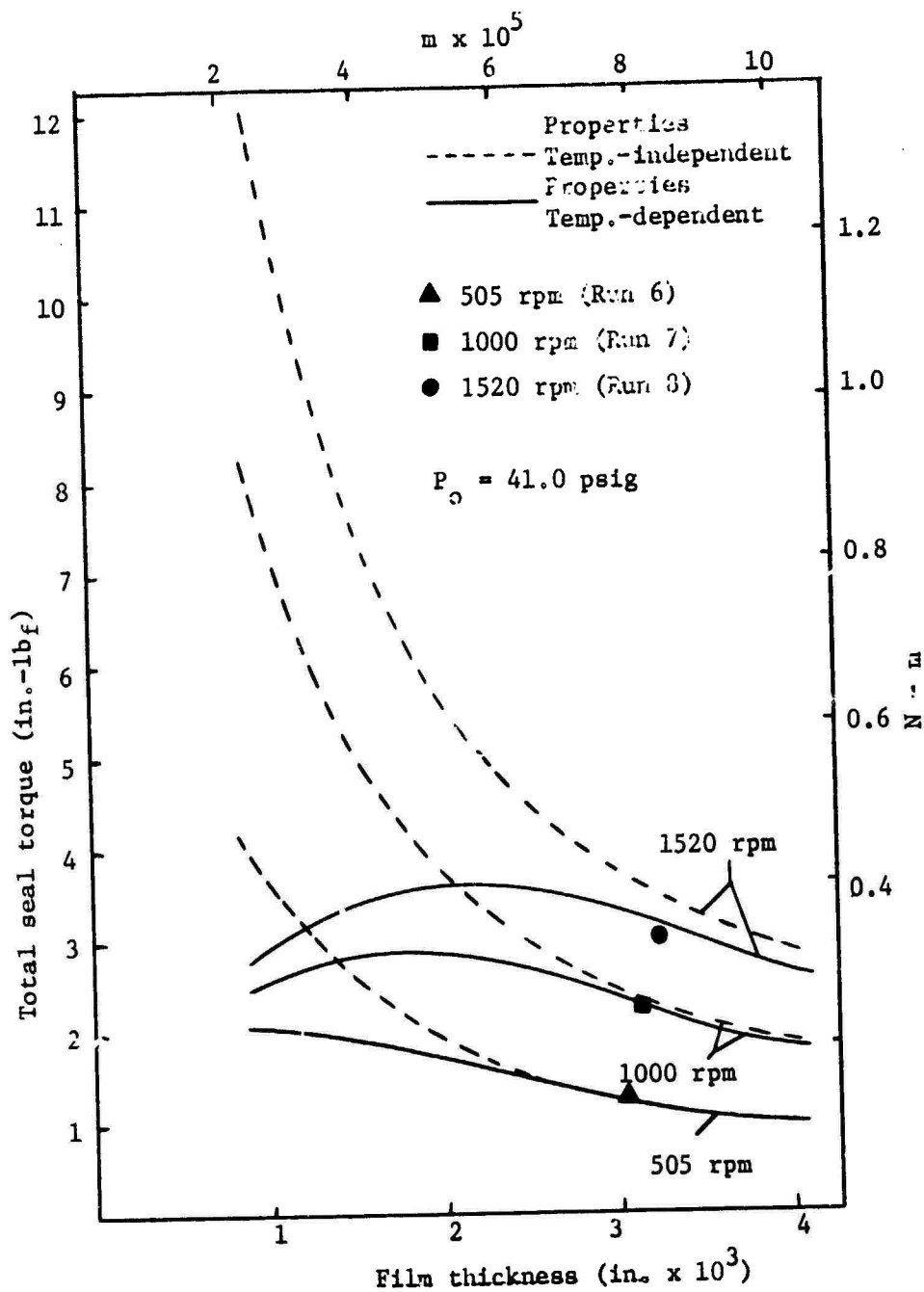


Figure 32. Seal Torque vs Clearance (Runs 6, 7, and 8).

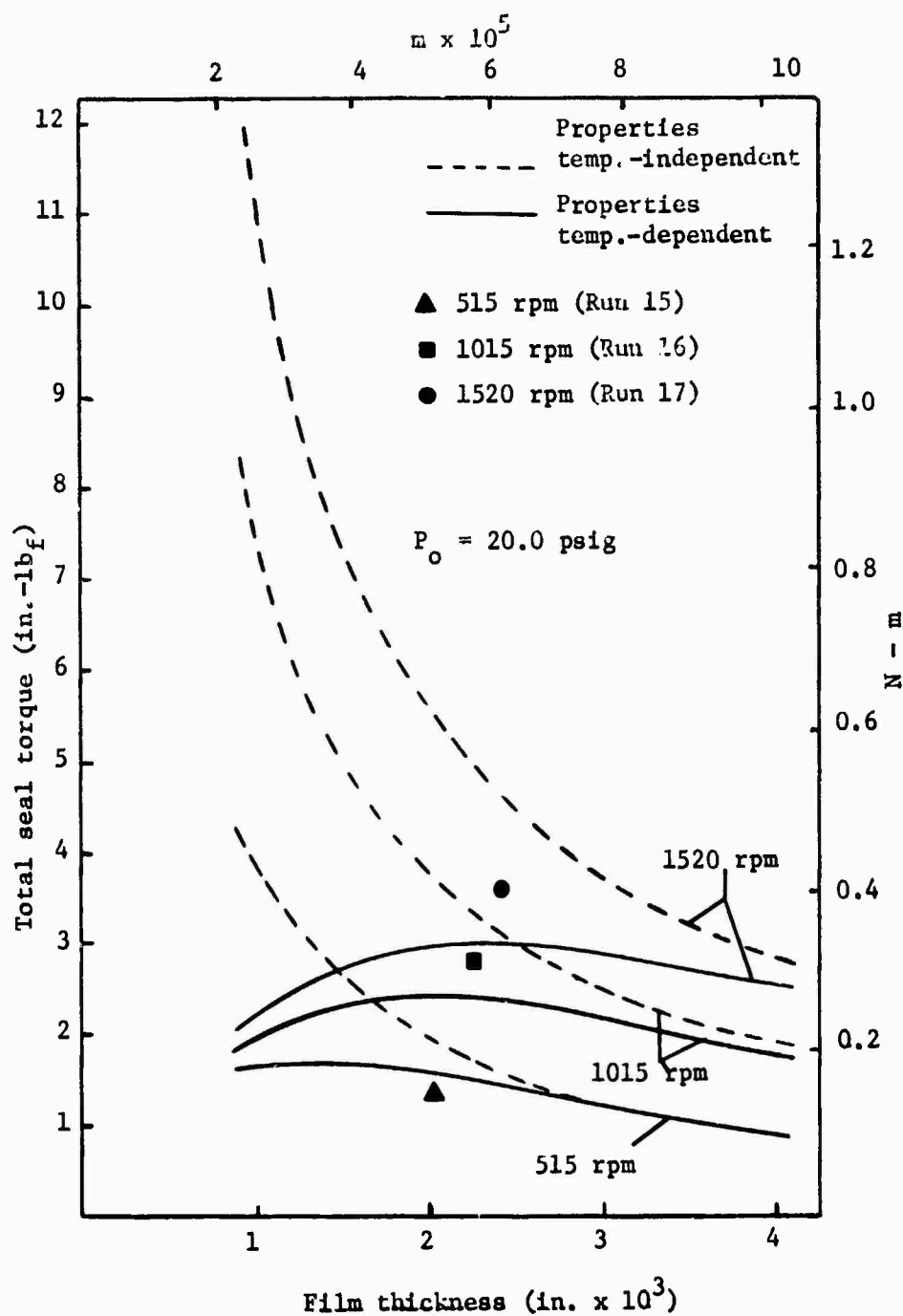


Figure 33. Seal Torque vs Clearance (Runs 15, 16 and 17).

figures show also that torque increased as seal rotational speed increased and that torque increased as clearance decreased.

Vertical load. Table IX shows vertical loads determined experimentally and also those predicted by theory. As Table IX illustrates, experimentally obtained loads were, in most cases, lower than those predicted. However, experimental values were occasionally slightly higher (Runs 5 and 6, high clearance and supply pressure). From these experimental runs, it seems that differences between theory and experiment decreased as supply pressure increased.

Numerical results indicate that loading decreases with increasing seal speed. Experimental evidence supports this somewhat but not consistently. Also, experimental findings lead to the consideration that loading is not strongly dependent on clearance or speed but mostly depends upon supply pressure which theory also indicates.

As mentioned previously, small load fluctuations were noticed at low clearances and high speeds. The mathematical model presented does not predict this experimentally observed phenomena; this should be expected since pressure oscillations are also unpredictable employing the presented model.

Interface temperature. Theoretical interface temperature profiles indicate fluid temperatures are greater towards the outer seal periphery. Figure 34 illustrates this along with typical experimental results at low clearances. However, as Figure 35 shows, at high clearances, the time involved in heating up the seal is longer, thus causing conduction back towards the seal centerline.

TABLE IX

EXPERIMENTAL, TEMPERATURE DEPENDENT, AND NON-TEMPERATURE-DEPENDENT FLUID  
PROPERTY VERTICAL LOAD COMPARISONS (RUNS 1 THROUGH 17)

Run No.	Supply Pressure (psig)	Average Clearance ( $\mu$ in.)	RPM	Vertical Load ( $lb_f$ )		
				Exp.	TO	TI
1	17.4	2858	0	96.2	118.7	118.7
2	17.4	2840	490	87.5	117.7	118.6
3	17.1	2953	980	96.2	113.2	116.3
4	17.1	3106	1513	91.8	110.8	115.8
5	41.0	3055	0	296.9	279.9	279.6
6	41.0	3043	505	303.4	281.4	279.5
7	41.0	3118	1000	275.1	276.4	279.3
8	41.2	3175	1510	270.7	272.9	280.1
9	87.5	3528	0	523.9	598.4	596.8
10	41.5	2282	0	279.1	283.4	283.0
11	36.1	2238	505	210.4	243.4	246.1
12	33.8	2378	1020	171.8	222.6	230.1
13	34.4	2564	1520	171.8	223.2	233.8
14	20.8	1995	0	-	141.9	141.9
15	20.0	2022	513	-	131.3	136.3
16	19.5	2194	1013	-	125.2	132.6
17	19.2	2401	1520	-	118.7	130.1

Exp = experimental; TO = properties temperature-dependent,  
TI = properties temperature-independent.

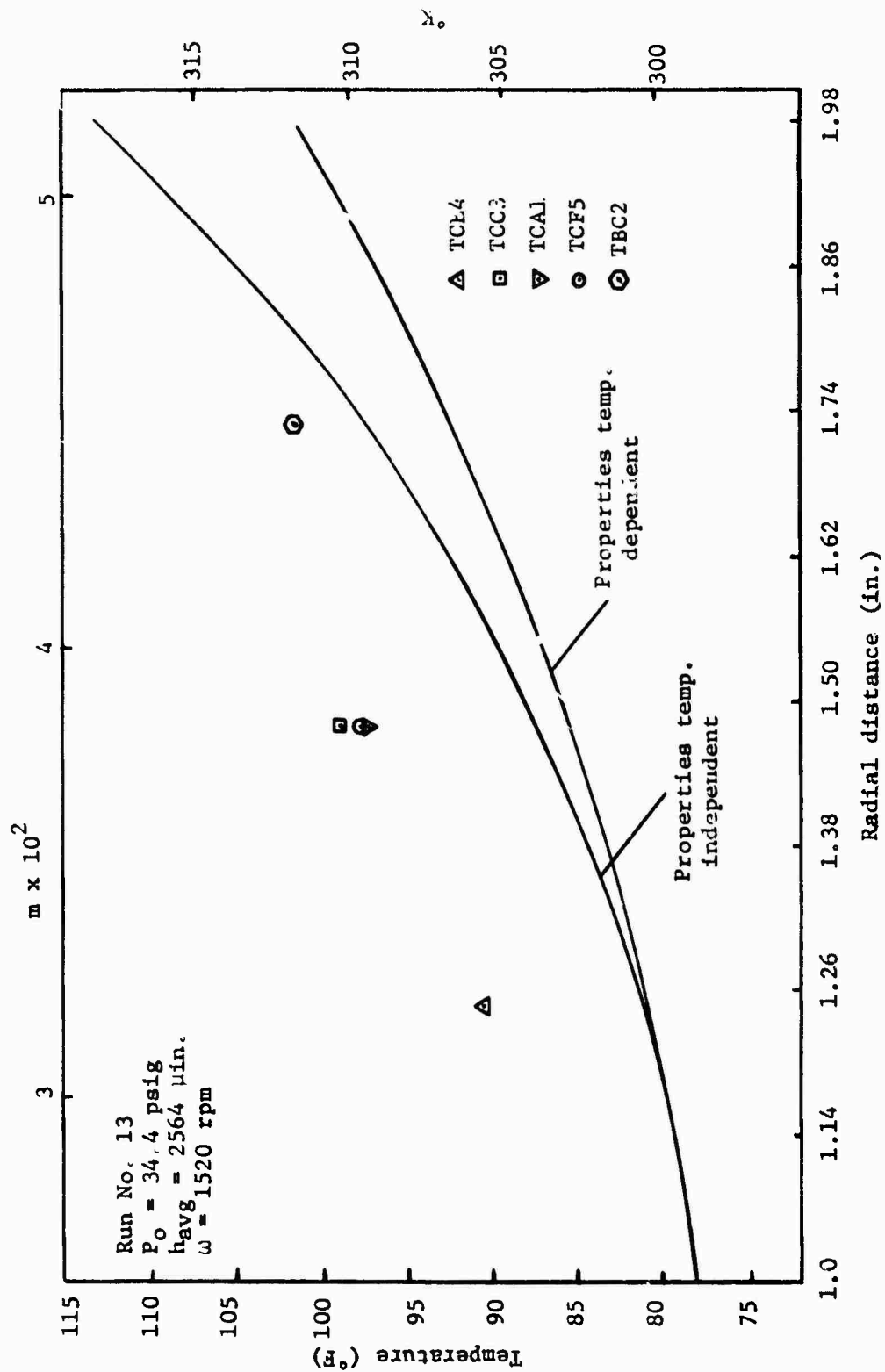


Figure 34. Temperature vs Radius (Run 13).



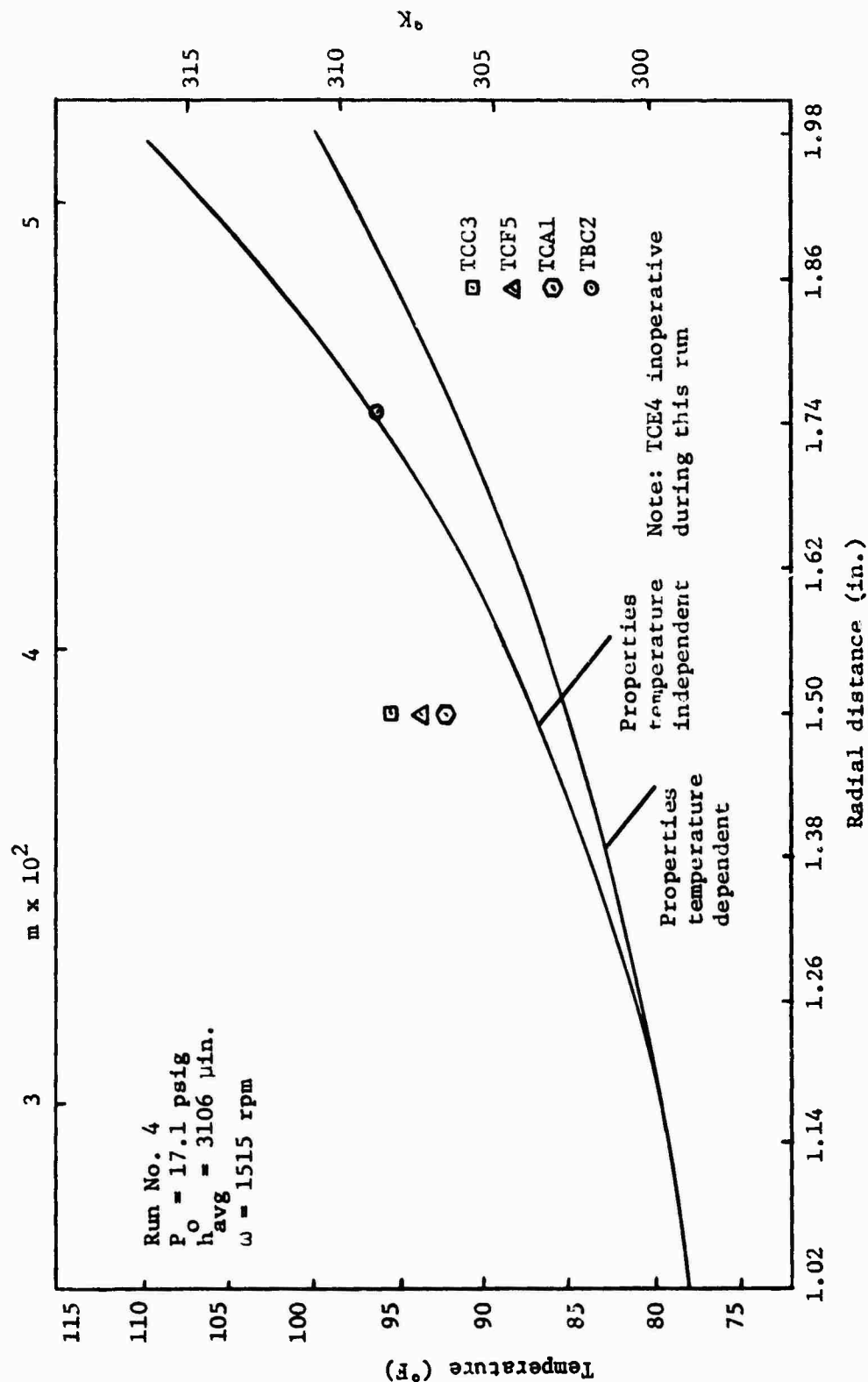


Figure 35. Temperature vs Radius (Run 4).

This was especially true towards the end of each testing period. Figure 36 shows temperature results obtained after the seal had been rotated at 1500 rpm for about one minute, stopped, and then allowed to cool down with fluid still flowing at zero rpm. As Figure 36 illustrates, conduction has taken place due to the temperature difference between outer and inner radii.

It should be noted that the experimental temperature data which are used in Figure 36 were not obtained during runs which are presented in this investigation. Data concerning Figure 36 were obtained primarily to study flow rate values as the test seal cooled down.

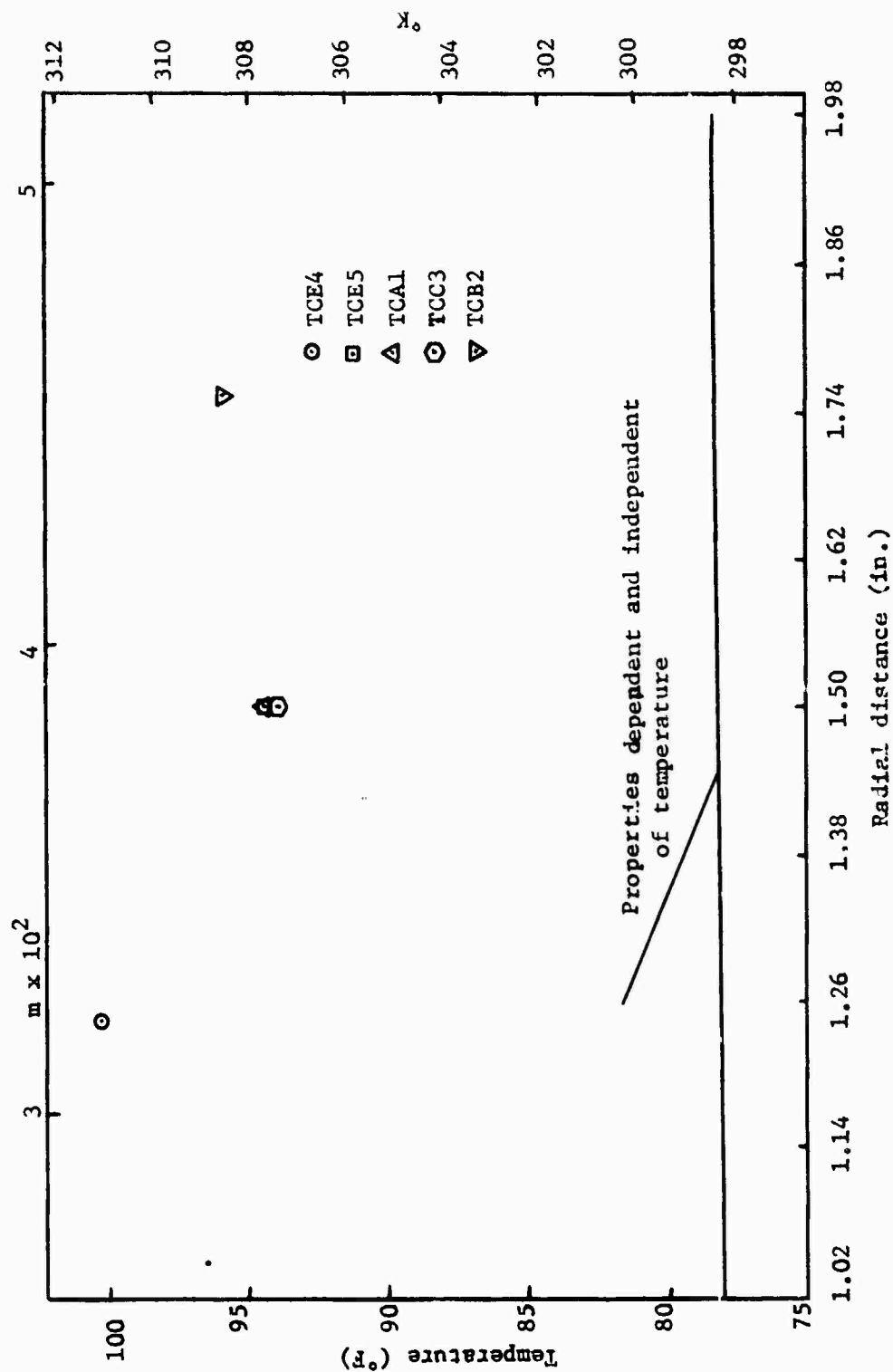


Figure 36. Temperature vs Radius.

## CHAPTER VI

### CONCLUSIONS AND RECOMMENDATIONS

As evidenced in Chapter V, significant differences between numerical predictions involving temperature-dependent and temperature-independent fluid properties arise if sealing conditions exist such that temperature rise across the seal face becomes appreciable. It is felt that the analytical approach taken regarding temperature-dependent fluid properties would suffice if laminar flow and non-boundary lubrication conditions existed and also if the two sealing surfaces were perfectly flat, aligned, and smooth. However, as shown by the experimental results concerning pressure and clearance fluctuation, conditions of seal face parallelism and flatness did not exist during the experimental testing. Therefore, it is concluded that the analytical approach described in Chapter II is an oversimplification of the flow phenomena which is actually occurring. It seems that an input variable concerning clearance as a function of angular position (with respect to the rotating surface) would be a more realistic condition in regard to the observed experimental data. Sneek (20, 21) did analytical studies of face seals considering sealing surface eccentricities and tangentially varying film thicknesses but assumed however that fluid properties were not affected by temperature across the seal face. As suggested above, consideration of sealing surface imperfections is certainly more realistic than

assuming ideal conditions prevail. Therefore, the coupling of Sneck's work plus the temperature-dependent fluid property model described in this investigation would yield yet a new model closely resembling the actual flow situation. Also, since fluid specific heat ( $C_p$ ) is temperature-dependent, a mathematical relationship needs to be developed such that any variation of this property (due to temperature) can be accounted for.

Temperatures calculated by the computer program are actual fluid temperatures whereas temperatures experimentally determined are the seal face diaphragm temperatures. Since the experimental data point to the possibility of heat conduction within the seal face, the program also needs to be modified such that any temperature time dependence concerning heat conduction within both seals can be accounted for.

The experimental test seal employed in this investigation was somewhat larger than commercial "off the shelf" radial face seals. Also, both surfaces were made of stainless steel. It is recognized that this is basically a disparity with respect to past experimental investigations since previous test seals were constructed of carbon. However, a test seal composed of a carbon compound is under consideration where the basic concern is with respect to the inductance clearance probes; i.e., clearance probe sensitivities will have to be of the same order of magnitude as those determined in this study employing a stainless steel test seal.

Experimental run times during any particular testing period never exceeded three to four minutes. Thus, the condition of thermal

equilibrium was not reached during any test. In effect, this means that the seal (both rotating and stationary) could actually have been thermally expanding during testing. The manner in which seal piece thermal expansion would take place is of prime importance when operating at low clearances and high rotational speeds. It is therefore recommended that tests be carried out for longer periods of time in order to study any possible thermal growth of the test seals. Since this thermal expansion could possibly result in the destruction (i.e., seizure) of the test seal apparatus, the above tests are necessary before any low clearance (1000 micro-inches or less) data can be obtained with reasonable safety.

The basic data acquisition system has proven to be extremely adequate in its ability to record numerous experimental parameters. With exception to torque sensitivity to vertical load, all transducers performed adequately during testing. It is therefore recommended that, if feasible, torque strain gages be installed such that an applied vertical load would have a nominal effect on torque output.

Pressure probe installation proved to be more difficult than originally estimated. The probes themselves were found to be extremely delicate with respect to the wire leads which are attached to the strain gage. Also, the author is not convinced that pressure probe diaphragm thicknesses are consistently 0.005 inch. As previously mentioned, one probe was destroyed during the installation process because the probe's diaphragm was apparently lapped off. It is believed that the probe's initial diaphragm thickness (prior to lapping) was not more than 0.003 inch since, at the time of

installation, the seal face was estimated to be not more than 1000 micro-inches out of flat. Nevertheless, if new pressure probes are to be installed, it is recommended that the seal face be lapped as flat as possible prior to probe installation to guard against any adverse conditions concerning the installation procedure.

It is believed that the clearance probes employed during this investigation are temperature sensitive. This possible temperature sensitivity needs to be investigated with respect to future investigations. Work is currently being directed toward this goal and results should be invaluable when operating at realistic face seal clearances and high rotational speeds.

The clearance probes used in this investigation were found to be much less pressure sensitive than those employed by Kiber (10). It is believed that this reduction of pressure sensitivity was primarily due to two differences in the basic seal design: (1) a machined-in-place diaphragm was employed in this study whereas Kiber used a diaphragm which had been epoxied to the seal face, and (2) Devcon Aluminum Putty provided a clearance probe adhesive in this investigation while Kiber employed a commercial epoxy.

As discussed in Chapter V, fluctuating pressures and clearances could have been due to the "wobble" in the rotating seal piece. To reduce the magnitude of this "wobble," it is suggested that the rotating seal be removed from the air spindle and checked for parallelism between sealing surface and the air spindle mounting surface. After this is accomplished, re-installation of the rotating seal should be carried out very carefully, i.e., to be confident that both pieces fit together properly.

From a physical standpoint, it certainly seems more realistic to assume that fluid properties would vary with temperature across the seal face. However, insufficient experimental evidence was gathered to substantiate this assumption. Therefore, it is recommended that tests be carried out at lower clearances in order to validate the temperature-dependent fluid property theory.

The overall purpose of this thesis was to present face seal analyses from both analytical and experimental aspects. Substantial amounts of data have been presented and it is believed that implementation of the suggestions given, particularly those concerning the integration of Sneek's (19, 20) model and the model presented in Chapter II, could very well result in a complete and accurate interface region description concerning a radial face seal.



## BIBLIOGRAPHY

## BIBLIOGRAPHY

1. Denny, D. F., "Some Measurements of Fluid Pressures Between Parallel Thrust Surfaces with Special Reference to Radial Face Seals," *Wear*, 4, pp. 64-83, 1961.
2. Ishiwata, H. and Hirabayashi, H., "Friction and Sealing Characteristics of Mechanical Seals," First International Conference on Fluid Sealing, B.H.R.A. Paper D5, April, 1961.
3. Summers-Smith, D., "Laboratory Investigation of the Performance of a Radial Face Seal," First International Conference on Fluid Sealing, B.H.R.A. Paper D1, April, 1961.
4. Batch, B. A. and Iny, E. H., "Pressure Generation in Radial Face Seals," Second International Conference on Fluid Sealing, B.H.R.A. Paper F4, April, 1964.
5. Bremner, G. F., "Experimental Study of Balance Conditions, Leakage Rates, and Pressure Profiles for Stationary Radial Face Seals," Second International Conference on Fluid Sealing, B.H.R.A. Paper F2, April, 1964.
6. Pape, J. G., "Fundamental Research on a Radial Face Seal," *ASLE Transactions* 11, pp. 302-309, 1968.
7. Stanghan-Batch, B. A., "Face Lubrication in Mechanical Seals," *Tribology Convention-Institution of Mechanical Engineers*, pp. 54-59, 1971.
8. Wilhelm, L. R., "Turbulence and Inertia Effects in the Aligned Face Seal," Ph.D. Dissertation, The University of Tennessee, Knoxville, Tennessee, August, 1971.
9. Snapp, R. B., "Theoretical Analysis of Face-Type Seals with Varying Radial Face Profiles," *ASME WA/LUB-6*, 1964.
10. Kiber, G. M., "An Experimental Investigation of a Radial Face Seal," M.S. Thesis, The University of Tennessee, Knoxville, Tennessee, June, 1975.
11. Duncan, W. R., "Development of a Nonpenetrating Inductance Probe for Measuring Lubricating Film Thickness in a Dynamic Seal," Ph.D. Dissertation, The University of Tennessee, Knoxville, Tennessee, December, 1974.

12. Fuller, D. D., Theory and Practice of Lubrication for Engineers. New York: John Wiley and Sons, Inc., 1956.
13. Fisher, C. F., Jr. et al., "Basic Research in Dynamic Sealing," Mechanical and Aerospace Engineering Department Report ME 71-T57-13, The University of Tennessee, Knoxville, Tennessee, 1971.
14. Fisher, C. F., Jr. et al., "Basic Research in Dynamic Sealing," Mechanical and Aerospace Engineering Department Report ME 71-T57-14, The University of Tennessee, Knoxville, Tennessee, 1972.
15. Wilkerson, H. J., personal communication, June, 1974.
16. Bliem, C. J., personal communication, August, 1975.
17. Galyon, M. E., personal communication, November, 1975.
18. Zimmerman, G. P., personal communication, August, 1975.
19. Littrell, J. J., personal communication, November, 1975.
20. Sneck, H. J., "The Misaligned, Eccentric Face Seal," Fourth International Conference on Fluid Sealing, A.S.M.E., April, 1969.
21. Sneck, H. J., "The Eccentric Face Seal with a Tangentially Varying Film Thickness," Fourth International Conference on Fluid Sealing, A.S.M.E., April, 1969.

APPENDICES

## APPENDIX A

### COMPUTER PROGRAM

The FORTRAN IV computer program employed in this investigation is given below. The program considers the possibility of temperature-dependent fluid properties as the fluid flows across the seal face.

Program input consists of supply pressure, seal rotational speed, and average clearance. It should be noted that no provision has been made for the possibility of wavy seal surfaces or any time-dependent heat conduction within the sealing surfaces themselves.

Typical central processing unit run time for "moderate" sealing conditions (low speed, medium clearance) was approximately 30 seconds. However, at low clearances and supply pressures, run time often exceeded two minutes.

SWAFFORD'S VARIABLE PROPERTY SEAL PROGRAM  
DEPARTMENT OF MECHANICAL AND AEROSPACE ENGINEERING  
UNIVERSITY OF TENNESSEE

THIS PROGRAM EVALUATES THE CHARACTERISTICS OF A PARALLEL FACED SEAL AS A FUNCTION OF RADIAL DISTANCE. THE PROPERTIES OF THE OIL (DENSITY AND VISCOSITY) ARE FOUND FOR EACH DELTA R INCREMENT THROUGHOUT THE TOTAL RADIUS OF THE SEAL.

THE FOLLOWING VARIABLES ARE EMPLOYED IN THE PROGRAM:

1.  $\dot{M}$ DOT1=MASS FLOW RATE DETERMINED FROM COMPUTER RUNS ASSUMING CONSTANT PROPERTIES (UNITS OF LBF-SEC/IN)
2.  $R$ =RADIAL DISTANCE FROM THE CENTERLINE OF THE SEAL
3.  $P$ OLD=PRESSURE AT THE BEGINNING OF EACH DELTA R INCREMENT (INITIALLY AT THE SUPPLY PRESSURE)
4.  $P$ NEW=PRESSURE EVALUATED FROM ASSUMING CONSTANT PROPERTIES OVER THE SMALL DELTA R
5.  $\dot{M}$ DOT=MASS FLOW RATE EVALUATED AT EACH DELTA R INCREMENT (SAME UNITS AS ABOVE)
6.  $Q$ =VOLUMETRIC FLOW RATE (UNITS OF IN\*\*3/SEC)
7. SPECIFIC HEAT IS ASSUMED CONSTANT AT 0.45 BTU/LBM-F
8.  $R$ 1=RECESS RADIUS (UNITS OF INCHES)
9.  $R$ 2=OUTSIDE RADIUS (UNITS OF INCHES)
10. OIL IS ASSUMED TO ENTER SEAL RIG AT "TFIRST" DEG F

[illegible]





SEAL0530  
SEAL0540  
SEAL0550  
SEAL0560  
SEAL0570  
SEAL0580  
SEAL0590  
SEAL0600  
SEAL0610  
SEAL0620  
SEAL0630  
SEAL0640  
SEAL0650  
SEAL0660  
SEAL0670  
SEAL0680  
SEAL0690  
SEAL0700  
SEAL0710  
SEAL0720  
SEAL0730  
SEAL0740  
SEAL0750  
SEAL0760  
SEAL0770  
SEAL0780  
SEAL0790  
SEAL0800  
SEAL0810  
SEAL0820  
SEAL0830  
SEAL0840  
SEAL0850

```

      KK=0
      LL=0
      R63 T=TFIRST
      DELT=0.12
      IFLAG=1

C     SINCE THE ACTUAL VALUES OF DATA ARE NOT PRINTED OUT UNTIL A
C     CORRECT VALUE OF MASS FLOW RATE HAS BEEN DETERMINED, THE SUPPLY
C     PRESSURE HAS TO BE REINITIALIZED
      POLD=R=SETP

C
      PJ=POLD
      L=0
      JJ=0
      N=0
      ZOT=PI
      MUMENT=0.000
      CP=0.4500
      VM=0
      K=0
      PING=0.000
      TOTALM=0.000
      TOTAL=P*PI*R1*H1

C     USE SUBROUTINE TO INITIALIZE VARIABLES
C     CALL INITL(PING,POLD,TOTALM,T,PI,MDOUL,R1,TOTALL,I,H,W,RPM,LL,
C     IFLAG,PPLDT,PPLDT,MPLDT,TPLDT,LPLDT)
C
C     ASSUME SMALL DELTA R FOR GOOD ACCURACY
      5 DELTA=5.00-3

```

```

J=0
EQU FOR SQ WAS DERIVED EMPIRICALLY
10 SG=-4.05685E-4*T+0.903076500
   RHQ=53*(62.400/(172800*32.171900*12.000))
   XX=T+460.000
   X=-3.8046600* DLOG10(   XX   )+10.5381200
   XX=10.000**X
EQUATION FOR NJ FROM "THEORY AND PRACTICE OF LUBRICATION FOR
ENGINEERS", BY FULLER(P. 49,EQN. 24)
   MU=(-0.800+10.000**XX)*1.080-5*144.000
   MU=MU*240
   T=DELTA*PI*NG
   VY=(P+DELTA)*R
EQU FOR P,CM,Q,AND MOMENT DERIVED FROM ASSUMING CONSTANT PROPERTIES
ACROSS THE SMALL DELTA R
   PHEX=0.000+13.000*(**2.000)*RHO*(2.000*R*DELTA+DELTA**2.000)/
120.000 - ((DLOG(VY))*6.000*MOD(1*NJ))/(PI*(H**3.000))
   DELTAP=PNEW-POLD
   Q=((PI*(R+DELTA)*H**3.000)/(6.000*U))*((3.000*KHO*(R+DELTA))*
1W**2.000)/10.000-DELTAP/DELTA
   C1=(2.0*PI*U*W)/(4.000*H)
   C2=4.000*(R**3.000)*DELTA+6.000*(P**2.000)*(DELTA**2.000)+4.000*R*
1(DELTA**3.000)+DELTA**4.000
   MOMENT=C1+C2
   K1=776.000
   K2=144.000
   EF=M*MOMENT +Q*QABS(DELTA)

```

```

C      DELTAT=EG/(G*RH0=CP*K1*K2*32.171900)
C      C=DELTA T
C      CHECK TO SEE IF TEMPERATURE RISE HAS AFFECTED PROPERTIES OF OIL
C
C      CALL CHECKLIT,MOOT,R,W,DELTAR,PI,H,DELTAP)
C
C      IF YES, CHANGE DELTA R AND START AGAIN
C      IF NO, PRINT VALUES
C
C      IF (DABS(MOOT1/MOOT-1.000).GT.1.00-2)    CALL FIND(DELTAR,J,T,
C      IDELTA T)
C      IF (DABS(MOOT1/MOOT-1.000).GT.1.00-2)    GO TO 10
C      IF (DABS(MOOT1/MOOT-1.000).LE.1.00-2)    CALL FOUND(R1,R2,DELTAR,
C      1PI,DELTAR,PNEW,T,J,I,Q,SS,MOMENT,TOTAL,M,TOTAL,K,RING,R,DLOAD,I,
C      2J,POLD,ZJ,N,L,MOOT1,PO,KK,MM,IFLAG,RPLDT,PPLDT,TPLDT,LPLDT)
C      IF (MM.EQ.1)    GO TO 100
C      GO TO 5
C
C      CHECK TO SEE IF EXIT PRESSURE IS CLOSE ENOUGH TO ZERO
C      IF NO, INCREMENT MOOT1 AND START AGAIN
C      IF YES, STOP
C
C      100 IF ((PO-DABS(PNEW))/FD).LT.0.99 DO)    CALL MASS2(JJ,MOOT1,PNEW,PO,
C      101)
C      IF (JJ.EQ.1)    GO TO 888
C      IF (KK.EQ.1)    GO TO 888
C      MOOT2=MOOT1*32.1719*12.0*60.0
C
C      CALL SUBROUTINE TO EVALUATE CONSTANT PROPERTY PRESSURE AND TEMP-
C      ERATURE DISTRIBUTION(FOR COMPARISON PURPOSES)
C
C      CALL CONPRP(RPM,H,PO,PPLCON,RPLCON,TPLCON,TFIRST,CONLG ,CON

```

SEAL1190  
 SEAL1200  
 SEAL1210  
 SEAL1220  
 SEAL1230  
 SEAL1240  
 SEAL1250  
 SEAL1260  
 SEAL1270  
 SEAL1280  
 SEAL1290  
 SEAL1300  
 SEAL1310  
 SEAL1320  
 SEAL1330  
 SEAL1340  
 SEAL1350  
 SEAL1360  
 SEAL1370  
 SEAL1380  
 SEAL1390  
 SEAL1400  
 SEAL1410  
 SEAL1420  
 SEAL1430  
 SEAL1440  
 SEAL1450  
 SEAL1460  
 SEAL1470  
 SEAL1480  
 SEAL1490  
 SEAL1500  
 SEAL1510

```

      ITO,CONMA,CONT3)
      VAPL7 =LPLOT(97)
      VAP10=MPLT(97)
      VAPM7 =MDGT2
      VAP10 =TPLOT(97)
      IF(NELAG.EQ.1) GO TO 400
      CALL PLOT3(LB9F,1000,48.0,'SWAFFORD4','DDJGHERY#')
      CALL FACTOR(0.857)
      CALL FORMS('0010')
      CALL ZIPOFF
      CALL PLOT(0.0,0.5,-3)
      RPLT(98)=R1
      RPLT(99)=DFLR
      CALL SCALE(PPLT,6.0,97,1)
      RPLT(98)=0.0
      CALL SCALE(TPLOT,6.0,97,1)
      TPLOT(98)=TFIRST
      IF(KFL-G.EQ.1) GO TO 2000
      CALL AXIS(0.0,0.0,14-PRESSURE(P5IG),14.0,0,90.0,PPLT(98),
      1PPLT(99))
      CALL PLOT(0.5,0.0,-3)
      CALL AXIS(0.0,0.0,13-TEMPERATURE(UEG F),18.6,0,90.0,TFIRST
      1TPLOT(99))
      CALL PLOT(0.5,0.0,-3)
      CALL SCALE(MPLT,6.0,97,1)
      CALL AXIS(0.0,0.0,14-TORQUE(IN-LBF),14.6,0,90.0,1PLOT(98),
      1MPLOT(99))
      CALL PLOT(0.5,0.0,-3)
      CALL SCALE(LPLOT,6.0,97,1)
      CALL AXIS(0.0,0.0,18-HVERTICAL LOAD(LBF),18.6,0,90.0,LPLOT(98),
      1LPLOT(99))
      CALL PLOT(0.0,0.0,-3)

```

SEAL1515  
 SEAL1520  
 SEAL1521  
 SEAL1522  
 SEAL1523  
 SEAL1524  
 SEAL1525  
 SEAL1530  
  
 SEAL1540  
 SEAL1550  
 SEAL1560  
 SEAL1570  
 SEAL1580  
 SEAL1590  
 SEAL1600  
 SEAL1605  
 SEAL1608  
 SEAL1610  
 SEAL1620  
 SEAL1630  
 SEAL1640  
 SEAL1650  
 SEAL1660  
 SEAL1670  
 SEAL1680  
 SEAL1690  
 SEAL1700  
 SEAL1710  
 SEAL1720  
 SEAL1730  
 SEAL1740  
 SEAL1750

```

RSCALE=(P2-R1)/DELTA+0.1
TSCALE=(ABS(FPLOT(97)-TPLOT(11))/TPLOT(99))
MSCALE=(ABS(MPLOT(97)-MPLT(11))/MPLT(99))
LSCALE=(ABS(LPLOT(97)-LPLOT(11))/LPLOT(99))
CALL AXIS(0.0,0.0,19,RADIAL DISTANCE(IN),-19,8.0,0.0,R1,DELTA)
CALL FLINER(PLOT,PLOT,97,1,0,0)
CALL PLOT(RSCALE,0.1,3)
CALL SYMBOL(PSCALE,0.1,0.07,8,HYPRESSURE,0.0,8)
CALL FLINER(FPLOT,TPLOT,97,1,0,0)
CALL PLOT(PSCALE,TSCALE,3)
CALL SYMBOL(RSCALE,TSCALE,0.07,1,HTEMPERATURE,0.0,11)
CALL FLINER(FPLOT,MPLT,97,1,0,0)
CALL PLOT(RSCALE,MSCALE,3)
CALL SYMBOL(RSCALE,MSCALE,0.07,6,HTORQUE,0.0,6)
CALL FLINER(RPLOT,LPLOT,97,1,0,0)
CALL PLOT(RSCALE,LSCALE,3)
CALL SYMBOL(RSCALE,LSCALE,0.07,10,VERT. LOAD,0.0,10)
CALL SYMBOL(1.0,6.5,0.21,22,HVARIABLE PROPERTY SEAL,0.0,22)
CALL SYMBOL(1.0,6.1,0.07,19,HMASS FLOW(LB/MIN)= ,0.0,19)
CALL NUMBER(99,0.6,1,0.07,MDET2,0.0,3)
CALL SYMBOL(1.0,5.95,0.07,18,H SUP. PRES.(PSIG)= ,0.0,18)
CALL NUMBER(99,0.5,95,0.07,PJ,0.0,1)
CALL SYMBOL(1.0,5.8,0.07,16,H CLEARANCE(IN.)= ,0.0,16)
CALL NUMBER(99,0.5,8,0.07,H,0.0,4)
CALL SYMBOL(1.0,5.65,0.07,17,H SEAL SPEED(RPM)= ,0.0,17)
CALL NUMBER(99,0.5,65,0.07,SPM,0.0,1)

2000 CONTINUE
IF(JFLAG.EQ.1) GO TO 3000
IF(KFLAG.EQ.1) GO TO 2500
CALL PLOT(12.0,0.0,-3)

2500 CONTINUE
CALL AXIS(0.0,0.0,14,HYPRESSURE(PSIG),14,6.0,90.0,PLOT(98),PLOT
1(99))

```

SEAL1770  
 SEAL1780  
 SEAL1790  
 SEAL1800  
 SEAL1810  
 SEAL1820  
 SEAL1830  
 SEAL1840  
 SEAL1850  
 SEAL1860  
 SEAL1870  
 SEAL1880  
 SEAL1890  
 SEAL1900  
 SEAL1910  
 SEAL1920  
 SEAL1930  
 SEAL1940  
 SEAL1950  
 SEAL1960  
 SEAL1970  
 SEAL1980  
 SEAL1990  
 SEAL2000  
 SEAL2010  
 SEAL2020  
 SEAL2030  
 SEAL2040  
 SEAL2050  
 SEAL2060  
 SEAL2070  
 SEAL2080  
 SEAL2090

```

CALL AXIS(0.0,0.0,0.0,19,RAIDIAL DISTANCE(IN),-19,8.0,0.0,0.0,R1,DELR)
CALL LINE(PLOT,PPLT,97,1,0,0)
CALL SCALE(PPLCON,6.0,97,1)
PPLCON(96)=6.0
CALL FLINE(RPLOT,PPLCON,57,1,0,0)
CALL SYMBOL(1.0,0.1,0.07,11,HRJN NUMBER ,0.0,11)
CALL NUMBER(99,0.6,1,0.07,RUN,0.0,1)
CALL SYMBOL(4.0,0.6,1,0.07,14,HVERT.LOAD(LBF),0.0,14)
CALL SYMBOL(4.0,0.5,95,0.07,14,HTORQUE(IN-LBF),0.0,14)
CALL SYMBOL(4.0,0.5,8,0.07,18,HMASS FLOW(LBM/MIN),0.0,18)
CALL SYMBOL(4.0,0.5,65,0.07,18,HOUTLET TEMP(DEG F),0.0,18)
CALL SYMBOL(5.75,6.25,0.07,16,HVP CP,0.0,16)
CALL NUMBER(5.55,6.1,0.07,VARLG ,0.0,2)
CALL NUMBER(5.55,5.95,0.07,VARLQ,0.0,3)
CALL NUMBER(5.55,5.8,0.07,VARMA ,0.0,4)
CALL NUMBER(5.55,5.65,0.07,VARTR ,0.0,2)
CALL NUMBER(6.0,5.1,0.07,CONLC ,0.0,2)
CALL NUMBER(6.65,5.95,0.07,CONLQ,0.0,3)
CALL NUMBER(6.65,5.8,0.07,CONMA ,0.0,4)
CALL NUMBER(6.65,5.65,0.07,CONTC ,0.0,2)
CALL PLOT(3.75,5.5,3)
CALL PLOT(7.25,5.5,2)
CALL PLOT(7.25,6.5,2)
CALL PLOT(3.75,6.5,2)
CALL PLOT(3.75,5.5,2)
CALL PLOT(5.35,5.5,3)
CALL PLOT(5.35,6.5,2)
CALL PLOT(6.35,5.5,3)
CALL PLOT(6.35,6.5,2)
CALL PLOT(0.75,5.5,3)
CALL PLOT(2.75,5.5,2)
CALL PLOT(2.75,6.5,2)
CALL PLOT(0.75,6.5,2)

```

SEAL2100  
 SEAL2110  
 SEAL2120  
 SEAL2125  
 SEAL2130  
 SEAL2140  
 SEAL2150  
 SEAL2160  
 SEAL2161  
 SEAL2162  
 SEAL2163  
 SEAL2164  
 SEAL2165  
 SEAL2166  
 SEAL2167  
 SEAL2168  
 SEAL2169  
 SEAL2170  
 SEAL2171  
 SEAL2172  
 SEAL2173  
 SEAL2174  
 SEAL2175  
 SEAL2176  
 SEAL2177  
 SEAL2178  
 SEAL2179  
 SEAL2180  
 SEAL2181  
 SEAL2182  
 SEAL2183  
 SEAL2184  
 SEAL2185

SEAL2186  
SEAL2187  
SEAL2190  
SEAL2200  
SEAL2210  
SEAL2220  
SEAL2230  
SEAL2231  
SEAL2232  
SEAL2233  
SEAL2234  
SEAL2235  
SEAL2236  
SEAL2237  
SEAL2238  
SEAL2239  
SEAL2240  
SEAL2241  
SEAL2242  
SEAL2243  
SEAL2244  
SEAL2245  
SEAL2246  
SEAL2247  
SEAL2248  
SEAL2249  
SEAL2250  
SEAL2260  
SEAL2270  
SEAL2280  
SEAL2290  
SEAL2300  
SEAL2310

```

CALL PLCT(0.75,5.5,2)
CALL SYM50L(1.0,5.95,0.07,18MSJP. PRES.(PSIG)= ,0.0,18)
CALL NUMBR(999.0,5.95,0.07,0.0,1)
CALL SYM30L(1.0,5.8,0.07,16HCLEARANCE(IN.)= ,0.0,16)
CALL NUMBR(999.0,5.8,0.07,4)
CALL SYM30L(1.0,5.65,0.07,17HSEAL SPEED(RPM)= ,0.0,17)
CALL NUMBR(999.0,5.65,0.07,8PM,0.0,1)
XV=(RPLCT(13)-RPLCT(1))/DELR
YV=PPLCT(13)/HPLCT(99)
XV1=XV+2.0
YV1=YV+1.0
XV2=XV1+0.05
YV2=YV1+0.05
XC=(PPLCT(61)-RPLCT(1))/DELR
YC=PPLCON(61)/PPLCON(99)
XC1=XC+0.5
YC1=YC+0.5
XC2=XC1+0.05
YC2=YC1+0.05
CALL PLCT(XV,YV,3)
CALL PLCT(XV1,YV1,2)
CALL SYM30L(XV2,YV2,0.07,17HVARIABLE PROPERTY,0.0,17)
CALL PLCT(XC,YC,3)
CALL PLCT(XC1,YC1,2)
CALL SYM30L(XC2,YC2,0.07,17HCONSTANT PROPERTY,0.0,17)
3000 CONTINUE
IF(MFLAG.EQ.1) GO TO 4000
CALL PLCT(12.0,0.0,-3)
CALL SCALE(TPLCON,6.0,97,1)
TFLCT(98)=TPLCON(98)
TPLCT(99)=TPLCON(99)
CALL AXIS(0.0,0.0,13HTEMPERATJRE(DEG F),18.6,0.9,0.0,TPLCON(98),
ITPLCON(99))

```

```

CALL AXIS(0.0,0.0,0.19HPADIAL DISTANCE(IN),-19.8,0.0,0.0,RI,DELR)
CALL FLIN2(FPLOT,TPLCON,97,1,0,0)
CALL FLIN2(FPLOT,TPLCON,97,1,0,0)
CALL SYMBOL(1.0,6.1,0.07,11HRUN NUMBER ,0.0,11)
CALL NUMBER(999.0,6.1,0.07,RUN,0.0,1)
CALL SYMBOL(4.0,6.1,0.07,14HVERT.LOAD(LBF),0.0,14)
CALL SYMBOL(4.0,5.95,0.07,14HTORQUE(IN-LBF),0.0,14)
CALL SYMBOL(4.0,5.8,0.07,18HMACS FLOW(LBM/MIN),0.0,18)
CALL SYMBOL(4.0,5.65,0.07,18HOUTLET TEMP(DEG F),0.0,18)
CALL SYMBOL(5.75,6.25,0.07,16HVP
CP,0.0,0,16)
CALL NUMBER(5.55,6.1,0.07,VARLO ,0.0,2)
CALL NUMBER(5.55,5.95,0.07,VARTQ,0.0,3)
CALL NUMBER(5.55,5.8,0.07,VARMA ,0.0,4)
CALL NUMBER(5.55,5.65,0.07,VARTO ,0.0,2)
CALL NUMBER(5.55,6.1,0.07,CONL),0.0,2)
CALL NUMBER(6.65,5.95,0.07,CONTO,0.0,3)
CALL NUMBER(6.65,5.8,0.07,CONMA ,0.0,4)
CALL NUMBER(6.65,5.65,0.07,CONTO ,0.0,2)
CALL PLOT(3.75,5.5,3)
CALL PLOT(7.25,5.5,2)
CALL PLOT(7.25,6.5,2)
CALL PLOT(3.75,6.5,2)
CALL PLOT(3.75,5.5,2)
CALL PLOT(5.35,5.5,3)
CALL PLOT(5.35,6.5,2)
CALL PLOT(6.35,5.5,3)
CALL PLOT(6.35,6.5,2)
CALL PLOT(0.75,5.5,3)
CALL PLOT(2.75,5.5,2)
CALL PLOT(2.75,6.5,2)
CALL PLOT(0.75,5.5,2)
CALL PLOT(0.75,5.5,2)
CALL SYMBOL(1.0,5.95,0.07,18HSUP. PRES.(PSIG)= ,0.0,18)

```

```

SEAL2320
SEAL2330
SEAL2340
SEAL2350
SEAL2360
SEAL2370
SEAL2371
SEAL2372
SEAL2373
SEAL2374
SEAL2375
SEAL2376
SEAL2377
SEAL2378
SEAL2379
SEAL2380
SEAL2381
SEAL2382
SEAL2383
SEAL2384
SEAL2385
SEAL2386
SEAL2387
SEAL2388
SEAL2389
SEAL2390
SEAL2391
SEAL2392
SEAL2393
SEAL2394
SEAL2395
SEAL2396
SEAL2397

```



```

CALL NUMBER(999.0,5.95,0.07,PD,0.0,1)
CALL SYMREL(1.0,5.8,0.07,16HCLEARANCE(IN.)= ,0.0,16)
CALL NJMREL(999.0,5.3,0.07,H,0.0,4)
CALL SYMREL(1.0,5.65,0.07,17HSEAL SPEED(RPM)= ,0.0,17)
CALL NJMREL(999.0,5.65,0.07,PPH,0.0,1)
TCX=(RPLDT(61))-5PLDT(1))/DELF
TCY=(TPLCN(61))-TPLCN(58))/TPLCN(99)
TCX1=TCX-2.0
TCY1=TCY+1.0
TCX2=TCX1
TCY2=TCY1+0.05
TVX=TCX
TVY=(TPLOT(61))-TPLOT(98))/TPLOT(99)
TVX1=TVX+1.0
TVY1=TVY-0.5
TVX2=TVX1+0.05
TVY2=TVY1
CALL PLOT(TCX,TCY,3)
CALL PLOT(TCX1,TCY1,2)
CALL SYMREL(TCX2,TCY2,0.07,17HCONSTANT PROPERTY,0.0,17)
CALL PLOT(TVX,TVY,3)
CALL PLOT(TVX1,TVY1,2)
CALL SYMREL(TVX2,TVY2,0.07,17HVARIAIBLE PROPERTY,0.0,17)
4000 CONTINUE
CALL PLOT(12.0,0.0,999)
300 CONTINUE
500 CONTINUE
400 CONTINUE
STOP
END
SUBROUTINE INITL(RING,POLD,TOTAL,T,PI,MDOT1,R1,TOTALL,I,H,W,RPM,
ILL,TFEAS,RPLDT,PPLDT,MPLDT,TPLOT,LPLDT)
DOUBLE PRECISION RING,POLD,TOTALM,T,PI,MDOT1,R1,TOTALL,DLOG10,SG,

```

```

SEAL2400
SEAL2410
SEAL2420
SEAL2430
SEAL2440
SEAL2441
SEAL2442
SEAL2443
SEAL2444
SEAL2445
SEAL2446
SEAL2447
SEAL2448
SEAL2449
SEAL2450
SEAL2451
SEAL2452
SEAL2453
SEAL2454
SEAL2455
SEAL2456
SEAL2457
SEAL2458
SEAL2459
SEAL2460
SEAL2470
SEAL2480
SEAL2490
SEAL2500
SEAL2510
INIT0100
INIT0110
INIT0120

```

```

12HQ,X,XX,XX,NU,0.4,W,RPM,M0CT2
DOUBLE PRECISION REYNUM
COMMON FUM
REAL M0CT,LPL0T
DIMENSION FPL0T( 99),MPL0T( 99),TPLOT( 99),LPL0T( 99)
IF(1.0W.0) GO TO 79
M0CT2=M0CT1*32.171900*12.000*60.000
WRITE(6,24)
24 FORMAT(1H1,20A,'*****')
1*****
WRITE(6,101) RUN
101 FORMAT(1H0,40X,'TEST CONDITION NO. ',F5.1)
WRITE(6,25) LI
25 FORMAT(1H0,45X,'CONDITIONS FOR THIS RUN: (',I2,')')
WRITE(6,35) P0L0
35 FORMAT(1H0,40X,'SUPPLY PRESSURE =',D12.5,1X,'PSIG')
WRITE(6,36) H
36 FORMAT(1H0,40X,'MINIMUM FILM THICKNESS =',D12.5,1X,'INCHES')
WRITE(6,37) W,RPM
37 FORMAT(1H0,40X,'SEAL ROTATIONAL SPEED =',D12.5,1X,'RAD/SEC (',D11.
15,1X,'RPM)')
WRITE(6,34) M0CT1,M0CT2
34 FORMAT(1H0,40A,'MASS FLOW RATE =',D12.5,1X,'LBF-SEC/IN (',D11.5,
11X,'LPM/MIN)')
M=0
SG=-4.05685E-4*(0.903076500
2H7=SG*(32.400/(172850*32.171900*12.000))
XXX=T+460.000
X=-3.6046600* PLUG10( XXX )+10.5381200
XX=10.000**X
NU=(-0.800+10.000**XX)*1.080-5*144.000
U=NU*RH0
Q=M0CT1/RH0
INIT0130
INIT0140
INIT0145
INIT0150
INIT0160
INIT0170
INIT0180
INIT0190
INIT0200
INIT0210
INIT0211
INIT0212
INIT0220
INIT0230
INIT0240
INIT0250
INIT0260
INIT0270
INIT0280
INIT0290
INIT0300
INIT0310
INIT0320
INIT0330
INIT0340
INIT0350
INIT0360
INIT0370
INIT0380
INIT0390
INIT0400
INIT0410
INIT0420

```



```
C
C
C      XXXX=I+460.000
C      X=-3.8046600*DLOG10(   XXXX   )+10.5361200
C      XX=10.000**X
C      YU=(-0.800+10.000**XX)*1.08D-5*144.000
C      U=YU*RTG
C      Q=((PI*(P+DELTA)*((H**3.0))/(6.000*U))*((3.000*RHO*(R+DELTA))*
C      14**2.0)/10.000-DELTAP/DELTAR)
C
C      CALCULATE MASS FLOW USING NEW RHO AND Q (EVALUATED AT NEW TEMPERATURE)
C      MOOT=Q*RHO
C      RETURN
C      END
C      SUBROUTINE CHECK2(PNEW,PO,I,KK,MM)
C
C      THIS SUBROUTINE USED TO CHECK WHAT SEAL EXIT PRESSURE IS
C
C      DOUBLE PRECISION PNEW,PO,DARS
C      MM=1
C      IF((PO-DARS(PNEW))/PO).LT.0.99 D0)    GO TO 541
C      I=I+1
C      KK=KK+1
C      CONTINUE
C      RETURN
C      END
C      SUBROUTINE FIND(DELTAR,J,T,DELTAT)
C
C      THIS SUBROUTINE USED IF DELTA R IS TOO LARGE FOR PROPERTIES NOT TO
C      CHANGE SIGNIFICANTLY
C
C      DOUBLE PRECISION DELTAR,T,DELTAT
```

```

C      J=J+1
C      INCREMENT DELTA R
C      DELTA=DELTA/2.000
C      INITIALISE TEMPERATURE
C      T=DELTA
C      PF=URN
C      END
C      SUBROUTINE FOUND(R1,R2,DELTA,PI,DELTA,PVIEW,T,U,H,Q,SG,MOMENT,
C      ITOTALM,TOTALL,K,RING,R,DLOAD,I,J,POLD,ZOT,N,L,MDOT1,PG,KK,MM,
C      ZIFLAG,KPLOT,PPLOT,MPLOT,TPLOT,LPLLOT)
C      THIS SUBROUTINE IS CALLED ONLY WHEN THE MASS FLOW RATE HAS
C      CHANGED SIGNIFICANTLY ACROSS DELTA R
C
C      DOUBLE PRECISION R1,R2,PI,DELTA,DELTA,PVIEW,U,H,T,Q,SG,MOMENT,
C      ITOTALM,TOTALL, RING,R,DAERA,DLOAD,POLD,ZOT,DABS ,MDOT1,PG,PAVG,
C      ZIFLAG
C      REAL KPLOT,LPLLOT
C      DIMENSION KPLOT( 99),PPLOT( 99),MPLOT( 99),TPLOT( 99),LPLLOT( 99)
C      CALCULATE INCREMENTAL AREA
C      DAERA=2.000*PI*R*DELTA
C      ...AND INCREMENTAL LOAD ACTING ON THIS AREA
C      PAVG=(POLD+PVIEW)/2.000
C      DLOAD=PAVG*DAERA
C
C      FOUN0160
C      FOUN0170
C      FOUN0180
C      FOUN0190
C      FOUN0200
C      FOUN0210
C      FOUN0220
C      FOUN0230
C      FOUN0240
C      FOUN0250
C      FOUN0260
C      FOUN0100
C      FOUN0110
C      FOUN0120
C      FOUN0130
C      FOUN0140
C      FOUN0150
C      FOUN0160
C      FOUN0170
C      FOUN0180
C      FOUN0190
C      FOUN0200
C      FOUN0210
C      FOUN0220
C      FOUN0230
C      FOUN0240
C      FOUN0250
C      FOUN0260
C      FOUN0270
C      FOUN0280
C      FOUN0290
C      FOUN0300
C      FOUN0310

```

```

C      CUM INCREMENTS OF SEAL LOAD AND MOMENT
C
      TOTAL=TOTAL+DLUAG
      TOTALM=TOTALM+MDMENT
C
C      PRINT OUT DATA EVERY 0.01 INCHES
C
      IF(I.EQ.0) GO TO 109
      IF((DABS(P-ZOT)).LT.0.0099D0) GO TO 109
      IFLAG=IFLAG+1
      WRITE(6,41) R,PNEW,TOTALM,T,SG,U,TOTAL,Q,J
41  FORMAT(1H, 'D12.5,3X,D12.5,3X,D12.5,3X,D12.5,3X,
      D12.5,3X,D12.5, 3X,I4)
      RPLDT(IFLAG)=R
      PPLDT(IFLAG)=PNEW
      MPLDT(IFLAG)=TOTALM
      TPLDT(IFLAG)=T
      LPLDT(IFLAG)=TOTAL
      ZOTEN
      P=0
109 K=1
      RING=RING+DELTA R
      N=N+1
C
C      INITIALIZE PRESSURE
C
      POLD=PNEW
C
C      CHECK TO SEE IF TOTAL SEAL RADIUS HAS BEEN TRANSVERSED
C
      IF(R.GE.R2) CALL CHECK2(PNEW,PO,I,KK,MM)
      RETURN
      END

```



```

XX=10.000**X
YU=(-0.800+10.000**XX)*1.080-5*144.000
J=J+RHC
Q=(PI*(H**3.000))*((POLD+C))/(6.000*U*DLOG(R2/R1))
WQNT1=Q*RHO
RETURN
END
SUBROUTINE COMP2P(RPM,H,PG,PPLCON,RPLCON,TPLCON,TFIRST,CONLO,
  1CONHT,CORNA,CONTO)
C
C THIS SUBROUTINE IS USED TO CALCULATE THE PRESSURE DISTRIBUTION.
C BY ASSUMING CONSTANT FLUID PROPERTIES. THESE VALUES ARE USED FOR
C PLOTTING PURPOSES ONLY.
C
DOUBLE PRECISION RPM,H,PG
DOUBLE PRECISION TFIRST
DIMENSION RPLCON(99),PPLCON(99),TPLCON(99)
REAL L,M,H,I,IPL,NIJ
REAL WQNT2
PI=3.14159
V=PP%
T=TFIRST
R1=1.02
R2=1.98
SC=-4.05685E-4*T+0.9030765E0
RHC=SG*(62.4E0/(1728E0*32.1719E0*12.0E0))
XXXX=T+460.0E0
X=-3.60466E0*ALOG10( XXXX )+10.53812E0
XX=10.000**X
NIJ=(-0.8E0+10.0E0**XX)*1.08E-5*144.0E0
J=J+RHC
U=NIJ/RHC
TPLCON(1)=TFIRST
RPLCON(1)=R1

```

MASS0290  
 MASS0300  
 MASS0310  
 MASS0320  
 MASS0330  
 MASS0340  
 MASS0350  
 CONP0100  
 CONP0105  
 CONP0110  
 CONP0120  
 CONP0130  
 CONP0140  
 CONP0150  
 CONP0160  
 CONP0170  
 CONP0180  
 CONP0190  
 CONP0195  
 CONP0200  
 CONP0210  
 CONP0220  
 CONP0230  
 CONP0240  
 CONP0250  
 CONP0260  
 CONP0270  
 CONP0280  
 CONP0290  
 CONP0300  
 CONP0310  
 CONP0320  
 CONP0330



```

RPLCON(1)=PC
CP=0.45
E=V2/2.0
F=P1/2.0
P2=0.0
V=N*(2.0*PI/60.0)
K=2
A=P2/PI
C=((3.0*RHD**2)*(R2**2-P1**2))/20.0
IP1=PC
I=H#1E4
ON 80 J=2.97
R=i.01+0.01*J
Y=(2.0*U**PI*((R**4-R1**4)/4.0))/(0.0001*I)
D=(PI*(0.0001*I)*R*(IP1-P2+C))/(5.0*U*ALOG(A))
L=PI*PC*R1*F1
1 + PI*(R2-P2-R1*R1)*(PD+C/2.0)
2 + (6.0*U*Q/(H*H*H))*
3 ((R2*P2-P1*P1)/2.0-R2*R2*ALOG(A))
CP/PI
P=IP1-((6.0*U*Q*ALOG(D))/(0.0001*I)**3*PI))+((3.0*RHD**2*(R**2-
P1**2))/20.0)
EP=Q*(IP1-P)
EF=((2.0*PI*N)/60.0)**2*((2.0*PI*U)/(0.0001*I))*(R**4-R1**4)
*/4.0
DELT=(EP+EF)/(PHU*Q*CP*778.0*32.1719*144.0)
T=TFIRST+DELT
RPLCON(J)=R
RPLCON(J)=P
TPLCON(J)=T
K=K+1
80 CONTINUE
90 CONTINUE

```

CONP0340  
 CONP0350  
 CONP0360  
 CONP0370  
 CONP0380  
 CONP0390  
 CONP0400  
 CONP0410  
 CONP0420  
 CONP0430  
 CONP0440  
 CONP0450  
 CONP0460  
 CONP0470  
 CONP0480  
 CONP0490  
 CONP0500  
 CONP0510  
 CONP0520  
 CONP0530  
 CONP0540  
 CONP0550  
 CONP0560  
 CONP0570  
 CONP0580  
 CONP0590  
 CONP0600  
 CONP0610  
 CONP0620  
 CONP0630  
 CONP0640  
 CONP0650  
 CONP0660

```

MDOT2=EMD*0.336.0*60.0
WRITE(6,10)
10 FORMAT(1-1,'CONSTANT PROPERTY EVALUATION FOR ABOVE CONDITIONS')
WRITE(6,11)
11 FORMAT(1-3,'RADIAL DISTANCE',3X,'PRESSURE',4X,'TEMPERATURE')
WRITE(6,12)
12 FORMAT(14,5X,'(IN)',10X,'(PSIG)',6X,'(DEG F)')
WRITE(6,13)
13 FORMAT(14,'-----',3X,'-----',4X,'-----')
WRITE(6,15) (RPLCON(K),PPLCON(K),TPLCON(K),K=1,97)
15 FORMAT(14,E12.4,3X,E12.4,3X,E12.5)
WRITE(6,20) %
20 FORMAT(1H0,10X,'TOTAL SEAL TORQUE =',E12.5,1X,'IN-LBF')
WRITE(6,30) L
30 FORMAT(1H0,10X,'TOTAL SEAL LOAD =',E12.5,1X,'LBF')
WRITE(6,40) MDOT2
40 FORMAT(1H0,10X,'MASS FLOW RATE =',E12.5,1X,'LBM/MIN')
CONLO = L
CONTO = M
CQUMA = MDOT2
CQUMF = TPLCON(97)
RETIEN
END
CONP0670
CONP0680
CONP0690
CONP0700
CONP0710
CONP0720
CONP0730
CONP0740
CONP0750
CONP0760
CONP0770
CONP0780
CONP0790
CONP0800
CONP0810
CONP0820
CONP0830
CONP0840
CONP0850
CONP0860
CONP0870
CONP0880
CONP0890

```

## APPENDIX B

### CLEARANCE PROBE INSTALLATION PROCEDURE

The following is the suggested step-by-step clearance probe installation procedure which was utilized in regard to the experimental portion of this investigation. From the performance of the test seal employed, the procedure below has proven to be an essential asset as far as clearance probe pressure sensitivity is concerned. It should also be pointed out that the adhesive compound (Devcon Aluminum Putty) utilized was instrumental in being able to successfully machine the 0.005-inch diaphragm to the required tolerances.

The recommended installation procedure is as follows:

1. Construct the desired type thermocouple with leads approximately 15 feet in length.
2. Mix up a substantial amount of Devcon Aluminum Putty without thinner.
3. Place thermocouple inside the clearance probe making sure the thermocouple is at the bottom of the clearance probe.
4. With a plastic syringe, inject Devcon Aluminum Putty alongside the thermocouple.
5. With remaining Devcon, fill test seal clearance probe hole about 1/4 full.

6. With small tweezers, carefully grasp top of probe and insert into test seal hole, being careful of wires.
7. With the probe vertical and on the bottom of test seal hole, grasp tweezers with holder to hold steady.
8. Allow this assembly to dry (approximately 24 hours).
9. Fill hole completely (if necessary) to protect probe and wires.
10. Allow to dry for 24 hours.

## APPENDIX C

### CALIBRATION RESISTOR ( $R_{CAL}$ ) CALCULATIONS

Actual  $R_{cal}$  values utilized in this investigation are given below. It should be noted that  $R_{cal}$  values are actually  $R_{cal} + R_a$  where  $R_a$  is the resistance of one arm of the bridge employed. However, in all cases considered,  $R_a$  values were insignificant when compared to values of  $R_{cal}$ .

#### Vertical Load

Maximum indicated strain = 575 micro-inches per inch.

Let 5-inch galvanometer deflection = 600 micro-inches per inch.

$$\text{Since } R_{cal} = \frac{R_a}{F \frac{\Delta L}{L}} = \frac{ER_a}{4M} \quad (C-1)$$

where

$R_a$  = resistance of one bridge arm

$F$  = gage factor

$\frac{\Delta L}{L}$  = maximum indicated strain

$E$  = bridge excitation voltage

$M$  = input parameter concerning amplifier balancing

then for a 5-inch deflection,

$$R_{cal} = \frac{190}{(3.17)(600 \times 10^{-6})} = 99.89 \text{ K}\Omega$$

But the actual resistor value was found to be 99.31 K $\Omega$ . Thus, solving for M in Equation (C-1) with E = 4.00 volts,

$$M = 1.909 \text{ mV}$$

A 1.909-mV input to the A20B amplifier should produce a 5.0-inch deflection.

### Torque

Maximum indicated strain = 30 micro-inches per inch.

Let 5-inch galvanometer deflection = 30  $\mu\text{in./in.}$  Then, from Equation (C-1),

$$R_{\text{cal}} = \frac{378.8}{(105.6)(30 \times 10^{-6})} = 119.57 \text{ K}\Omega$$

$$\text{Actual } R_{\text{cal}} \text{ value} = 117.57 \text{ K}\Omega$$

Thus, with E = 8.00 volts,

$$M = 6.42 \text{ mV.}$$

The A20B amplifier should be balanced such that an input of 6.42 mV produces a 5.0-inch deflection.

### Supply Pressure, SP1, SP2, SP3, SP5

Maximum indicated strain - 522 micro-inches per inch.

Let 4-inch galvanometer deflection = 522 micro-inches per inch.

Then, from Equation (C-1),

$$R_{\text{cal}} = \frac{120}{(2)(522 \times 10^{-6})} = 114.014 \text{ K}\Omega$$

$$\text{Actual supply pressure } R_{\text{cal}} \text{ value} = 114.5 \text{ K}\Omega$$

Actual SP1  $R_{cal}$  value = 115.65  $K\Omega$

Actual SP2  $R_{cal}$  value = 115.06  $K\Omega$

Actual SP3  $R_{cal}$  value = 115.17  $K\Omega$

Actual SP5  $R_{cal}$  value = 114.90  $K\Omega$

Thus, for  $E = 4.00$  volts, the A20B amplifiers should be balanced such that the following voltage inputs produce a 4.00-inch deflection:

Supply pressure:  $M = 10.48$  mV

SP1:  $M = 1.046$  mV

SP2:  $M = 1.052$  mV

SP3:  $M = 1.049$  mV

SP5:  $M = 1.054$  mV.

Note: Since during the final test seal lapping process probes SP1, SP2, and SP5 were made over-sensitive, the above calculated values of voltage input were too high. Therefore, the previously balanced amplifier gain was reduced such that the maximum observed pressure would not drive the galvanometer trace off the paper. Reducing the amplifier gain also meant reducing the  $R_{cal}$  deflection in proportion to the gain reduction.

## APPENDIX D

### CALIBRATION CURVES

Calibration curves of all external transducers (except thermocouples) are presented in this section. Also, calibration data in regard to the gage glass flow indicators are shown in Figures 37 through 49.



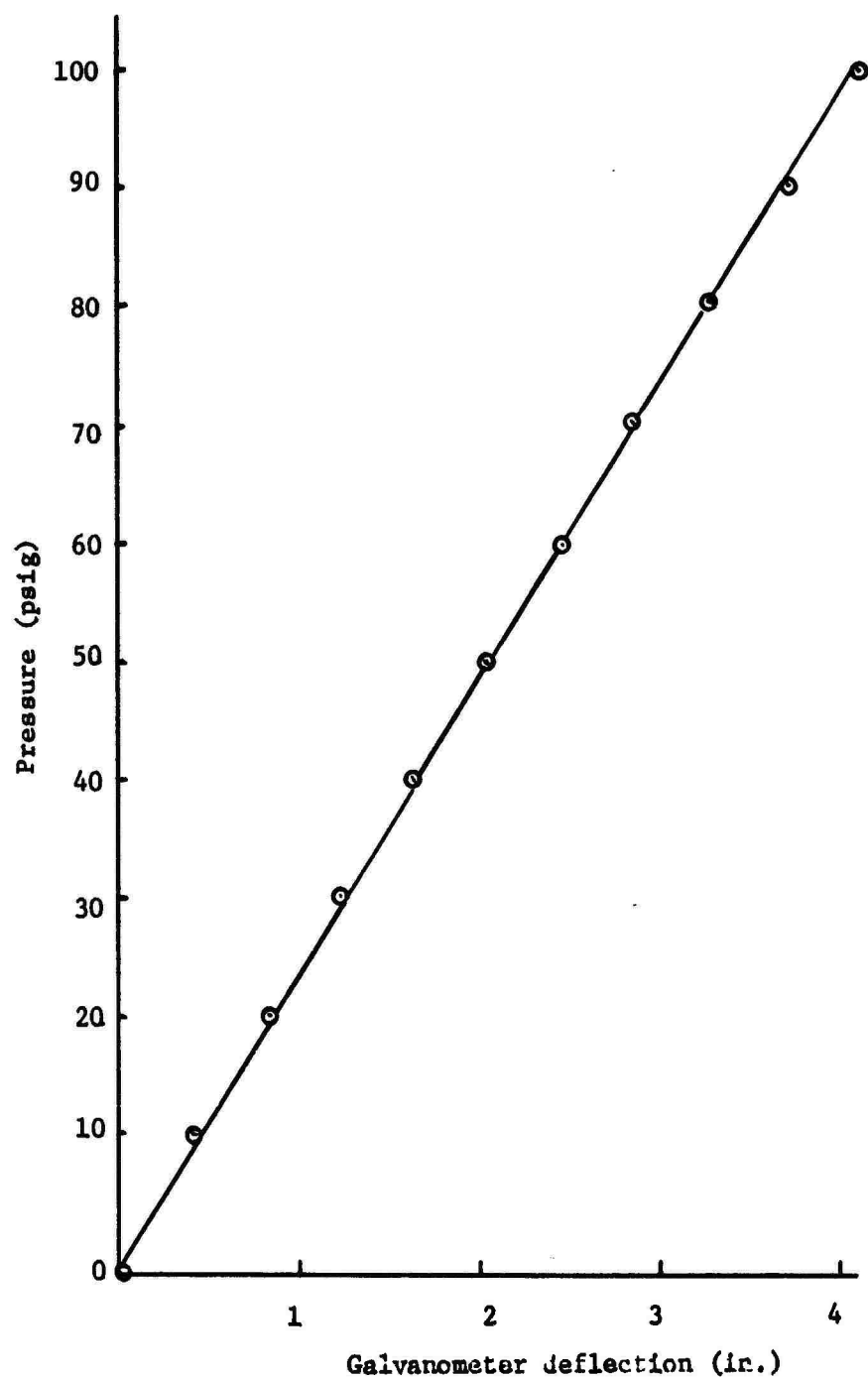


Figure 37. Supply Pressure Calibration Curve.

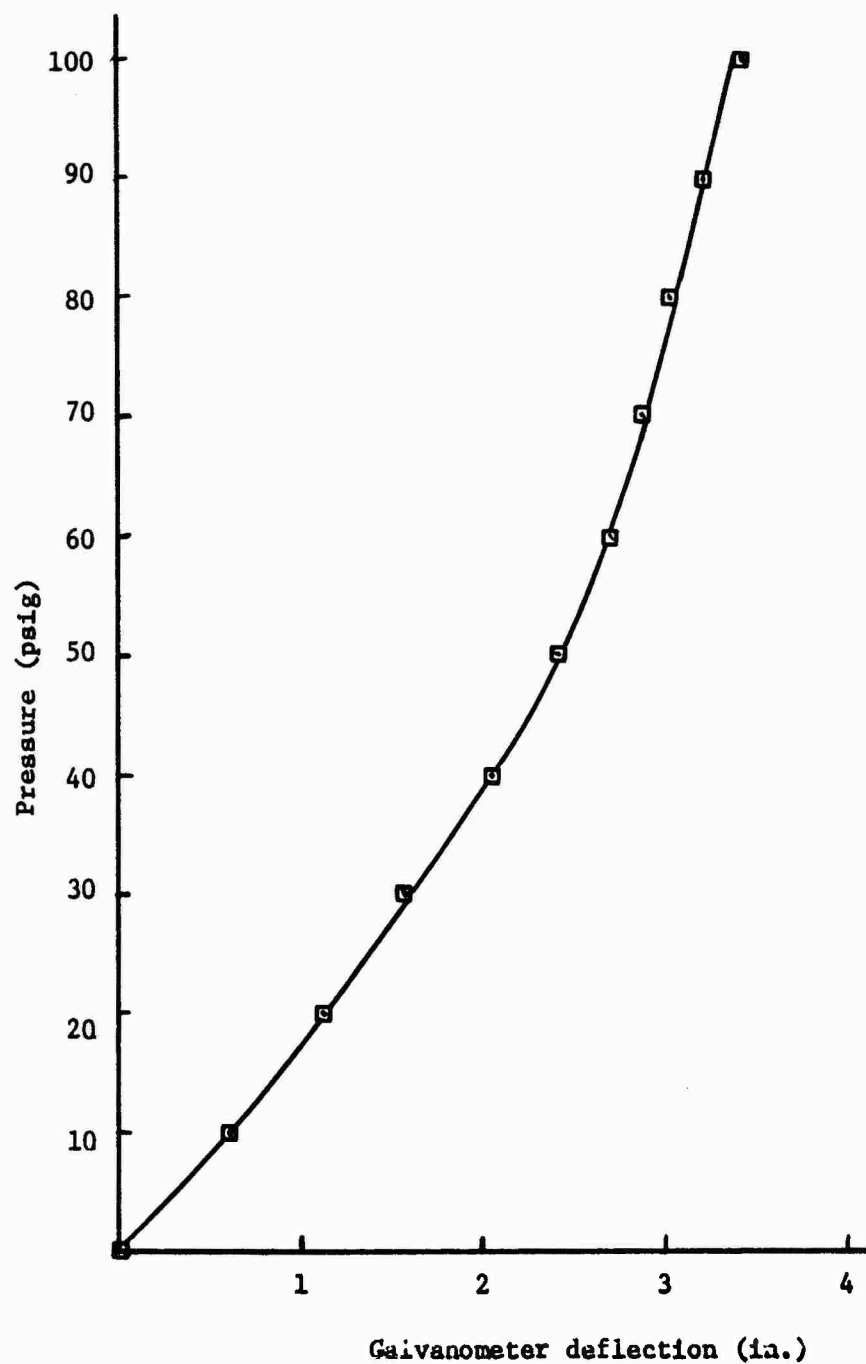


Figure 38. Pressure Probe SP1 Calibration Curve.

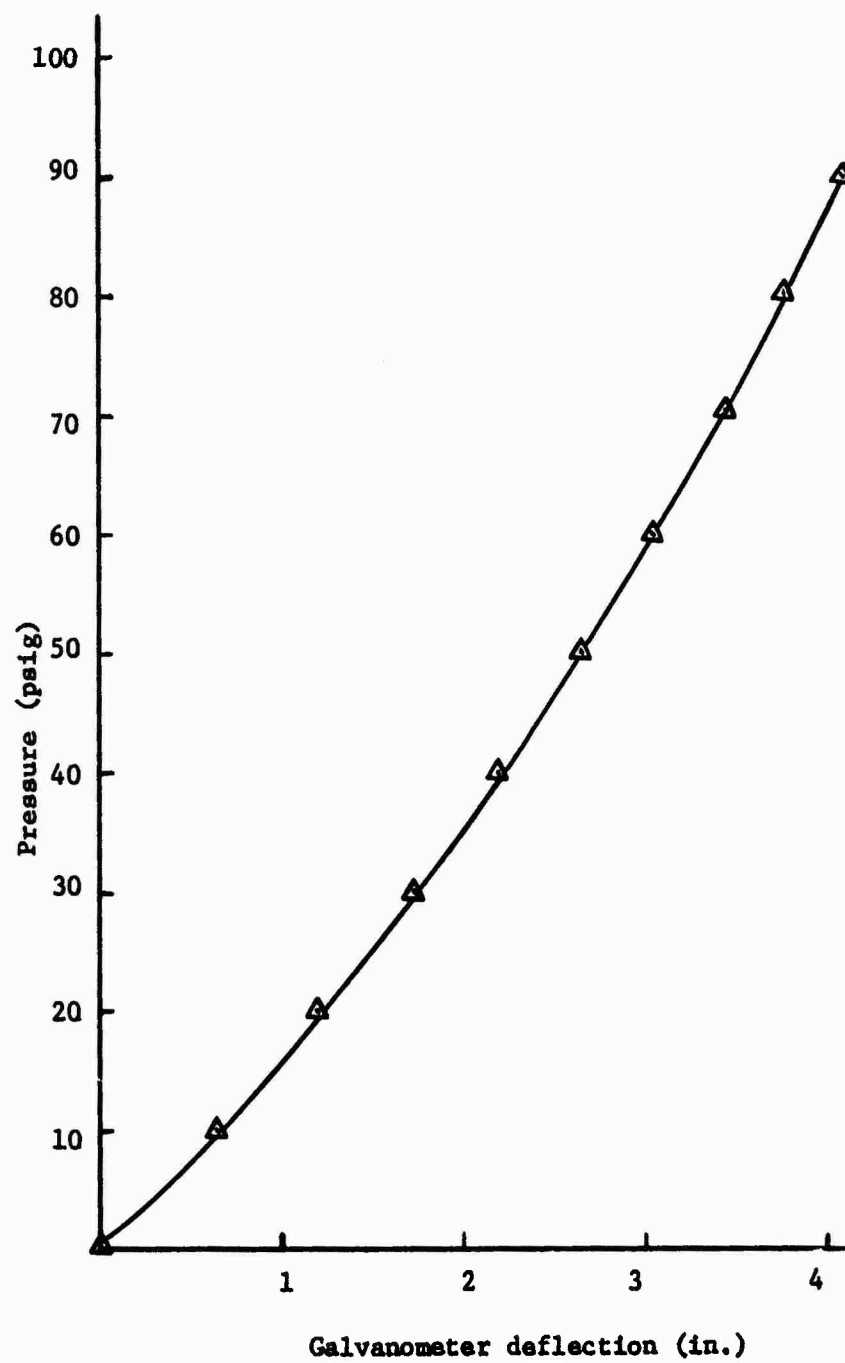


Figure 39. Pressure Probe SP2 Calibration Curve.

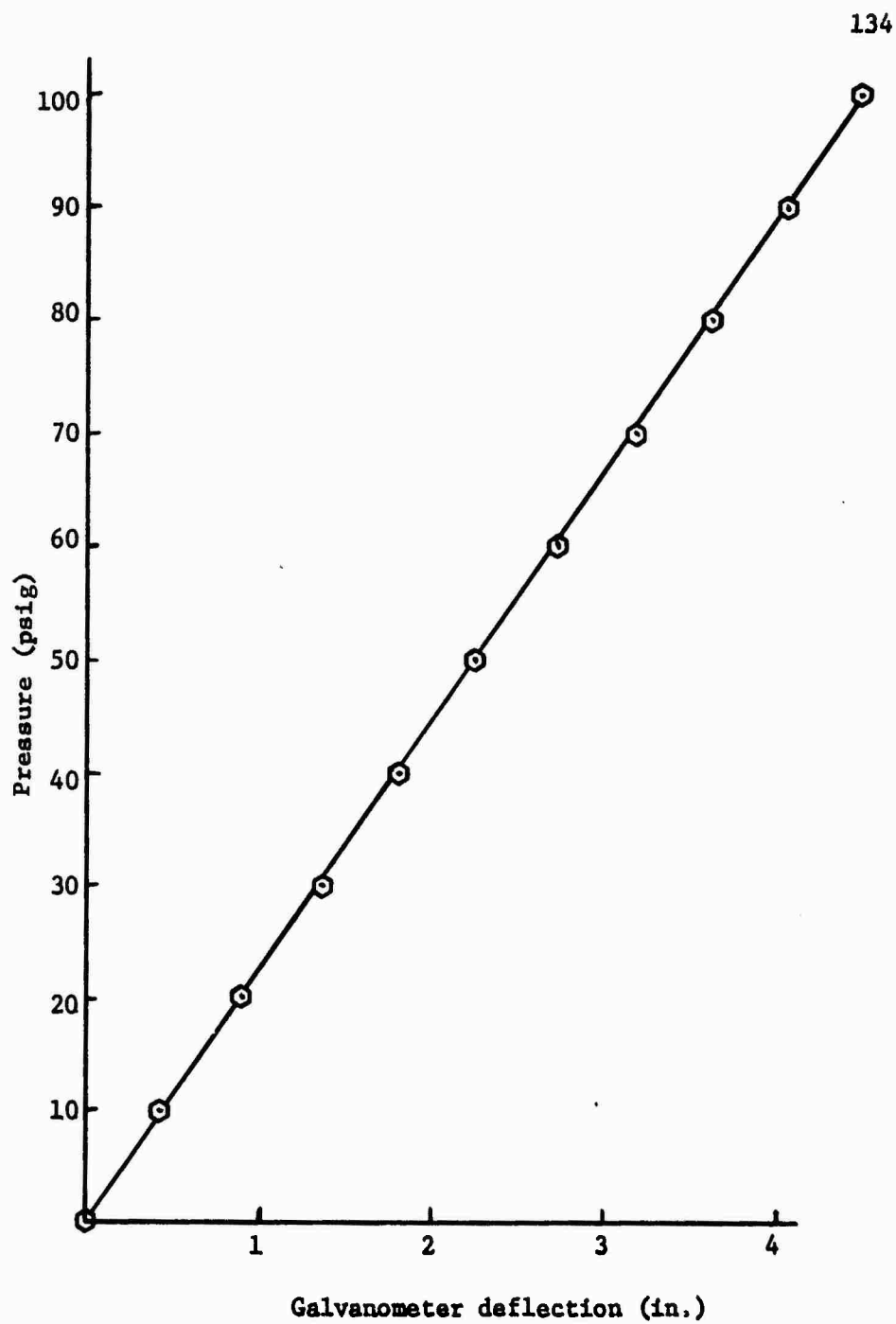


Figure 40. Pressure Probe SP3 Calibration Curve.

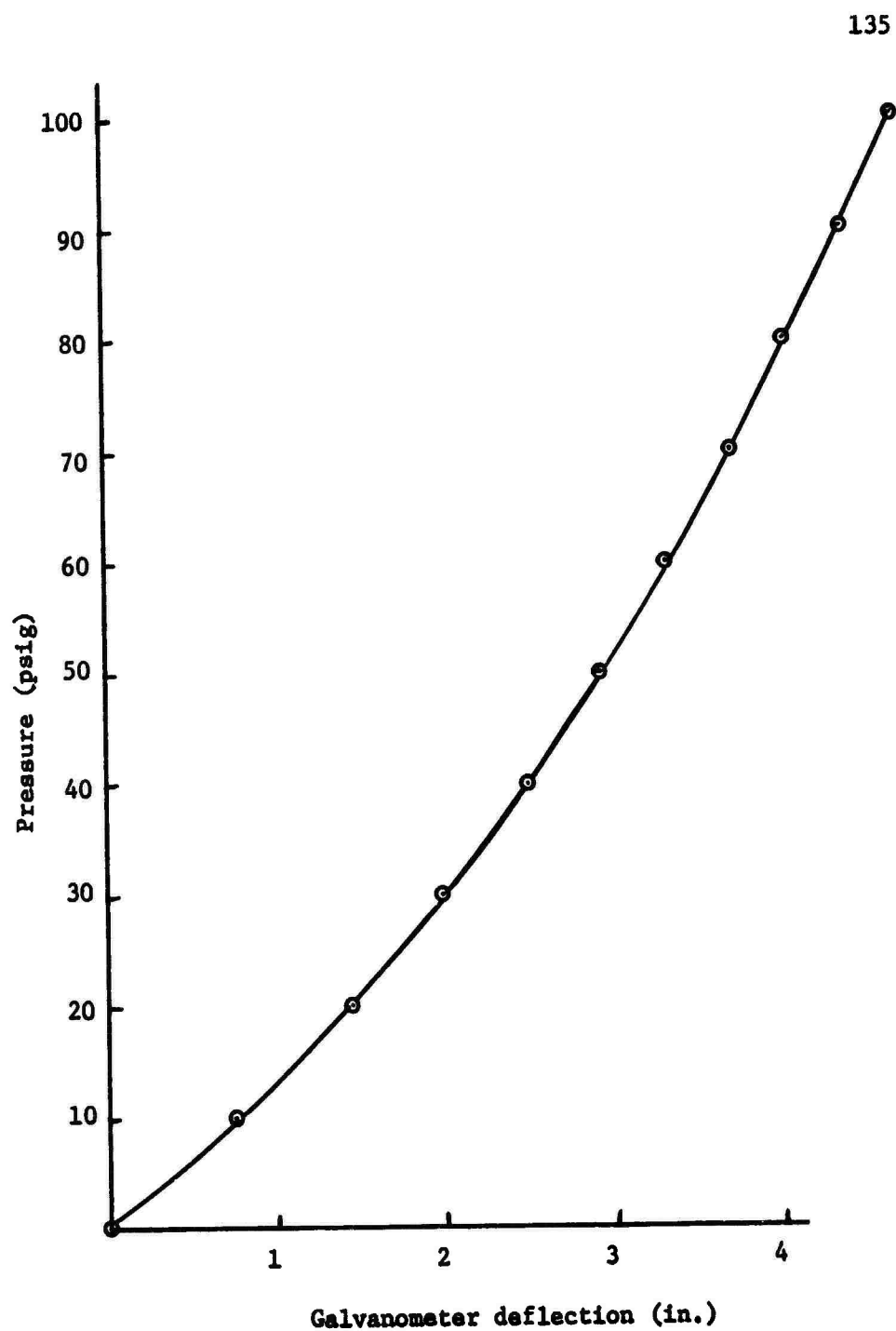


Figure 41. Pressure Probe SP5 Calibration Curve.

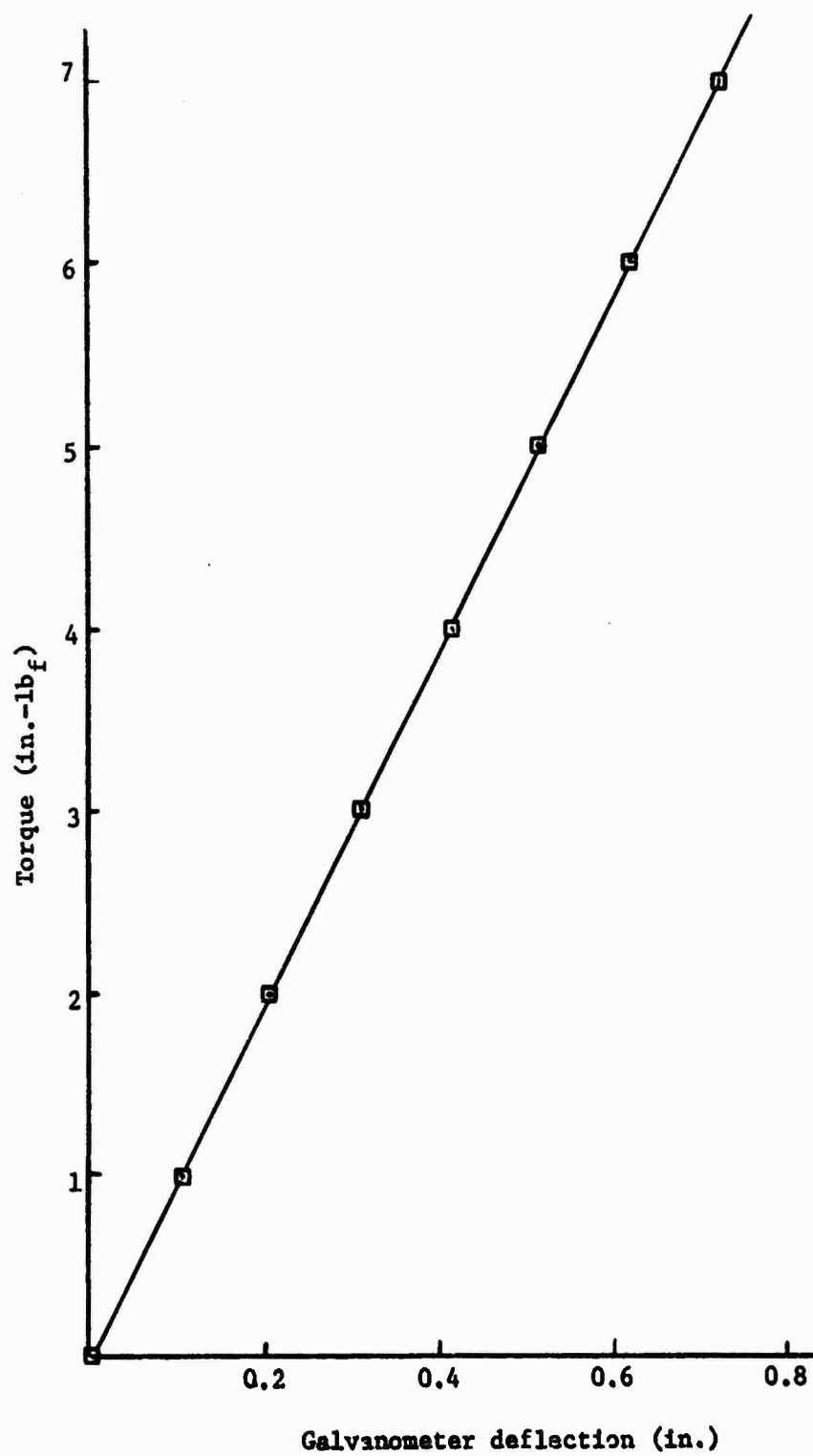


Figure 42. Torque Calibration Curve.

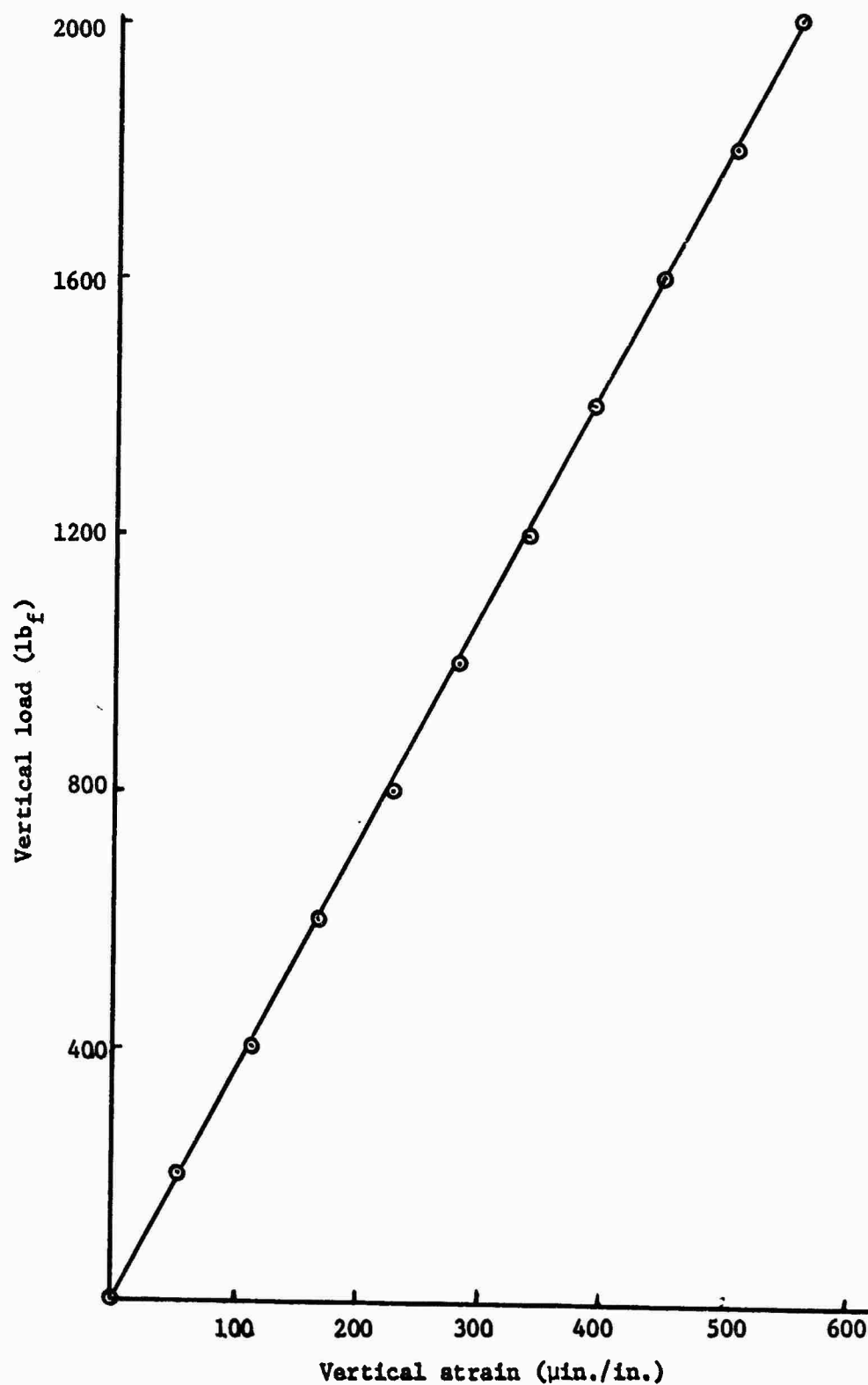


Figure 43. Vertical Load Calibration Curve.

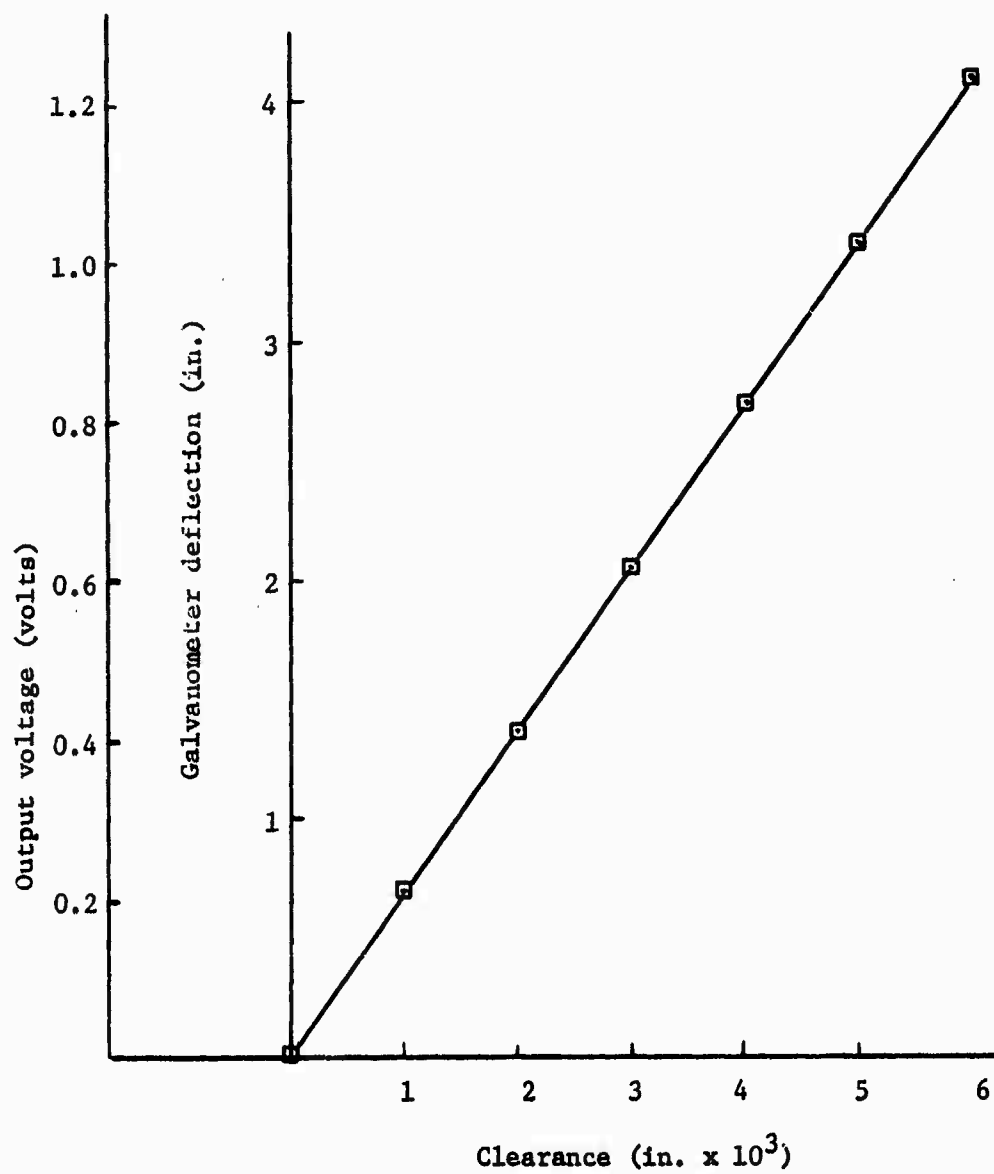


Figure 44. Clearance Probe A1 Calibration Curve.



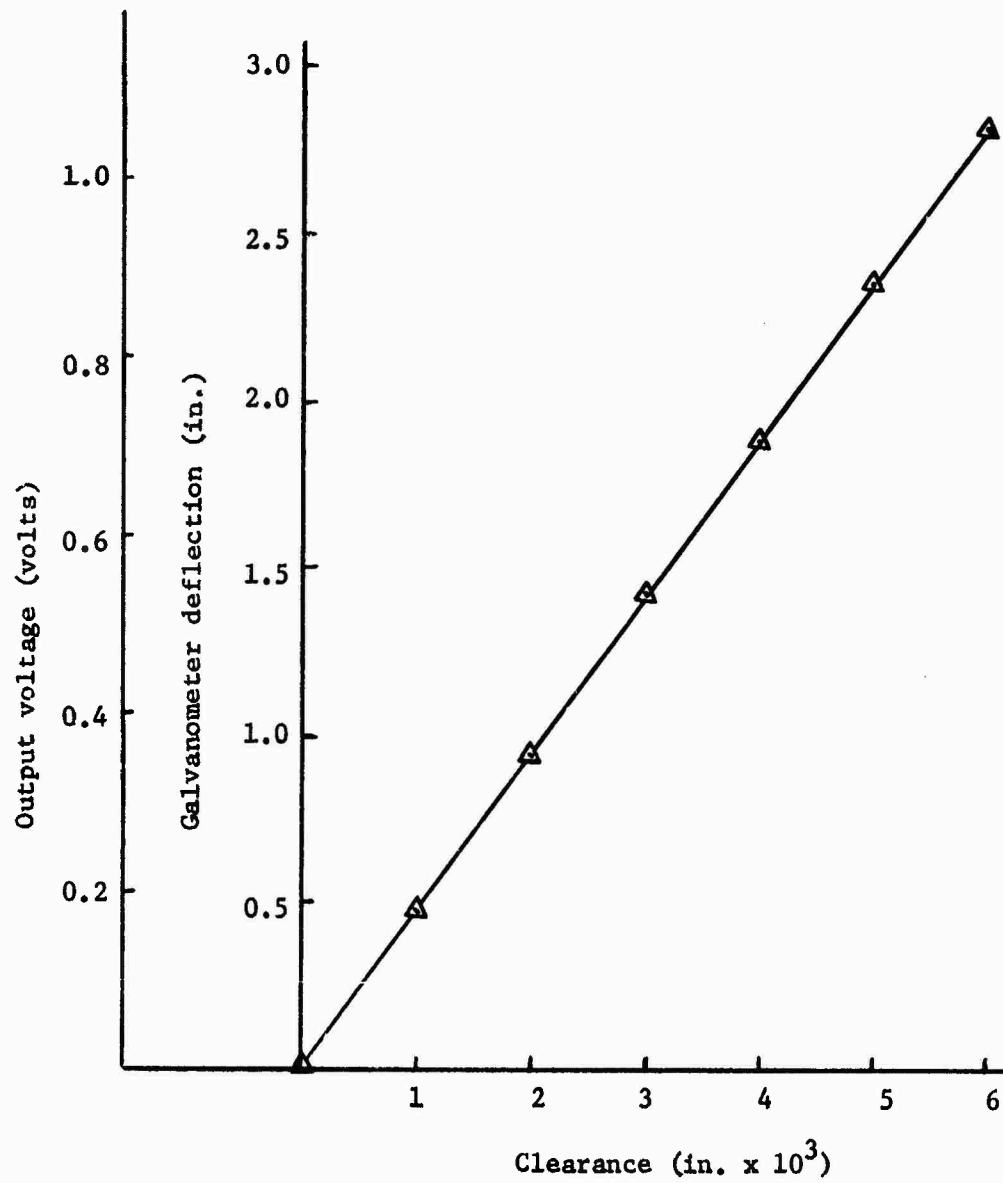


Figure 45. Clearance Probe B2 Calibration Curve.

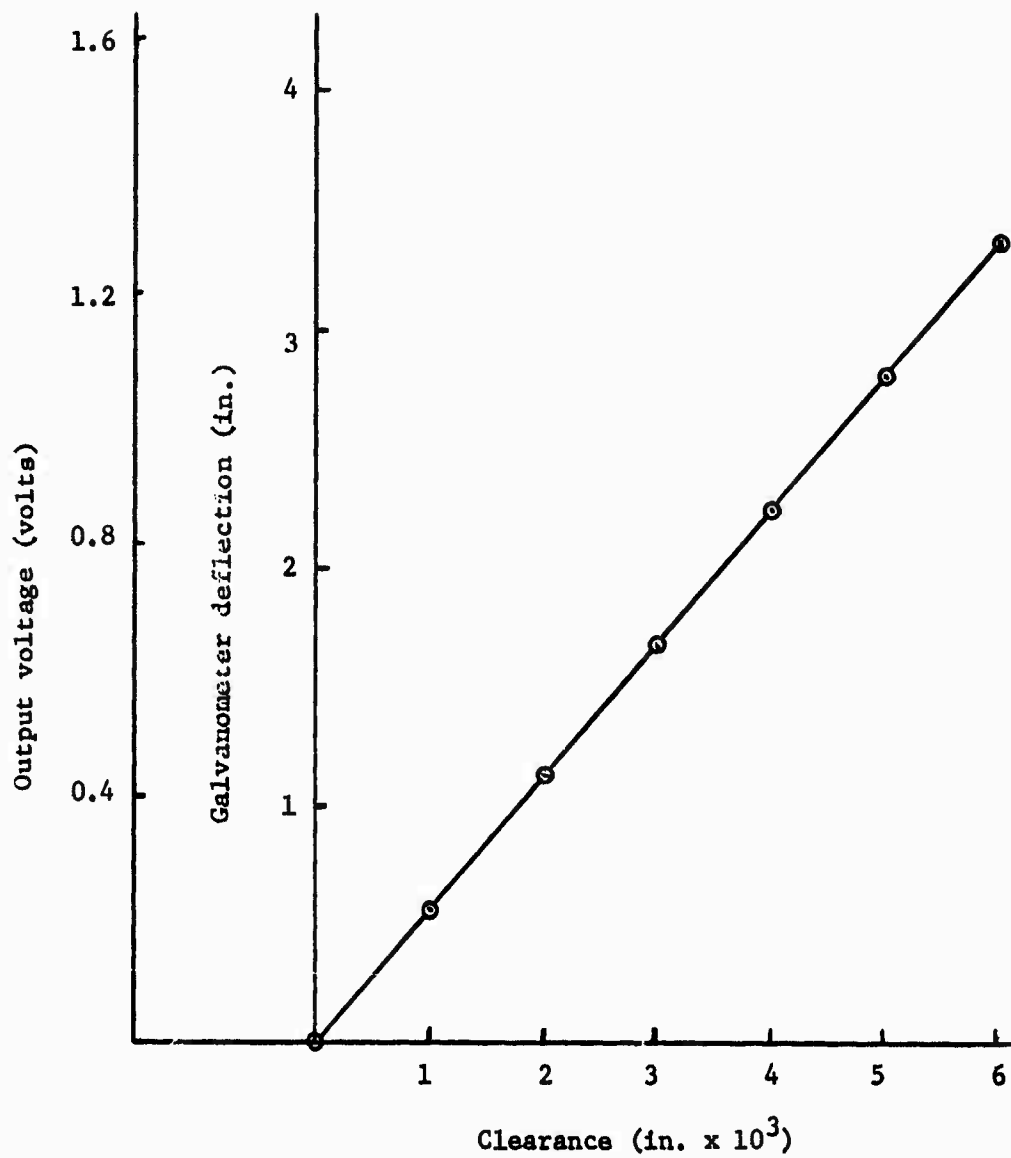


Figure 46. Clearance Probe C3 Calibration Curve.

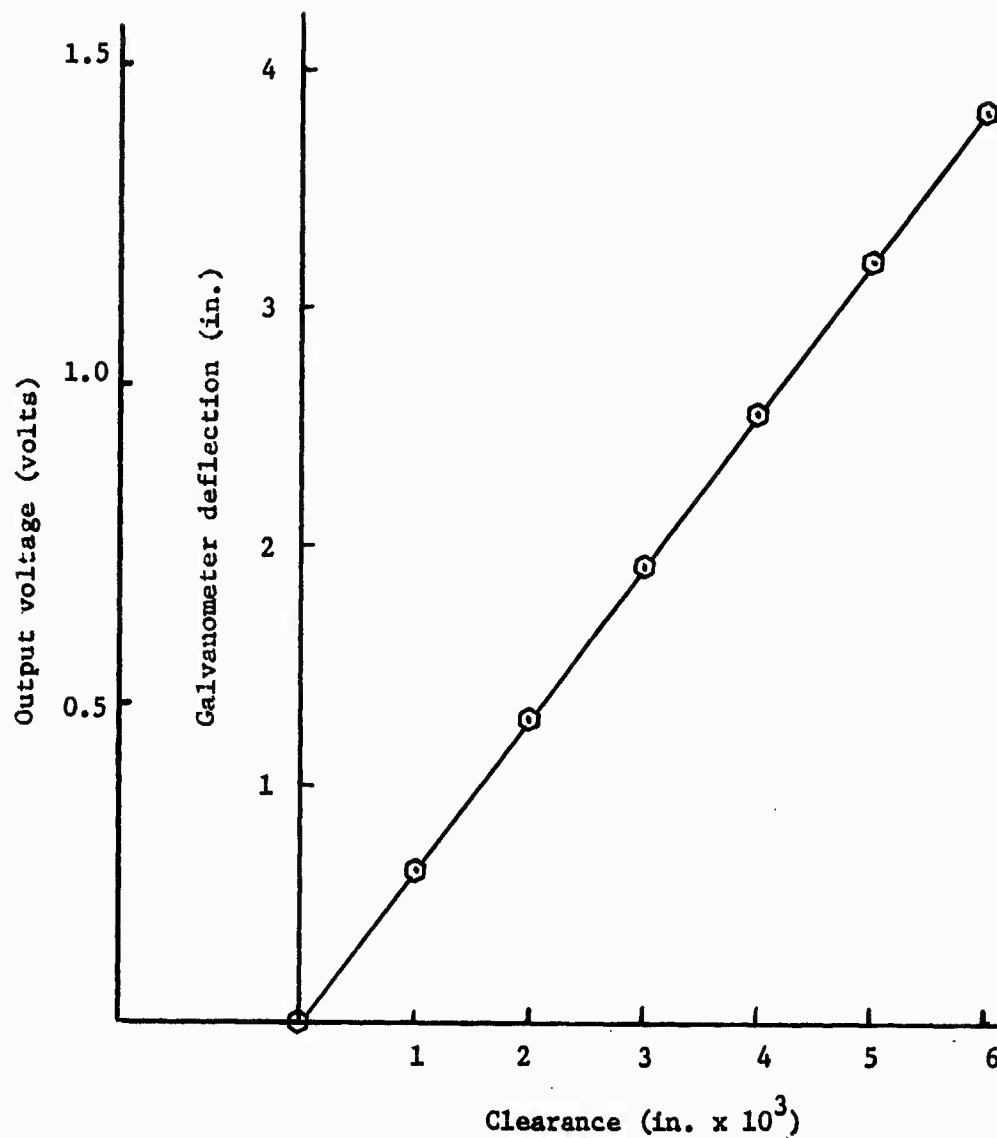


Figure 47. Clearance Probe F5 Calibration Curve.

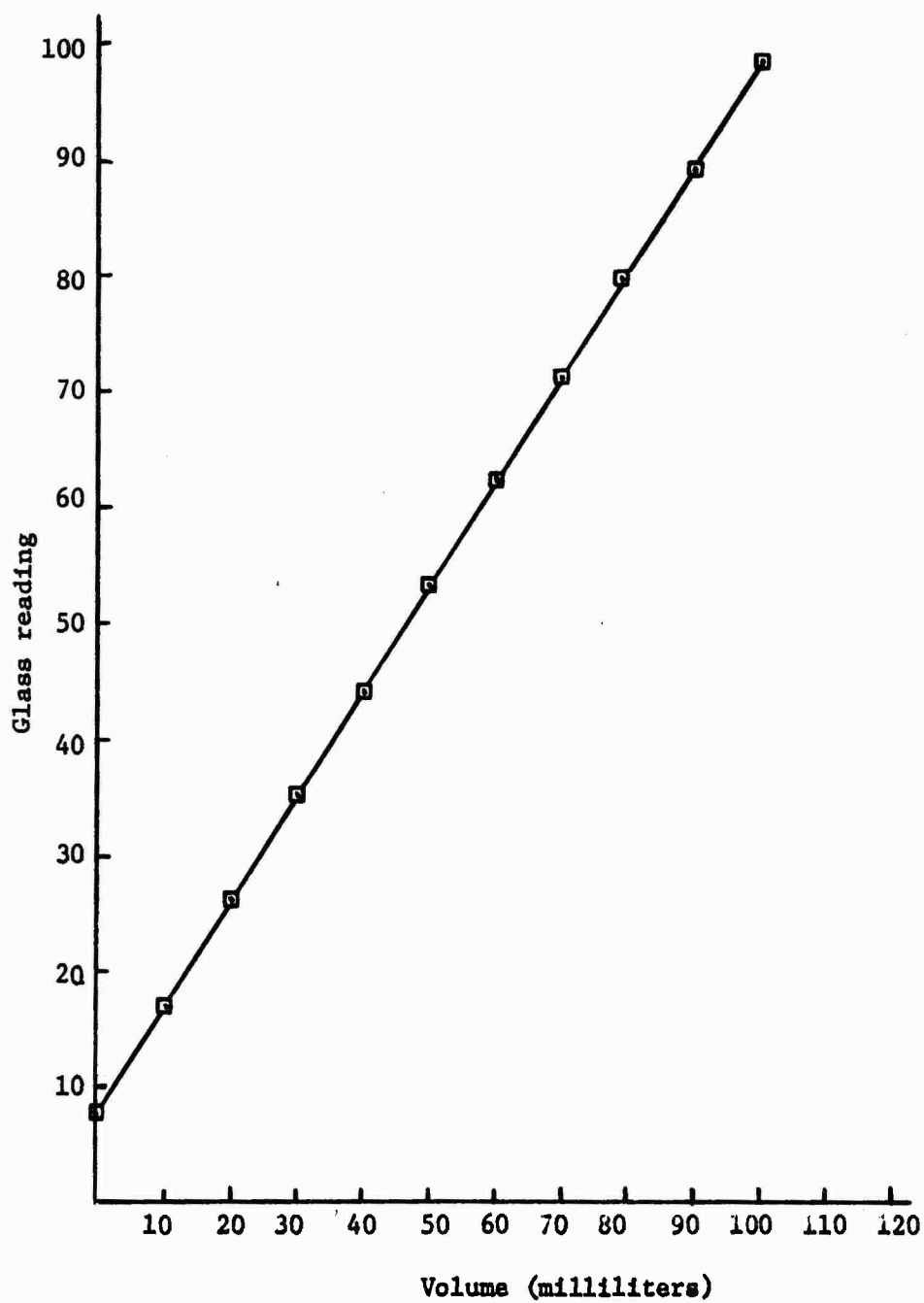


Figure 48. Flow Meter Calibration Curve (Large Glass).

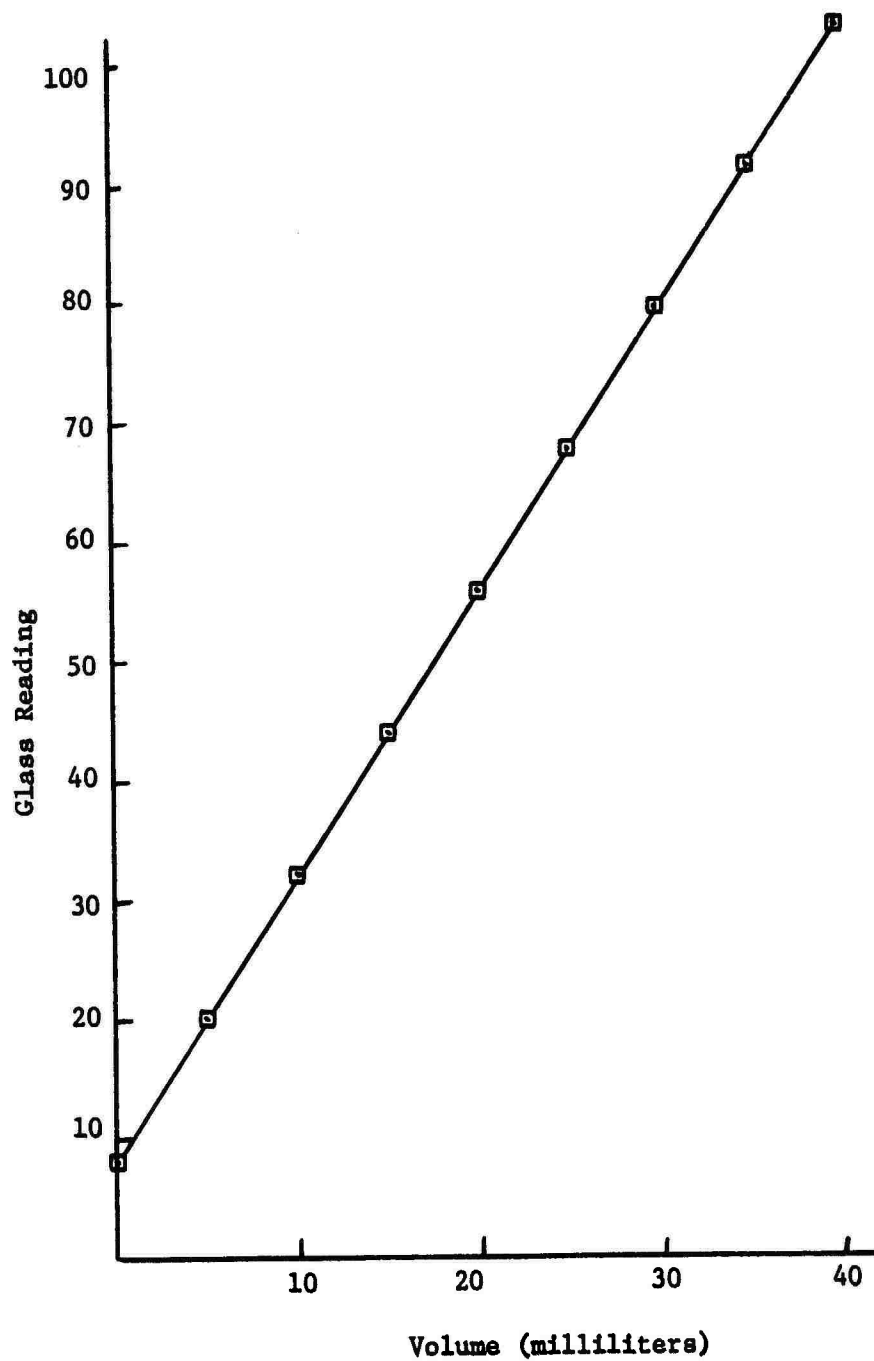


Figure 49. Flow Meter Calibration Curve (Small Glass).

## APPENDIX E

### CLEARANCE PROBE PRESSURE COMPENSATION-DETERMINATION OF ACTUAL CLEARANCE PROBE MOVEMENT

The method of determining actual clearance probe movement due to movement of the upper seal piece due to pressure is given in this section. The method basically involves finding the equation of a plane from three points making it possible to determine the coordinates of any point within that plane.

The clearance measured at zero pressure was taken as the reference plane. At each pressure, the upper sealing surface took on a different planar position (with respect to the reference plane) determined from the three probes of each external clearance indicating system. Since any three points determine a plane, the planar position of each clearance probe could be determined at each pressure, thus determining the actual movement of the upper sealing surface.

It was noticed that the Bentley-Nevada system produced less scatter in the "delta clearances" when compared to those determined from the Sheffield system, although similar trends existed between the two methods. Thus, Figure 18 (page 5b) was produced from points found employing the Bentley-Nevada system.

DISTRIBUTION LIST

Defense Documentation Center  
Cameron Station  
Alexandria, Virginia 22314

National Aeronautics and Space  
Administration (R-ASTR-GC)  
Marshall Space Flight Center  
Huntsville, Alabama 35812  
Attn: Mr. P. H. Broussard

Naval Air Systems Command  
Department of the Navy  
Washington, D. C. 20360  
Attn: Mr. J. R. Crowder, AIR 5303

Naval Air Systems Command  
Department of the Navy  
Washington, D. C. 20360  
Attn: Mr. John J. Gurtowski, AIR 52032C

Naval Air Systems Command  
Department of the Navy  
Washington, D. C. 20360  
Attn: Dr. H. Rosenwasser, AIR 510C

Naval Air Systems Command  
Department of the Navy  
Washington, D. C. 20360  
Attn: Technical Library, AIR 604

National Aeronautics and Space Administration  
Lewis Research Center  
Cleveland, Ohio 44135  
Attn: Mr. Robert L. Johnson, Chief,  
Lubrication Research Branch

National Aeronautics and Space Administration  
Lewis Research Center  
Cleveland, Ohio 44135  
Attn: Mr. Lawrence P. Ludwig, Head,  
Seals Section

Office of Naval Research  
Department of the Navy  
Arlington, Virginia 22217  
Attn: Mr. J. A. Ellingsworth, Code 473

Office of Naval Research  
Department of the Navy  
Arlington, Virginia 22217  
Attn: Mr. Stanley Doroff, Code 438

Office of the Director of Defense Research  
and Engineering  
Washington, D. C. 20501  
Attn: Assistant Director for Research

Oak Ridge National Laboratory  
Oak Ridge, Tennessee 37830  
Attn: Mr. Lloyd A. Wilson  
Reactor Engineering Division

U. S. Army Mobility Equipment Research and  
Development Center  
Fort Belvoir, Virginia 22060  
Attn: Director of Research

U. S. Army Mobility Equipment Research and  
Development Center  
Fort Belvoir, Virginia 22060  
Attn: Mr. Richard A. Belt

U. S. Tank Automotive Center  
Propulsion Systems Laboratory, AFPA RCP-4  
Warren, Michigan 48090  
Attn: Mr. Lloyd E. Cox

Naval Ship Systems Command  
Department of the Navy  
Washington, D. C. 20360  
Attn: Dr. J. H. Huth, Code 051

Naval Ship Systems Command  
Department of the Navy  
Washington, D. C. 20360  
Attn: Mr. Roy Peterson, Code 03413

Naval Ship Systems Command  
Department of the Navy  
Washington, D. C. 20360  
Attn: Technical Library

Naval Ship Research and Development Center  
Annapolis Division  
Annapolis, Maryland 21402  
Attn: Dr. Earl Quandt

Naval Ship Research and Development Center  
Annapolis Division  
Annapolis, Maryland 21402  
Attn: Library, Code A214

Naval Ordnance Laboratory  
White Oak  
Silver Spring, Maryland 20910  
Attn: Mr. Lyman Carlyle Fisher, Code 510  
Technical Library

Air Force Aero Propulsion Laboratory (APIP-1)  
Wright-Patterson Air Force Base, Ohio 45433  
Attn: Mr. John W. Zmurek

Air Force Office of Scientific Research  
1400 Wilson Boulevard  
Arlington, Virginia 22209  
Attn: Dr. Joseph F. Masi

Rome Air Development Center, EMEAM  
Griffiss Air Force Base, New York 13440  
Attn: Mr. Frank J. Mollura

U. S. Atomic Energy Commission  
Washington, D. C. 20545  
Attn: SEPO-Division of Space  
Nuclear Systems

U. S. Atomic Energy Commission  
Washington, D. C. 20545  
Attn: Mr. C. E. Miller, Jr.  
Division Reactor Development  
and Technology

U. S. Naval Oceanographic Office  
Suitland, Maryland 20390  
Attn: Library, Code 1640

U. S. Naval Postgraduate School  
Monterey, California 93940  
Attn: Library, Code 0212

Naval Ship Engineering Center  
Philadelphia Division  
Philadelphia, Pennsylvania 19112  
Attn: Technical Library

Naval Underwater System Center  
TB 142  
Newport, Rhode Island 02840  
Attn: Mr. John P. Arena

Mr. Vernon C. Westcott  
Trans-Sonics, Inc.  
P. O. Box 526  
Lexington, Massachusetts 02173

U. S. Atomic Energy Commission  
Argonne National Laboratory  
9700 South Cass Avenue  
Argonne, Illinois 60440  
Attn: Library

National Bureau of Standards  
Washington, D. C. 20025  
Attn: Library

Naval Undersea Warfare Center  
3202 East Foothill Boulevard  
Pasadena, California 91107  
Attn: Technical Library

Naval Underwater Systems Center  
Fort Trumbull  
New London, Connecticut 06320  
Attn: Technical Library

U. S. Naval Weapons Laboratory  
Damascus, Virginia 22448  
Attn: Technical Library

Naval Ship Engineering Center  
Pattersonville, Maryland 20782  
Attn: Mr. R. M. Petros, Code 6148D

Naval Ship Engineering Center  
Pattersonville, Maryland 20782  
Attn: Mr. R. A. Coulombe, Code 6146

Naval Weapons Center  
China Lake, California 93555  
Attn: Technical Library

Director  
Naval Research Laboratory  
Washington, D. C. 20390  
Attn: Technical Information Division

Strategic Systems Project Office  
Department of the Navy  
Washington, D. C. 20360  
Attn: Technical Library, NSP-43

Office of Naval Research  
Southeastern Area  
2110 G Street, N. W.  
Washington, D. C. 20037  
Attn: Mr. W. H. Grant, Contract Administrator

Battelle Memorial Institute  
505 King Avenue  
Columbus, Ohio 43201  
Attn: Library

Massachusetts Institute of Technology  
Cambridge, Massachusetts 02139  
Attn: Library

The Franklin Institute  
Benjamin Franklin Parkway at 20th Street  
Philadelphia, Pennsylvania 19103  
Attn: Library

Acrojet-General Corporation  
Von Karman Center  
Azusa, California 91702  
Attn: Library

University of Arizona  
Department of Aerospace and  
Mechanical Engineering  
Tucson, Arizona 85721  
Attn: Professor D. Kececioglu

AIResearch Manufacturing Company  
9851 Sepulveda Boulevard  
Los Angeles, California 90045  
Attn: Library

AIResearch Manufacturing Company  
402 South 36th Street  
Phoenix, Arizona 85034  
Attn: Library

General Electric Company  
Flight Propulsion Division  
Cincinnati, Ohio 45215  
Attn: Library

General Electric Company  
Mechanical Technology Laboratory  
Research and Development Center  
Schenectady, New York 12301  
Attn: Library

Naval Ships R & D Center  
Annapolis Laboratory  
Annapolis, Maryland 21402  
Attn: Code 2813/Mr. B. Miller

Power Information Center  
University City Science Institute  
3401 Market Street, Room 2210  
Philadelphia, Pennsylvania 19104

Professor Ralph Burton  
Dept. of Mech Engr & Astronautical Sci  
Northwestern University  
Evanston, Illinois 60201

Professor Nathan Cook  
Dept. of Mechanical Engr.  
Massachusetts Institute of Technology  
Cambridge, Massachusetts 02139

Mr. Anton Hehn  
General American Research Division  
General American Transport  
7449 North Natchez Avenue  
Niles, Illinois 60648

Professor A. O. Lebeck  
Mechanical Engineering Department  
University of New Mexico  
Albuquerque, New Mexico 87106



Unclassified

Security Classification

DOCUMENT CONTROL DATA - R & D

(Security classification of title, body of abstract and indexing annotation must be entered when the overall report is classified)

1. ORIGINATING ACTIVITY (Corporate author) The University of Tennessee Mechanical & Aerospace Engineering Department ✓ Knoxville, Tennessee 37916		2a. REPORT SECURITY CLASSIFICATION Unclassified	
3. REPORT TITLE "An Experimental & Analytical Investigation of a Radial Face Seal"		2b. GROUP	
4. DESCRIPTIVE NOTES (Type of report and inclusive dates) Interim			
5. AUTHOR(S) (First name, middle initial, last name) Timothy W. Swafford			
6. REPORT DATE January 30, 1976		7a. TOTAL NO. OF PAGES 155	7b. NO. OF REFS 21
8a. CONTRACT OR GRANT NO. N00014-75-C-390 ✓		9a. ORIGINATOR'S REPORT NUMBER(S) ME-76-T57-22 ✓	
b. PROJECT NO.		9b. OTHER REPORT NO(S) (Any other numbers that may be assigned this report)	
c.			
d.			
10. DISTRIBUTION STATEMENT This document has been approved for public release and sale; its distribution is unlimited.			
11. SUPPLEMENTARY NOTES None		12. SPONSORING MILITARY ACTIVITY	
13. ABSTRACT Abstract A complete description concerning the interface region of a parallel radial face seal has been conducted both experimentally and analytically. Analytical predictions stem from a FORTRAN IV computer program designed such that density and viscosity variation with temperature can be simulated. The equations of motion were solved on an incremental basis to yield a "closed form, finite difference" solution. For comparison purposes, predictions assuming non-temperature dependent fluid properties are also given. Experimentally determined parameters include vertical load, torque, interface pressures, and temperatures, while interface clearance, supply pressure, and rotational speed were externally set parameters affecting seal performance. Unlike most other investigators, the test seal was rigidly mounted and both surfaces were constructed of stainless steel. Numerically predicted temperature dependent and non-temperature dependent fluid property pressure profiles deviate substantially when fluid temperatures rise becomes significant; thus decreasing the load carrying capacity of the seal. Predictions involving a temperature-dependent fluid indicate higher leakage rates and lower torque values when compared to predictions assuming a non-temperature dependent fluid. Experimental testing was carried out under several sealing conditions. Supply pressures ranged from 17.1 to 87.5 psig ( $1.18 \times 10^5$ to $6.03 \times 10^5$ N/m <sup>2</sup> ) while average clearances and rotational speeds ranged from 1995 to 3428 micro-inches (50.7 to 89.6 microns) and from 0 to 1520 rpm, respectively. Vertical loads obtained experimentally were normally lower than those predicted although differences decreased at higher supply pressures. Experimentally determined torque agreed favorably with theoretical predictions while measured leakage rates were consistently lower than those predicted by theory. In contrast to several past experimenters reporting doubly fluctuating components of clearance and pressure per shaft revolution, this investigation revealed but a single clearance and pressure oscillation per shaft revolution. Measured average pressure values agreed somewhat with predictions although significant differences were noticed at high speeds and low clearances.			

DD FORM 1473

1 NOV 65

(PAGE 1)

S/N 0101-807-6801

Security Classification

### KEY WORDS

LINK A

LINK B

LINK C

	NAME	ROLE
1	Mr. J. Edgar Hoover	Director
2	Mr. Clegg	Chief Clerk
3	Mr. Glavin	Assistant Director
4	Mr. Ladd	Assistant Director
5	Mr. Nichols	Assistant Director
6	Mr. Rosen	Assistant Director
7	Mr. Tracy	Assistant Director
8	Mr. Carson	Assistant Director
9	Mr. Egan	Assistant Director
10	Mr. Gurnea	Assistant Director
11	Mr. Hendon	Assistant Director
12	Mr. Mumford	Assistant Director
13	Mr. Quinn	Assistant Director
14	Mr. Nease	Assistant Director
15	Mr. Tamm	Assistant Director
16	Mr. W.C. Sullivan	Assistant Director
17	Mr. Harbo	Assistant Director
18	Mr. Mohr	Assistant Director
19	Mr. Pennington	Assistant Director
20	Mr. Nease	Assistant Director
21	Mr. Tamm	Assistant Director
22	Mr. W.C. Sullivan	Assistant Director
23	Mr. Harbo	Assistant Director
24	Mr. Mohr	Assistant Director
25	Mr. Pennington	Assistant Director
26	Mr. Nease	Assistant Director
27	Mr. Tamm	Assistant Director
28	Mr. W.C. Sullivan	Assistant Director
29	Mr. Harbo	Assistant Director
30	Mr. Mohr	Assistant Director
31	Mr. Pennington	Assistant Director
32	Mr. Nease	Assistant Director
33	Mr. Tamm	Assistant Director
34	Mr. W.C. Sullivan	Assistant Director
35	Mr. Harbo	Assistant Director
36	Mr. Mohr	Assistant Director
37	Mr. Pennington	Assistant Director
38	Mr. Nease	Assistant Director
39	Mr. Tamm	Assistant Director
40	Mr. W.C. Sullivan	Assistant Director
41	Mr. Harbo	Assistant Director
42	Mr. Mohr	Assistant Director
43	Mr. Pennington	Assistant Director
44	Mr. Nease	Assistant Director
45	Mr. Tamm	Assistant Director
46	Mr. W.C. Sullivan	Assistant Director
47	Mr. Harbo	Assistant Director
48	Mr. Mohr	Assistant Director
49	Mr. Pennington	Assistant Director
50	Mr. Nease	Assistant Director
51	Mr. Tamm	Assistant Director
52	Mr. W.C. Sullivan	Assistant Director
53	Mr. Harbo	Assistant Director
54	Mr. Mohr	Assistant Director
55	Mr. Pennington	Assistant Director
56	Mr. Nease	Assistant Director
57	Mr. Tamm	Assistant Director
58	Mr. W.C. Sullivan	Assistant Director
59	Mr. Harbo	Assistant Director
60	Mr. Mohr	Assistant Director
61	Mr. Pennington	Assistant Director
62	Mr. Nease	Assistant Director
63	Mr. Tamm	Assistant Director
64	Mr. W.C. Sullivan	Assistant Director
65	Mr. Harbo	Assistant Director
66	Mr. Mohr	Assistant Director
67	Mr. Pennington	Assistant Director
68	Mr. Nease	Assistant Director
69	Mr. Tamm	Assistant Director
70	Mr. W.C. Sullivan	Assistant Director
71	Mr. Harbo	Assistant Director
72	Mr. Mohr	Assistant Director
73	Mr. Pennington	Assistant Director
74	Mr. Nease	Assistant Director
75	Mr. Tamm	Assistant Director
76	Mr. W.C. Sullivan	Assistant Director
77	Mr. Harbo	Assistant Director
78	Mr. Mohr	Assistant Director
79	Mr. Pennington	Assistant Director
80	Mr. Nease	Assistant Director
81	Mr. Tamm	Assistant Director
82	Mr. W.C. Sullivan	Assistant Director
83	Mr. Harbo	Assistant Director
84	Mr. Mohr	Assistant Director
85	Mr. Pennington	Assistant Director
86	Mr. Nease	Assistant Director
87	Mr. Tamm	Assistant Director
88	Mr. W.C. Sullivan	Assistant Director
89	Mr. Harbo	Assistant Director
90	Mr. Mohr	Assistant Director
91	Mr. Pennington	Assistant Director
92	Mr. Nease	Assistant Director
93	Mr. Tamm	Assistant Director
94	Mr. W.C. Sullivan	Assistant Director
95	Mr. Harbo	Assistant Director
96	Mr. Mohr	Assistant Director
97	Mr. Pennington	Assistant Director
98	Mr. Nease	Assistant Director
99	Mr. Tamm	Assistant Director
100	Mr. W.C. Sullivan	Assistant Director

WT

NAME	ROLE
1. [Name]	[Role]
2. [Name]	[Role]
3. [Name]	[Role]
4. [Name]	[Role]
5. [Name]	[Role]
6. [Name]	[Role]
7. [Name]	[Role]
8. [Name]	[Role]
9. [Name]	[Role]
10. [Name]	[Role]
11. [Name]	[Role]
12. [Name]	[Role]
13. [Name]	[Role]
14. [Name]	[Role]
15. [Name]	[Role]
16. [Name]	[Role]
17. [Name]	[Role]
18. [Name]	[Role]
19. [Name]	[Role]
20. [Name]	[Role]
21. [Name]	[Role]
22. [Name]	[Role]
23. [Name]	[Role]
24. [Name]	[Role]
25. [Name]	[Role]
26. [Name]	[Role]
27. [Name]	[Role]
28. [Name]	[Role]
29. [Name]	[Role]
30. [Name]	[Role]
31. [Name]	[Role]
32. [Name]	[Role]
33. [Name]	[Role]
34. [Name]	[Role]
35. [Name]	[Role]
36. [Name]	[Role]
37. [Name]	[Role]
38. [Name]	[Role]
39. [Name]	[Role]
40. [Name]	[Role]
41. [Name]	[Role]
42. [Name]	[Role]
43. [Name]	[Role]
44. [Name]	[Role]
45. [Name]	[Role]
46. [Name]	[Role]
47. [Name]	[Role]
48. [Name]	[Role]
49. [Name]	[Role]
50. [Name]	[Role]
51. [Name]	[Role]
52. [Name]	[Role]
53. [Name]	[Role]
54. [Name]	[Role]
55. [Name]	[Role]
56. [Name]	[Role]
57. [Name]	[Role]
58. [Name]	[Role]
59. [Name]	[Role]
60. [Name]	[Role]
61. [Name]	[Role]
62. [Name]	[Role]
63. [Name]	[Role]
64. [Name]	[Role]
65. [Name]	[Role]
66. [Name]	[Role]
67. [Name]	[Role]
68. [Name]	[Role]
69. [Name]	[Role]
70. [Name]	[Role]
71. [Name]	[Role]
72. [Name]	[Role]
73. [Name]	[Role]
74. [Name]	[Role]
75. [Name]	[Role]
76. [Name]	[Role]
77. [Name]	[Role]
78. [Name]	[Role]
79. [Name]	[Role]
80. [Name]	[Role]
81. [Name]	[Role]
82. [Name]	[Role]
83. [Name]	[Role]
84. [Name]	[Role]
85. [Name]	[Role]
86. [Name]	[Role]
87. [Name]	[Role]
88. [Name]	[Role]
89. [Name]	[Role]
90. [Name]	[Role]
91. [Name]	[Role]
92. [Name]	[Role]
93. [Name]	[Role]
94. [Name]	[Role]
95. [Name]	[Role]
96. [Name]	[Role]
97. [Name]	[Role]
98. [Name]	[Role]
99. [Name]	[Role]
100. [Name]	[Role]

W T

[illegible]

WT

### Interface Pressure Measurements